

Chapter-5

Synthesis of Schiff Base Derivatives of 6-Amino Coumarin as Mesogens



5.1 Introduction

Liquid crystals contain a variety of intriguing and practical qualities that make them suitable for use in various devices. The use of liquid crystals in various devices depends on a variety of features such as optical and dielectric anisotropy, birefringence behavior, etc. [1-3]. Compounds having liquid crystalline phases are created at certain transition temperatures by a combination of morphological structural components [4]. At a specific temperature range, a class of materials known as thermotropic liquid crystals exhibits both liquid-like and crystalline-like characteristics. These substances often consist of elongated or rod-like molecules that are capable of aligning themselves in an orderly manner to produce a liquid crystal phases [5-6]. Temperature has a major role on the behavior of thermotropic liquid crystals. Thermotropic liquid crystals are used in a variety of products, such as displays, sensors, and optical equipment. For instance, they are frequently employed in the production of liquid crystal displays (LCDs), where they enable the capacity to transit between various polarization states and so produce various colors [7-10]. Liquid crystal materials utilized in liquid crystal devices have hard rod-like molecules as their core molecular structure, functionalized with one or two flexible hydrocarbon tails. An extended, rigid structure that is extremely anisotropic appears to be the primary requirement for liquid crystalline behavior [11-13].

Synthetic coumarin derivatives are well studied for their biological and pharmacological applications. Coumarin derivatives have shown very distinctive photophysical characteristics and been explored for their material applications such as fluorescent sensors, laser dyes and organic light-emitting diodes (OLEDs) [7-8,14-15]. Recently, several new thermotropic compounds are designed containing coumarin as heterocyclic core and studied for their mesomorphic behavior [16-18]. Amino coumarins are important members of the coumarin, which can easily have synthesized for various applications [19-21]. Coumarin with imine (-CH=N-) linkage have played role in molecular conjugation as well as more suited to the fluorescence and mesogenic properties [22-24]. The properties related to mesomorphism in 7-alkoxy 3-amino coumarin were notably influenced by alterations in the linking groups and length of the terminal alkoxy chain [20, 25-26]. This influence stemmed from an overall modification in the polarity and alignment of dipole moments. The mesomorphic properties of coumarin Schiff base also underwent significant changes due to variations in the terminal polar group, as investigated within our group [27-28].

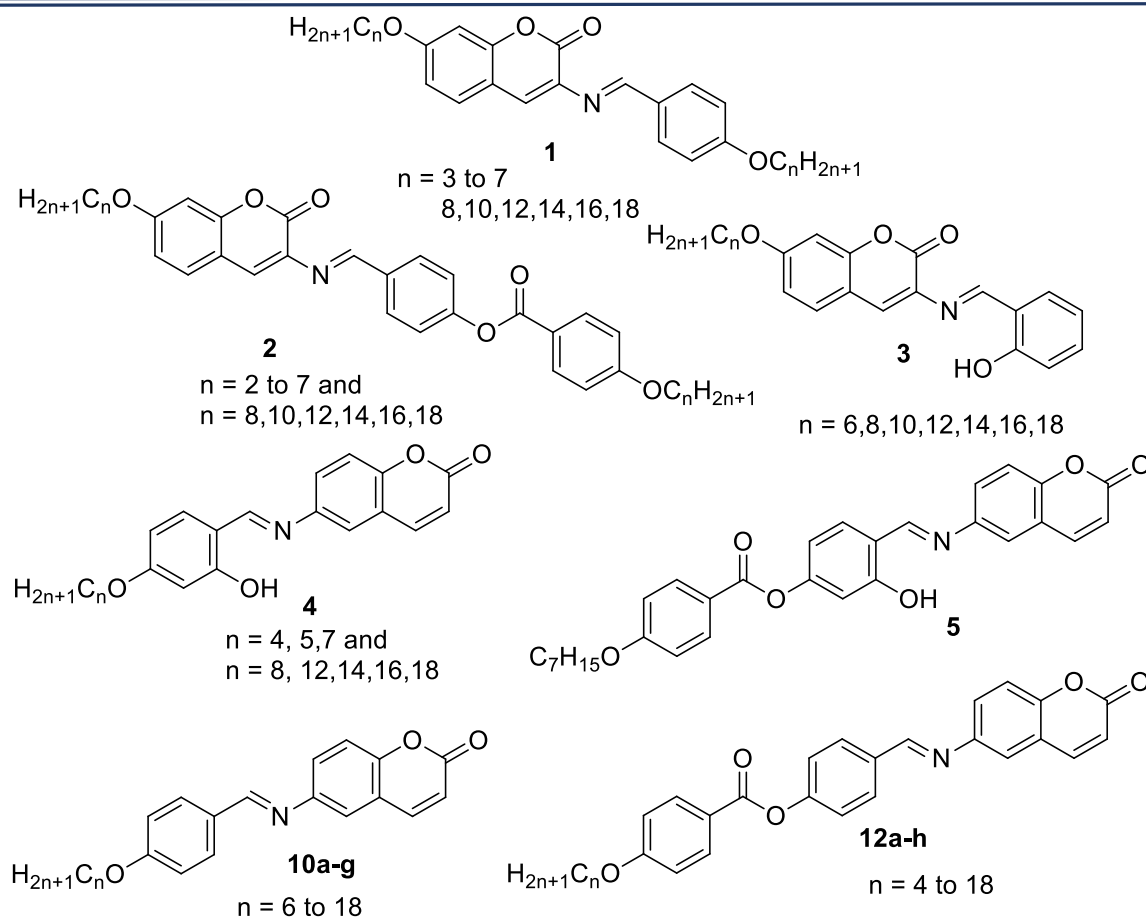


Figure- 5.1 Coumarin Schiff Base derivatives as thermotropic liquid crystalline material

Earlier, Schiff base derivatives **1** and Schiff base derivatives **2** with ester linkages of 7-alkoxy 3-amino coumarin with symmetrical alkoxy chain lengths at both ends of the molecules reported by our group (**Fig-5.1**). In this study, for compound **1** it was observed that shorter chain members displayed a nematic phase, whereas longer alkyl chain members exhibited a SmA mesophase [29] and for compounds **2** with ester linkage lower members showed nematic mesophase while higher alkoxy group showed Smectic C mesophases [30]. The structural stability, distinctive photosensitivity, and non-covalent intermolecular interactions of coumarin derivatives are well known. Very recently, Rina et al. have reported and studied the mesomorphic and photophysical properties of derivative **3** (**Fig-5.1**) [31]. In this series, Schiff base derivatives with intramolecular hydrogen bonding have also exhibited fluorescence due to excited state proton transfer properties.

6-amino coumarin is also one of the important members of the coumarin family which is a naturally occurring compound found in plants and also synthesized for various applications [19,10,32]. 6-amino coumarin has interesting properties, such as fluorescence, which makes it useful as a fluorescent probe in bio imaging and sensing applications [33]. Its properties can

be modified by careful chemical modification of the amino and coumarin groups, leading to the development of new compounds with novel properties and potential applications.

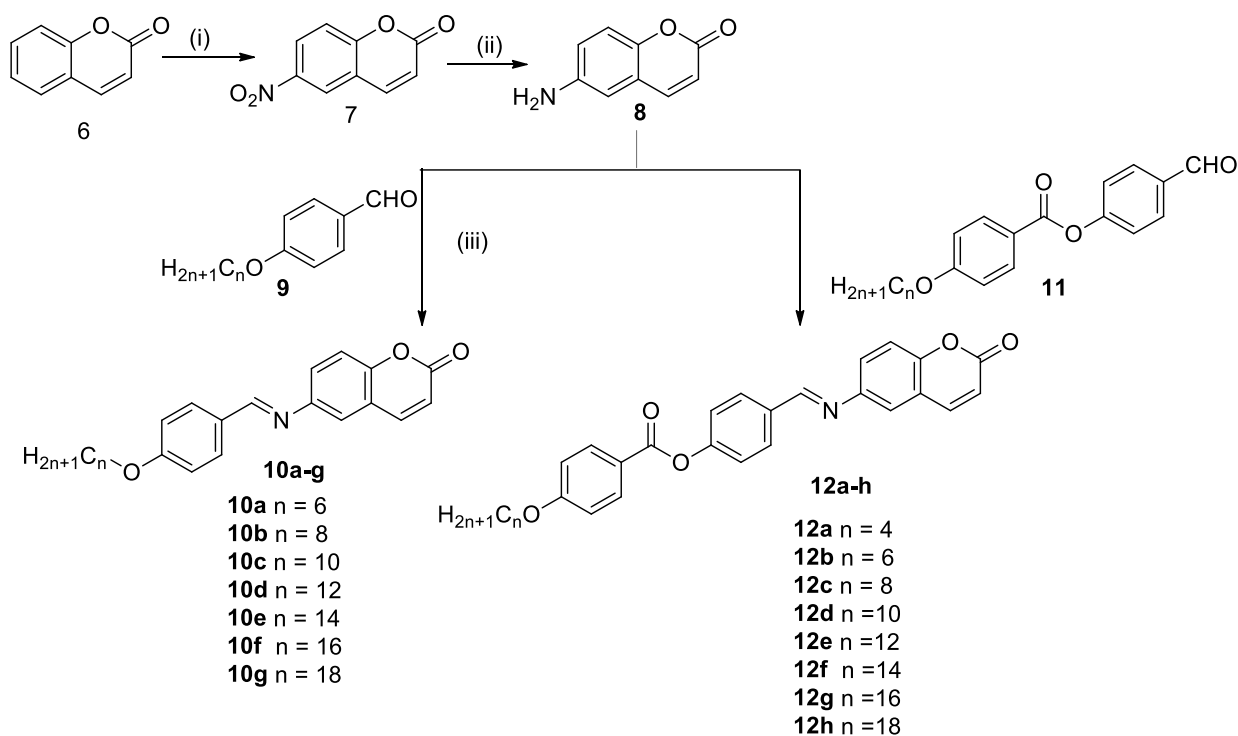
Paul et al, reported a homologous series of emissive novel coumarins that comprise rod-shaped Schiff bases and their Zn(II) complexes **4** (**Fig-5.1**). These compounds were shown to have intriguing photophysical characteristics, mesomorphic behavior, and gelation behavior [34]. A novel coumarin Schiff base compound with a significant Stokes shift was synthesized by Pegu et al. [35]. The structural and spectroscopic properties of the substance 6-(4-n-heptyloxybenzyloxy)-2-hydroxybenzylidene)amino)-2H chromen-2-one **5** were investigated both experimentally and theoretically. The first hyper polarizability value in particular, with its huge magnitude, showed its potential application in nonlinear optical devices.

As a part of our research work on development of coumarin containing liquid crystalline compounds [25,29,36] we have selected 6-aminocoumarin and designed compounds **10a-g** and **12a-h** with void of ortho hydroxyl group on aldehyde part. Removal of hydroxyl group will result in loss of intramolecular hydrogen bonding, which will further affect intermolecular interaction and hence mesomorphic properties as well as electronic properties of these compounds. DFT calculations are used to optimize the structures of both the series and literature reported compound **4** and important electronic properties such as dipole moment and polarizability are compared with mesomorphic trends for studied compounds.

5.2 Result and discussion

5.2.1 Chemistry

2*H*-chromen-2-one **6** was nitrated with HNO₃:H₂SO₄ at cooling condition. After addition of nitrating mixture, the reaction mixture was allowed to stir at room temperature for 2 hours (Scheme-5.1), which resulted in formation of 6-nitro-2*H*-chromen-2-one **7** with 96% yield. 6-amino-2*H*-chromen-2-one **8** was obtained by reduction of **7** using iron powder and NH₄Cl in water with 70% yield. Simultaneously, *n*-alkoxy benzaldehyde **9** was prepared by *o*-alkylation of 4-hydroxybenzaldehyde using *n*-alkyl bromide in presence of anhydrous K₂CO₃ and catalytic amount KI in DMF and yield compound **9** is 80%. Finally, the desired Schiff bases i.e. **10a-g** were obtained by reacting *n*-alkoxy benzaldehyde **9** with 6-aminocoumarin **8** in presence of 3-4 drops of glacial acetic acid in absolute ethanol under reflux condition with good yield between 75-88%.



Reagents and Conditions: (i) HNO₃:H₂SO₄ (1:3) Conc. H₂SO₄, RT, 2hr (ii) Fe (powder), NH₄Cl, H₂O Reflux, 80°C (iii) EtOH, Cat. AcOH, Reflux 16 hr

Scheme- 5.1 Synthesis of Schiff base derivatives **10a-g** and **12a-h**

In another variations 4-hydroxybenzoic acid was mono alkylated with *n*-alkyl bromide in KOH, methanol and acidified with HCl, gave 4-(alkyloxy) benzoic acid which was further esterified with 4-hydroxybenzaldehyde using EDC, HOBt and TEA in DCM which gave 4-formylphenyl 4-(alkyloxy) benzoate **11** Finally, the desired Schiff Bases i.e. **12a-h** were obtained by reacting **8** and **11** in presence of catalytic glacial acetic acid (3-4 drops) in absolute ethanol under reflux

condition (**Scheme-5.1**). All the new Schiff base derivatives **10a-g** and **12a-h** were characterized by different analytical techniques such as $^1\text{H-NMR}$, $^{13}\text{C-NMR}$, ESI-MS, IR and CHN analysis. In IR spectrum of compound **10a-g** (**Fig-5.2.1 to 5.8.4**) showed absorption band for $-\text{CH}$ stretching in the region of $2922\text{--}2834\text{ cm}^{-1}$ and one strong band for the carbonyl group of coumarin ring in the range of $1728\text{--}1711\text{ cm}^{-1}$, while the imine C-N stretching of Schiff Base in the range of $1624\text{ to }1626\text{ cm}^{-1}$. In $^1\text{H-NMR}$, compound **10a-g** showed alkyl chain methyl protons as triplet in the range of $\delta\ 0.90\text{--}0.94\text{ppm}$, methylene linkage protons as multiplet from $\delta\ 1.26\text{--}1.87$ and methyleneoxy ($-\text{OCH}_2-$) protons were observed as triplet at $\delta\ 4.01\text{--}4.04$ with coupling constant value of 6.4 Hz . For all the compounds, aromatic protons were appeared from $\delta\ 6.45\text{ to }6.47$ and imine proton in the range of $\delta\ 8.41\text{ to }8.42\text{ppm}$. In $^{13}\text{C-NMR}$ of compounds **10a-g**, methyl carbons were observed in the range of $\delta\ 14.03\text{ to }14.13\text{ ppm}$, methylene carbons from $\delta\ 22.59\text{--}31.93\text{ ppm}$ and methyleneoxy carbon was observed at $\delta\ 68.28\text{ ppm}$. While for all the compounds aromatic carbons were observed from $114.81\text{ to }160.77\text{ppm}$ in $^{13}\text{C-NMR}$ along with imine carbon and lactone carbonyl carbon at $\delta\ 160.77$ and 162.26 ppm respectively.

For all the compounds **12a-h**, (**Fig-5.9.1 to 5.16.2**) IR spectra showed the alkyl stretching in the region of $2925\text{--}2835\text{ cm}^{-1}$, coumarin carbonyl group and ester carbonyl group as strong band in the range of $1728\text{--}1711\text{ cm}^{-1}$ and the imine stretching of Schiff Base at 1624 cm^{-1} . The methyl and methylene group peaks for compounds **12a-h** were in the range of $0.91\text{--}1.88\text{ ppm}$ and a methylene group containing oxygen was seen at 4.07 ppm in $^1\text{H-NMR}$. Aromatic protons for all the compounds were appeared in the range of $6.49\text{--}8.17\text{ ppm}$ and imine proton as singlet at 8.52 ppm . In $^{13}\text{C-NMR}$ analysis of compound **12a-h**, the methyl and methylene carbons were appeared between $14.13\text{--}31.90\text{ ppm}$, methyleneoxy carbon at 68.41 ppm , aromatic carbons, lactone carbonyl carbon and ester carbonyl carbon appeared from $114.42\text{--}163.79\text{ ppm}$ and imine carbon was observed at 164.54 ppm .

Figure- 5.2.1 IR of (E)-6-((4-(hexyloxy)benzylidene)amino)-2H-chromen-2-one (10a)

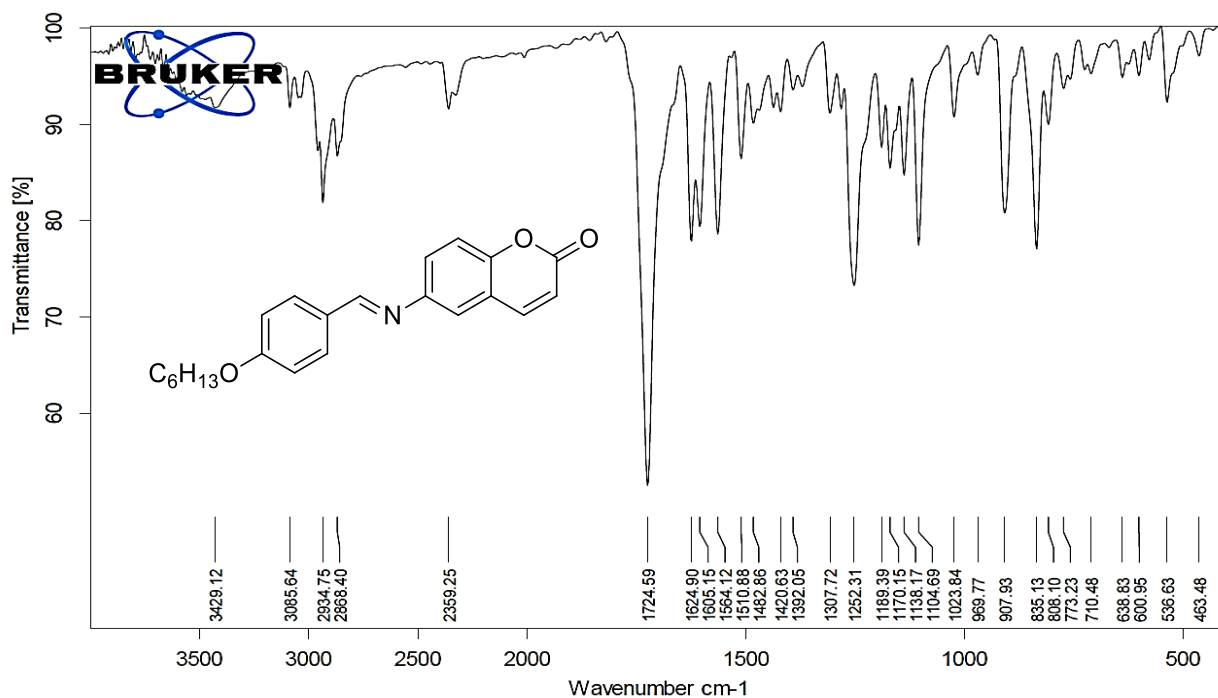
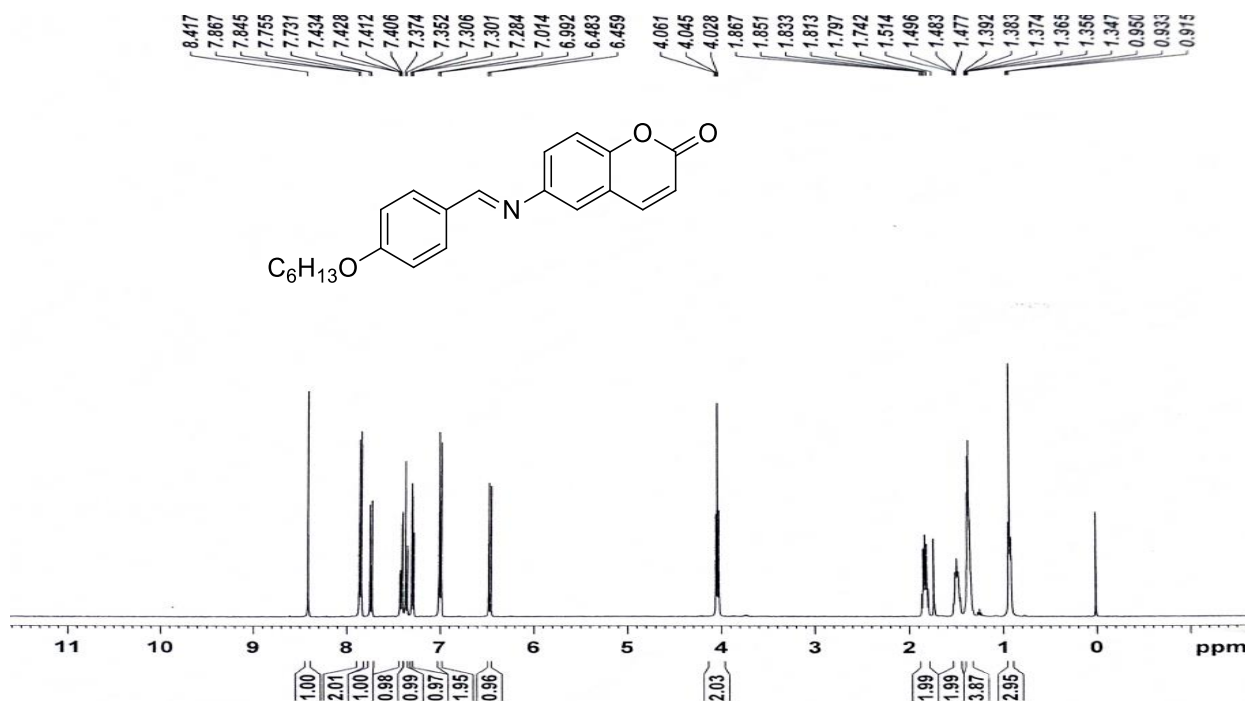
Figure- 5.2.2 ¹H-NMR of (E)-6-((4-(hexyloxy)benzylidene)amino)-2H-chromen-2-one (10a)

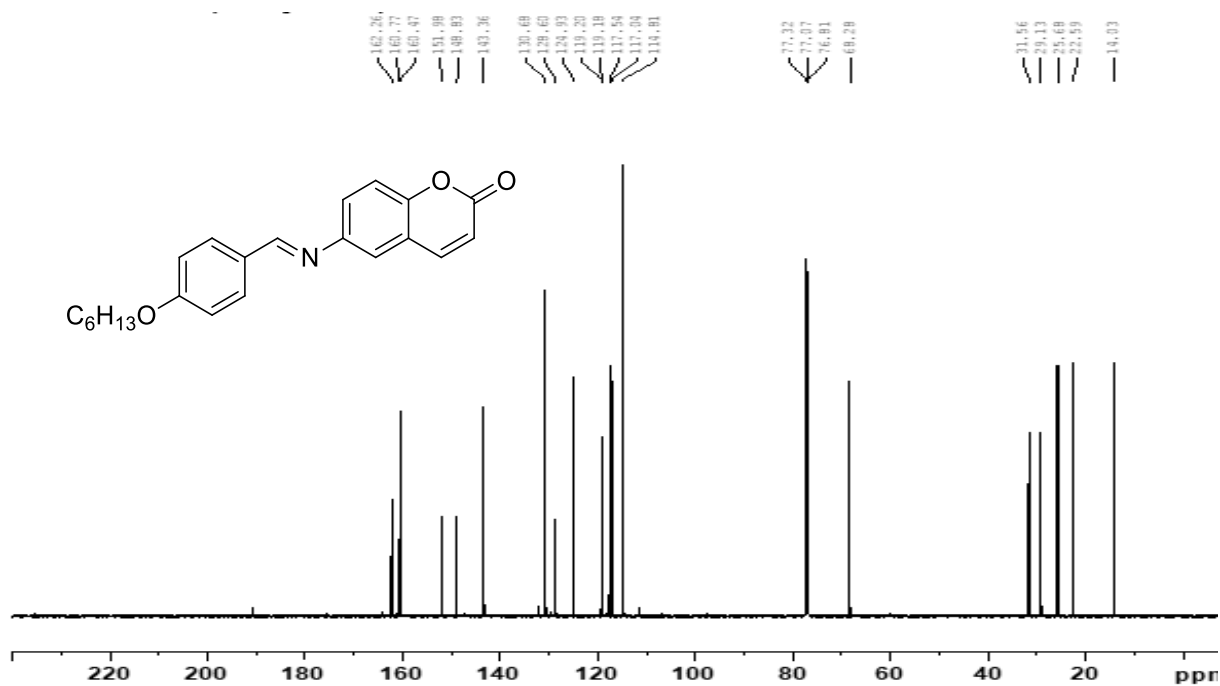
Figure- 5.2.3 ^{13}C -NMR of (E)-6-((4-(hexyloxy)benzylidene)amino)-2H-chromen-2-one (10a)

Figure- 5.3.1 IR of (E)-6-((4-(octyloxy)benzylidene)amino)-2H-chromen-2-one (10b)

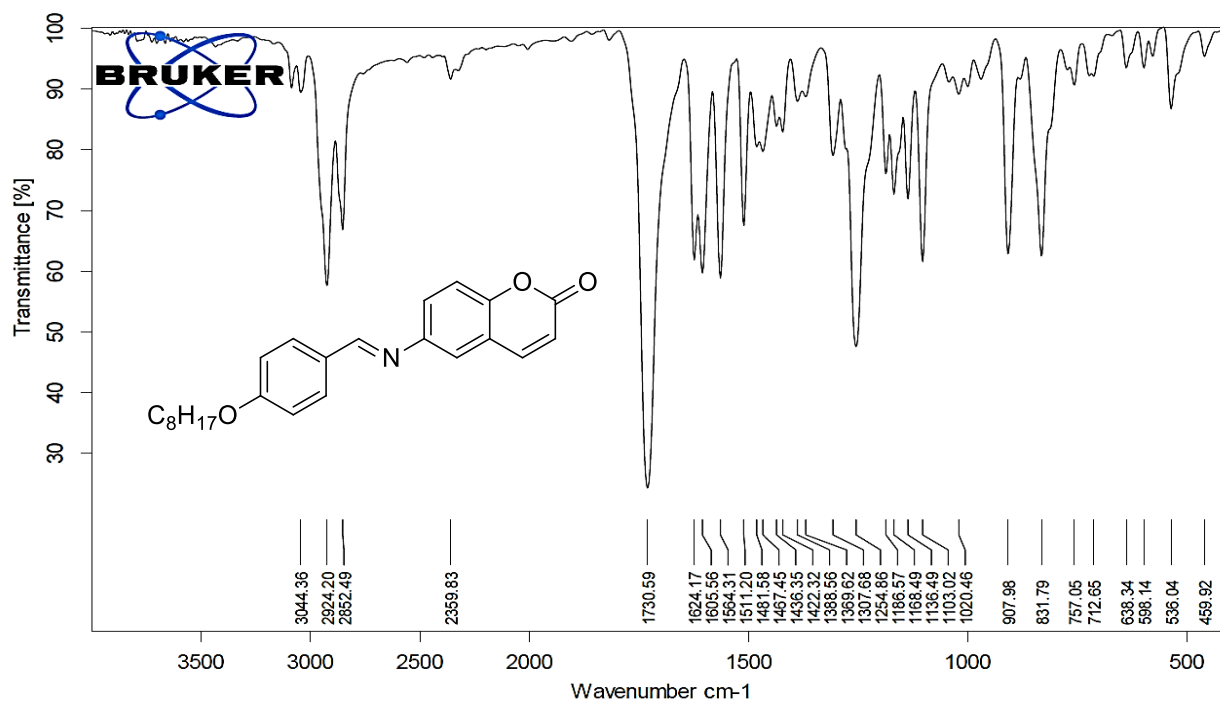


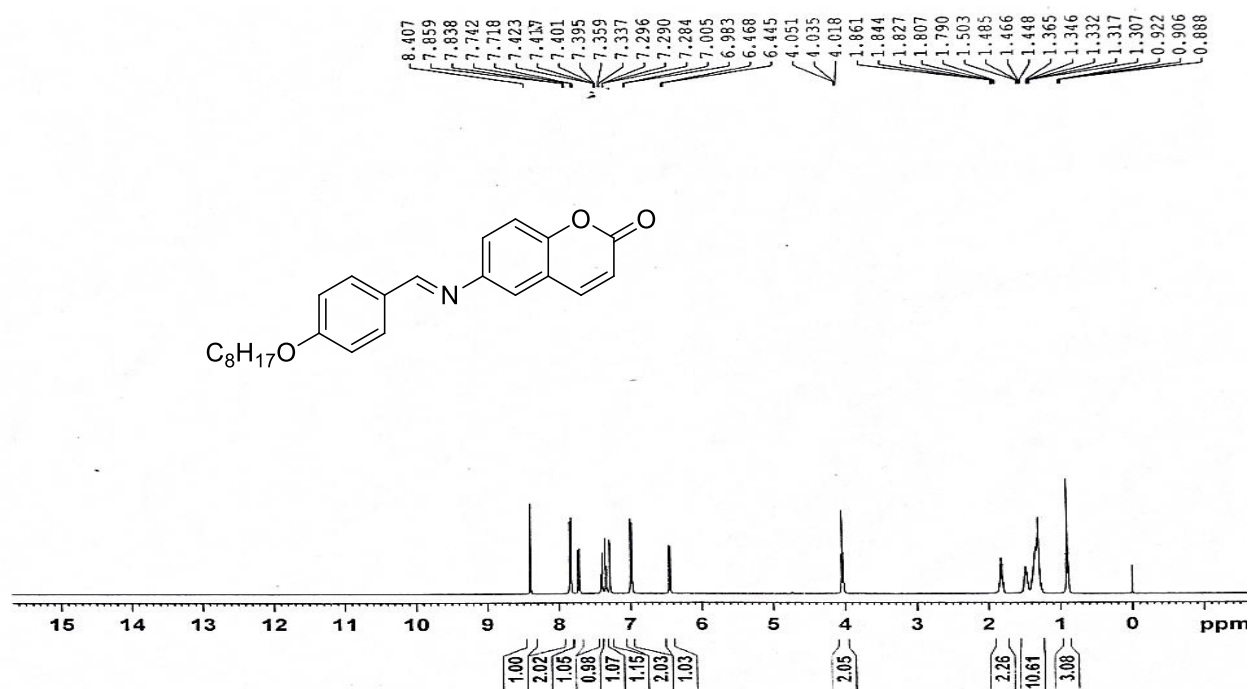
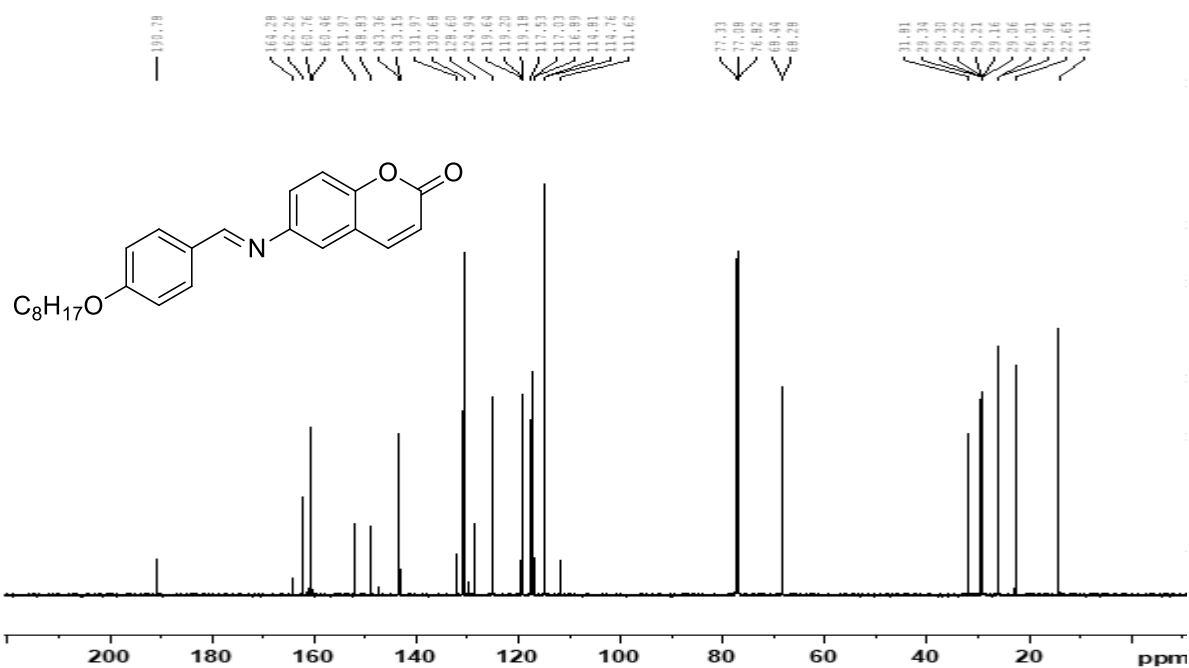
Figure- 5.3.2 $^1\text{H-NMR}$ of (E)-6-((4-(octyloxy)benzylidene)amino)-2H-chromen-2-one (10b)Figure- 5.3.3 $^{13}\text{C-NMR}$ of (E)-6-((4-(octyloxy)benzylidene)amino)-2H-chromen-2-one (10b)

Figure- 5.3.4 Mass of (E)-6-((4-(octyloxy)benzylidene)amino)-2H-chromen-2-one (**10b**)
M+H peak at 378.1

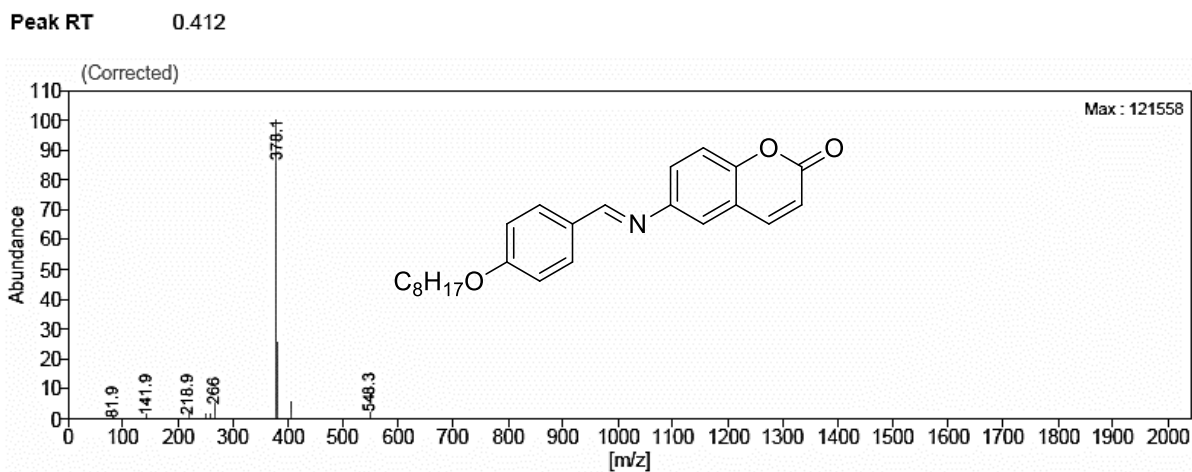


Figure- 5.4.1 IR of (E)-6-((4-(decyloxy)benzylidene)amino)-2H-chromen-2-one (**10c**)

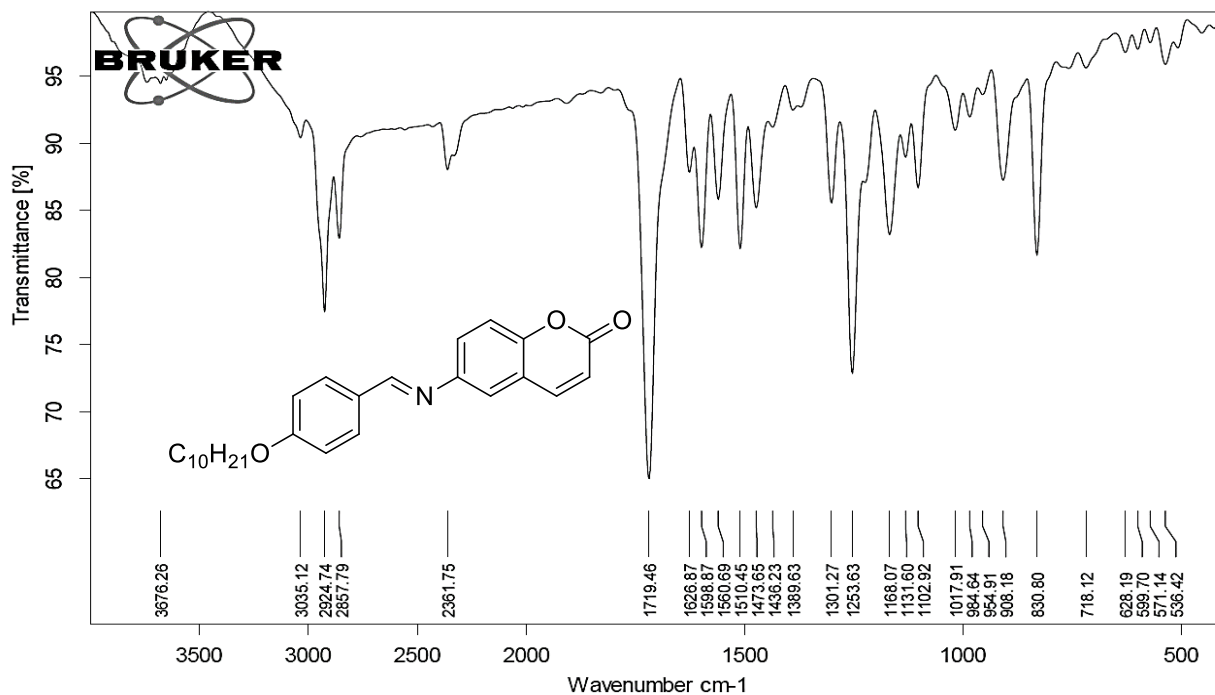


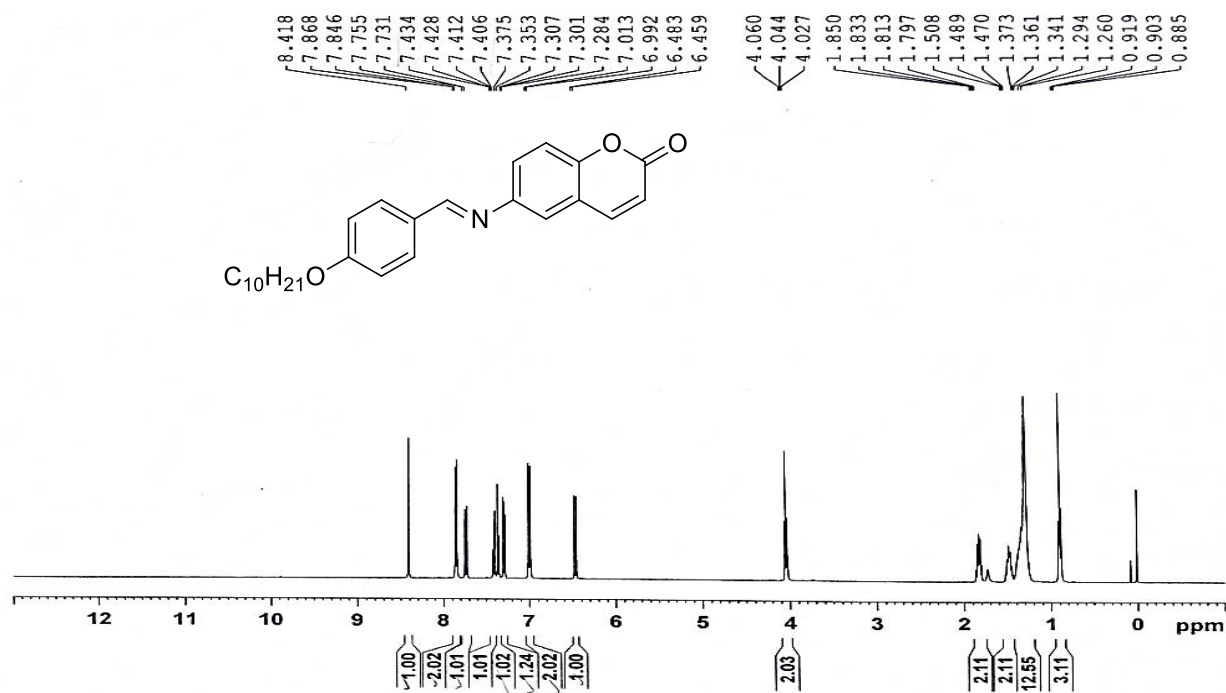
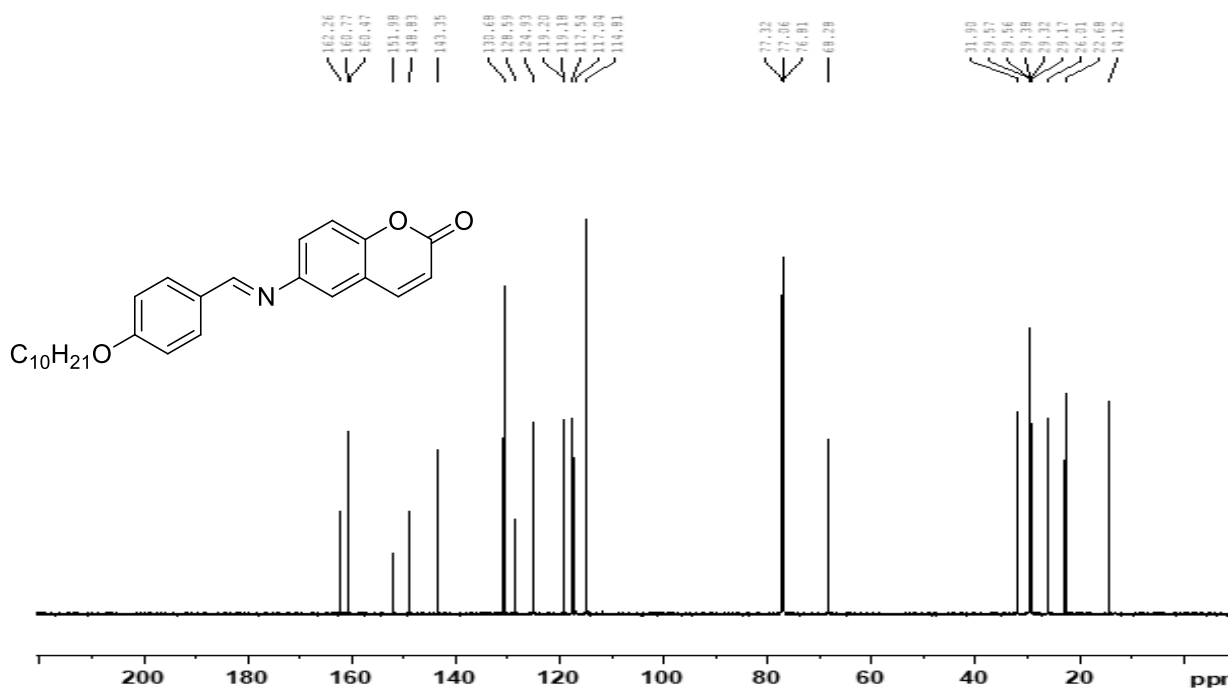
Figure- 5.4.2 $^1\text{H-NMR}$ of (E)-6-((4-(decyloxy)benzylidene)amino)-2H-chromen-2-one (**10c**)Figure- 5.4.3 $^{13}\text{C-NMR}$ of (E)-6-((4-(decyloxy)benzylidene)amino)-2H-chromen-2-one (**10c**)

Figure- 5.4.4 Mass of (E)-6-((4-(decyloxy)benzylidene)amino)-2H-chromen-2-one (**10c**) M+ peak at 405.52

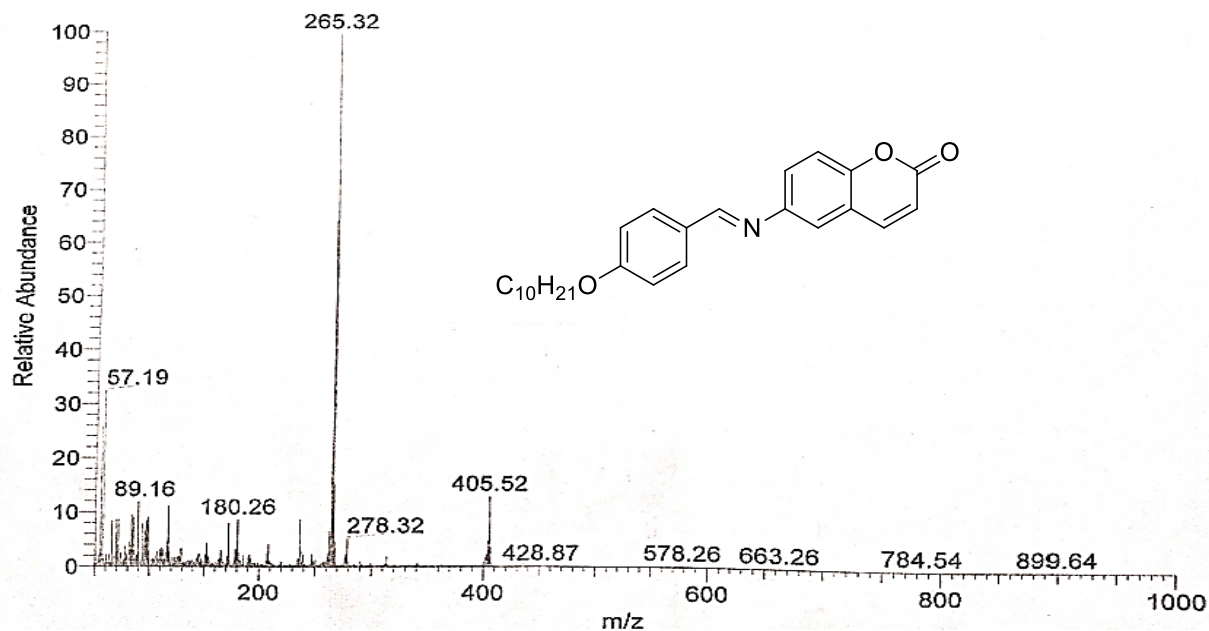


Figure- 5.5.1 IR of (E)-6-((4-(dodecyloxy)benzylidene)amino)-2H-chromen-2-one (**10d**)

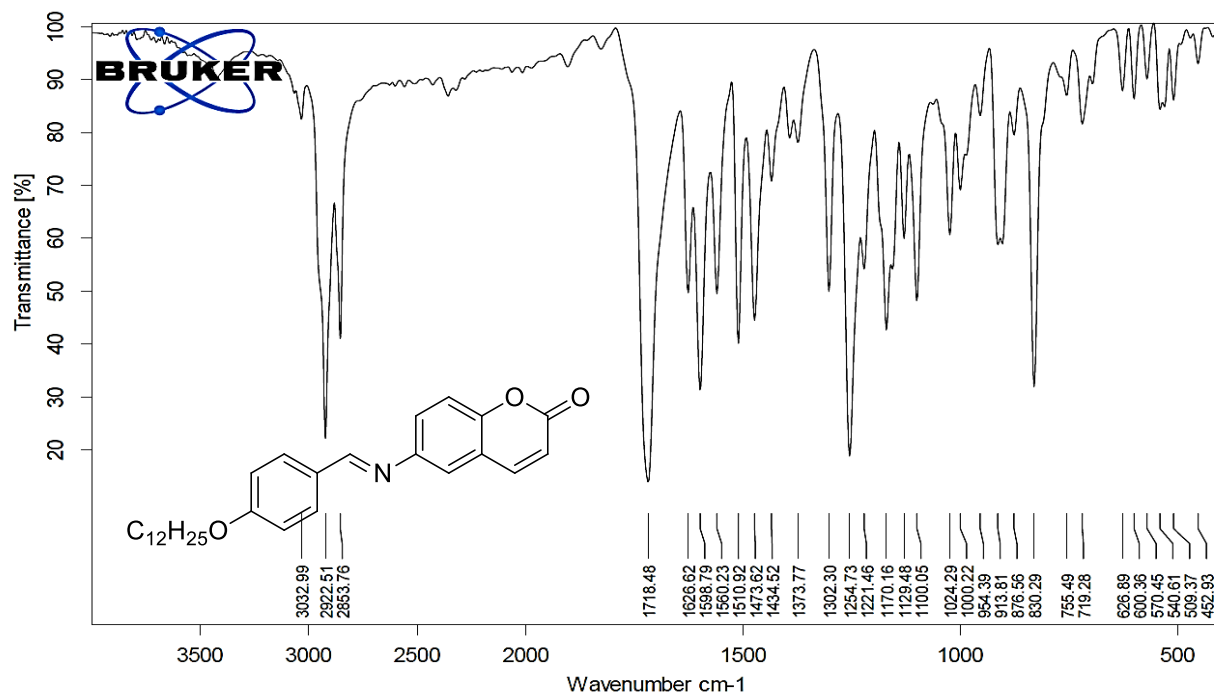


Figure- 5.5.2 $^1\text{H-NMR}$ of (E)-6-((4-(dodecyloxy)benzylidene)amino)-2H-chromen-2-one (10d)

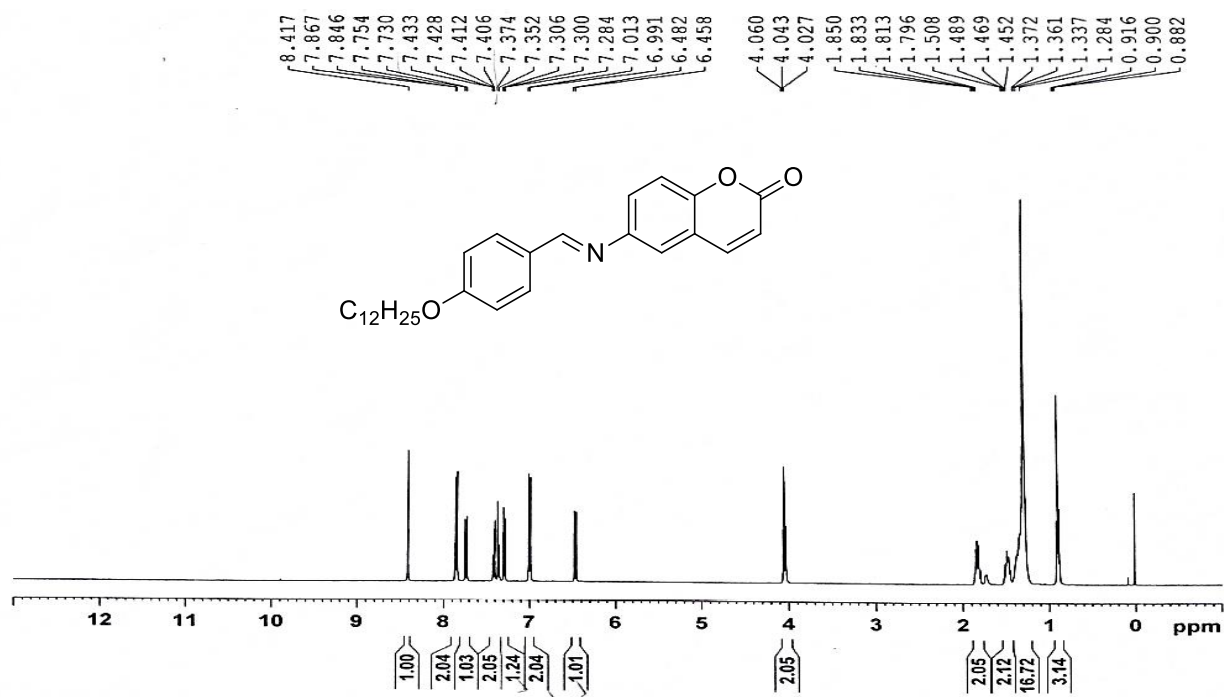


Figure- 5.5.3 $^{13}\text{C-NMR}$ of (E)-6-((4-(dodecyloxy)benzylidene)amino)-2H-chromen-2-one (10d)

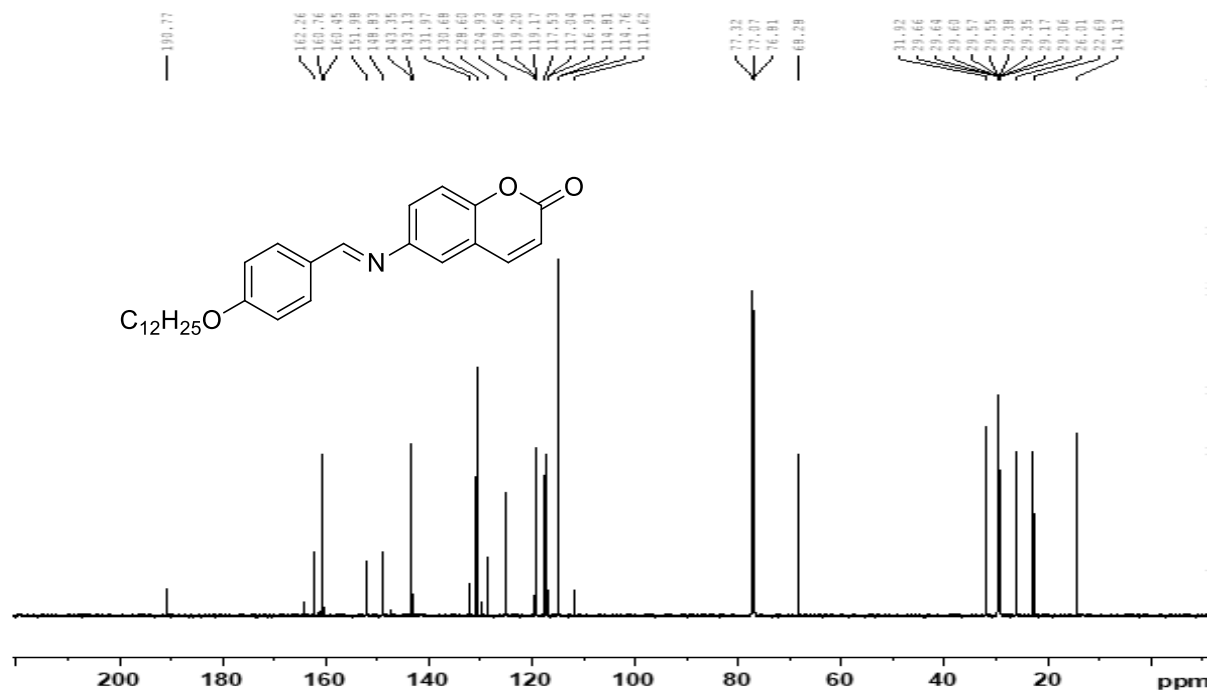


Figure- 5.5.4 Mass of (E)-6-((4-(dodecyloxy)benzylidene)amino)-2H-chromen-2-one (**10d**)

M+H peak at 434.26

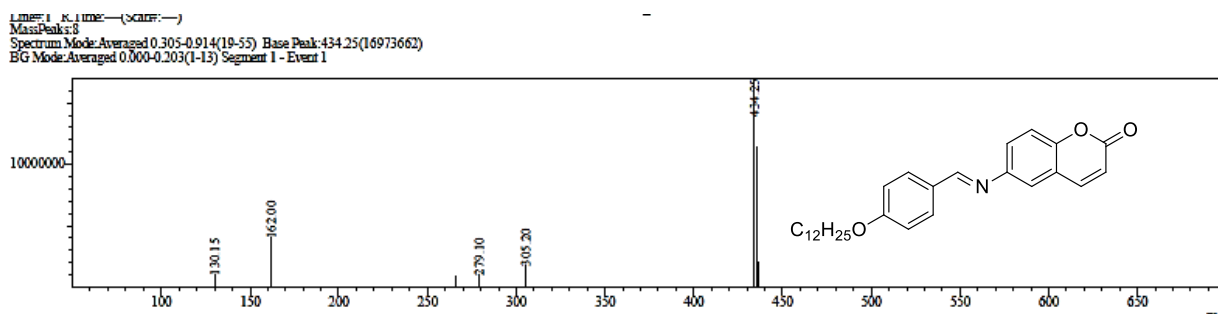
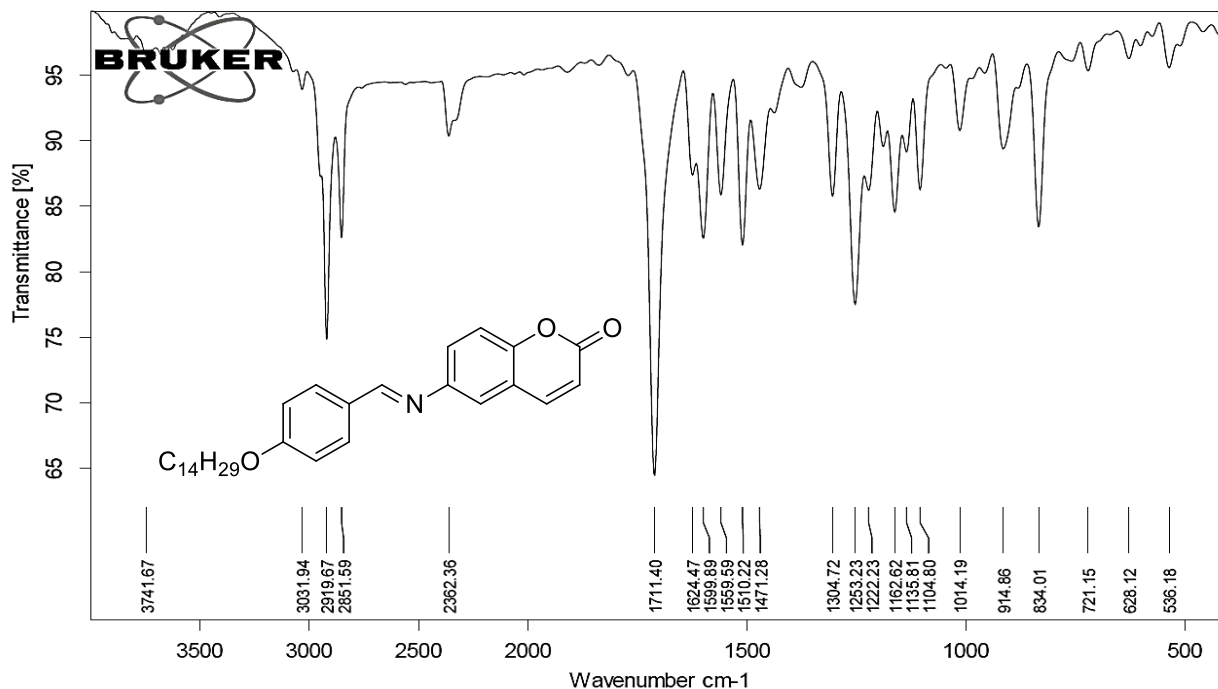
**Figure- 5.6.1** IR of (E)-6-((4-(dodecyloxy)benzylidene)amino)-2H-chromen-2-one (**10e**)

Figure- 5.6.2 $^1\text{H-NMR}$ of (E)-6-((4-(dodecyloxy)benzylidene)amino)-2H-chromen-2-one (10e)

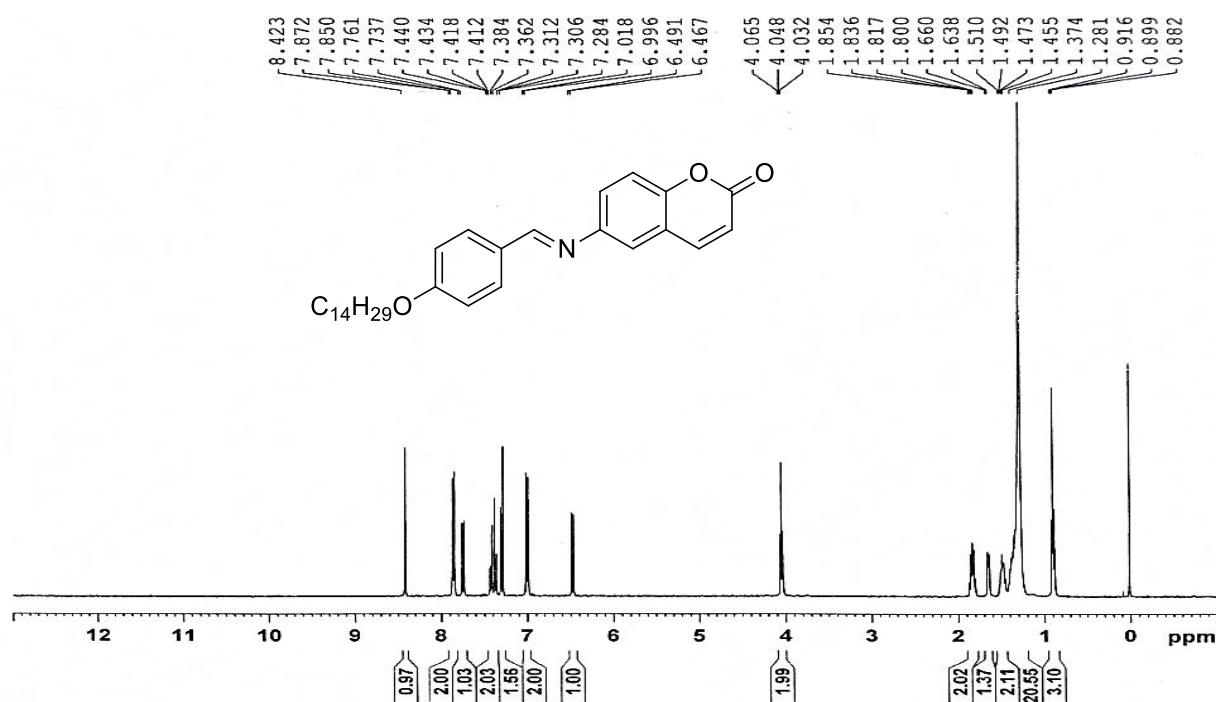


Figure- 5.6.3 $^{13}\text{C-NMR}$ of (E)-6-((4-(dodecyloxy)benzylidene)amino)-2H-chromen-2-one (10e)

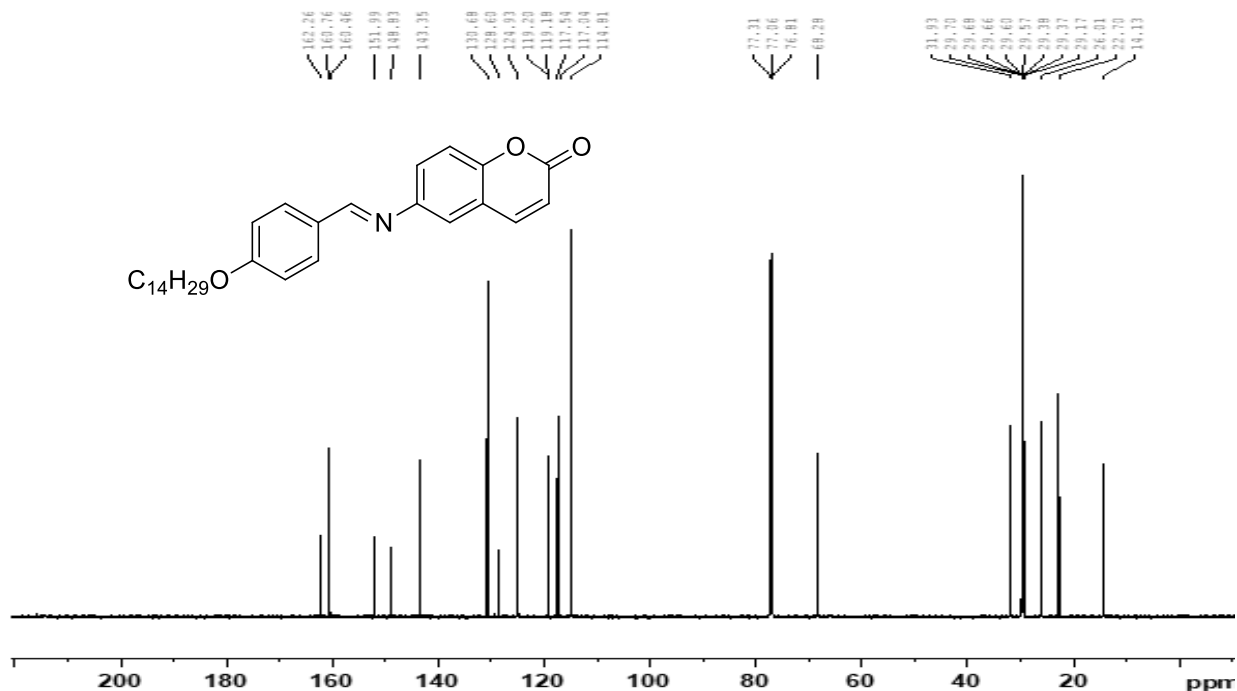


Figure- 5.7.1 IR of (E)-6-((4-(hexadecyloxy)benzylidene)amino)-2H-chromen-2-one (10f)

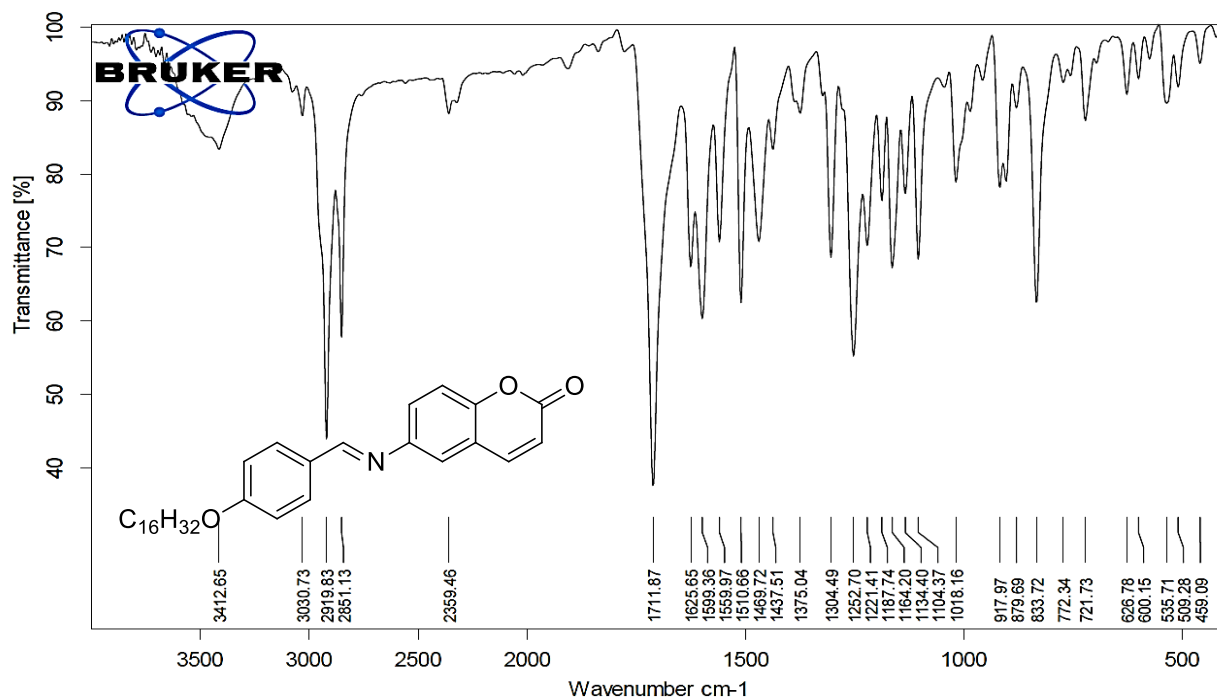
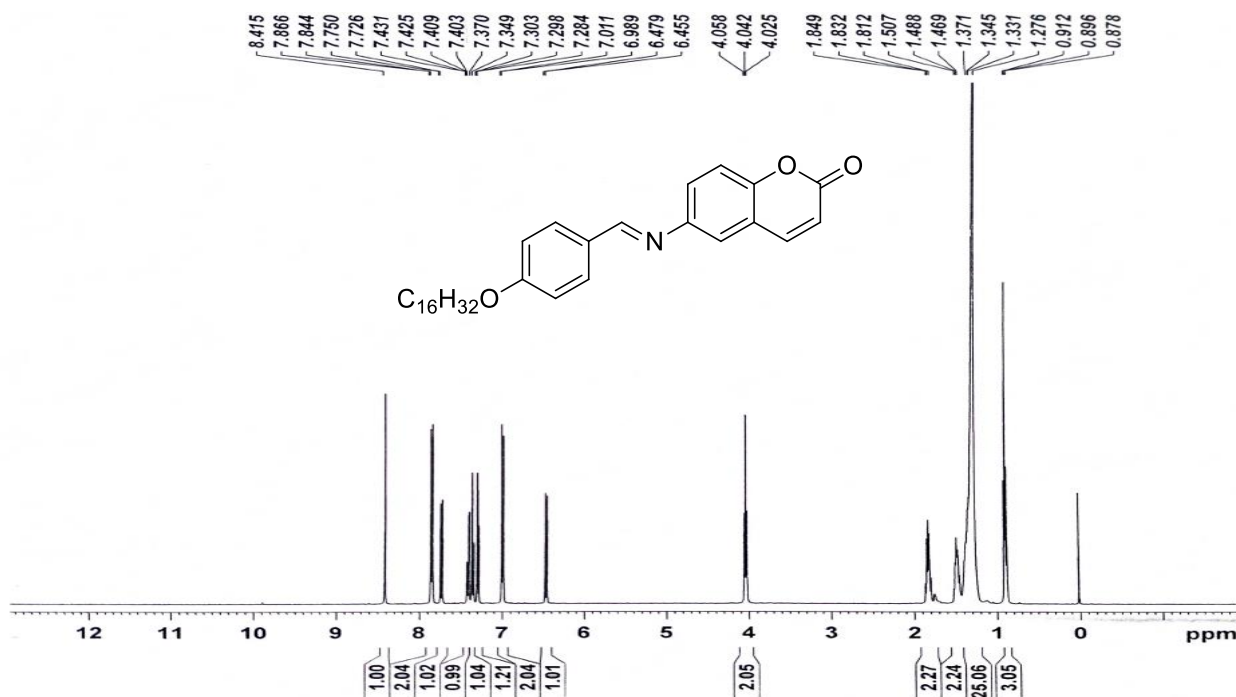
Figure- 5.7.2 ¹H-NMR of (E)-6-((4-(hexadecyloxy)benzylidene)amino)-2H-chromen-2-one (10f)

Figure- 5.7.3 ^{13}C -NMR of (E)-6-((4-(hexadecyloxy)benzylidene)amino)-2H-chromen-2-one (10f)

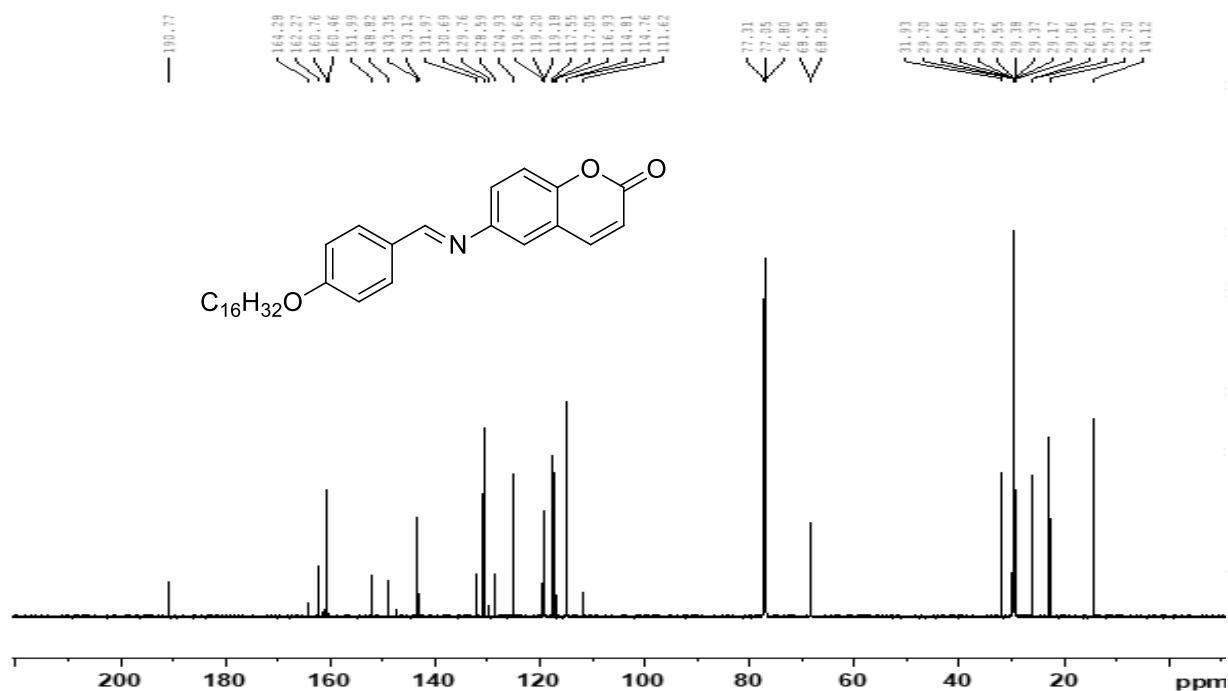


Figure- 5.7.4 Mass of (E)-6-((4-(hexadecyloxy)benzylidene)amino)-2H-chromen-2-one (10f) M+H peak at 489.46

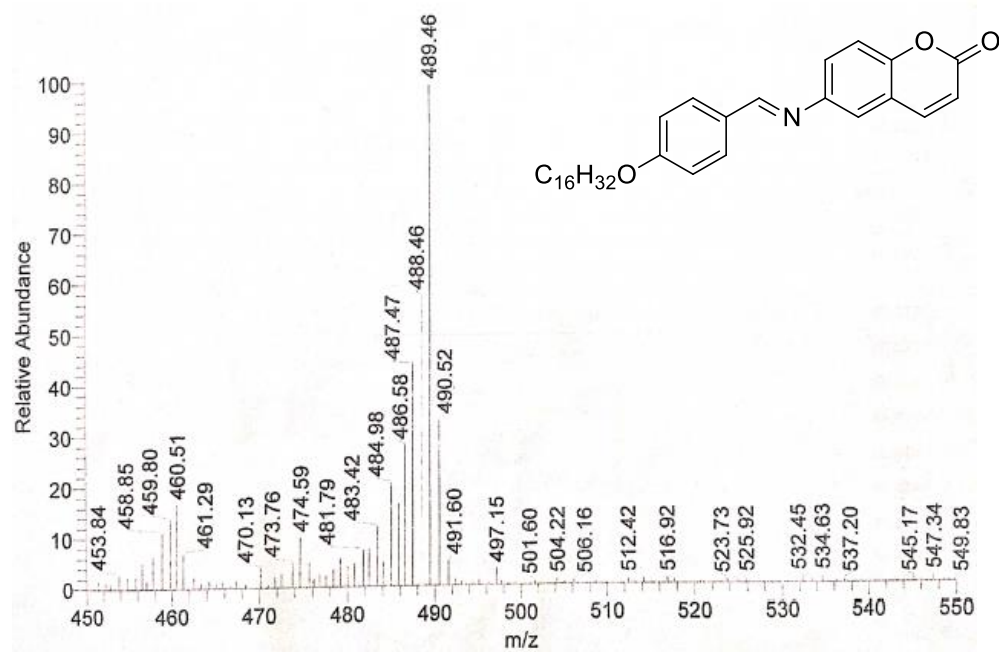


Figure- 5.8.1 IR of (E)-6-((4-(octadecyloxy)benzylidene)amino)-2H-chromen-2-one (10g)

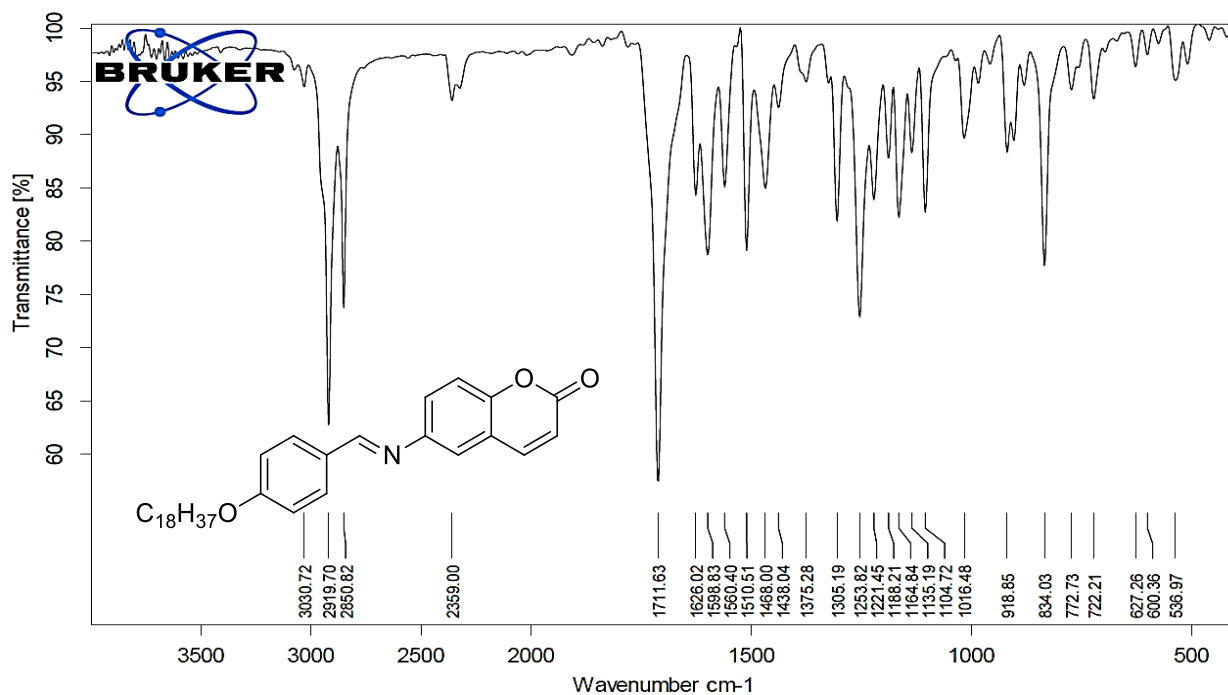
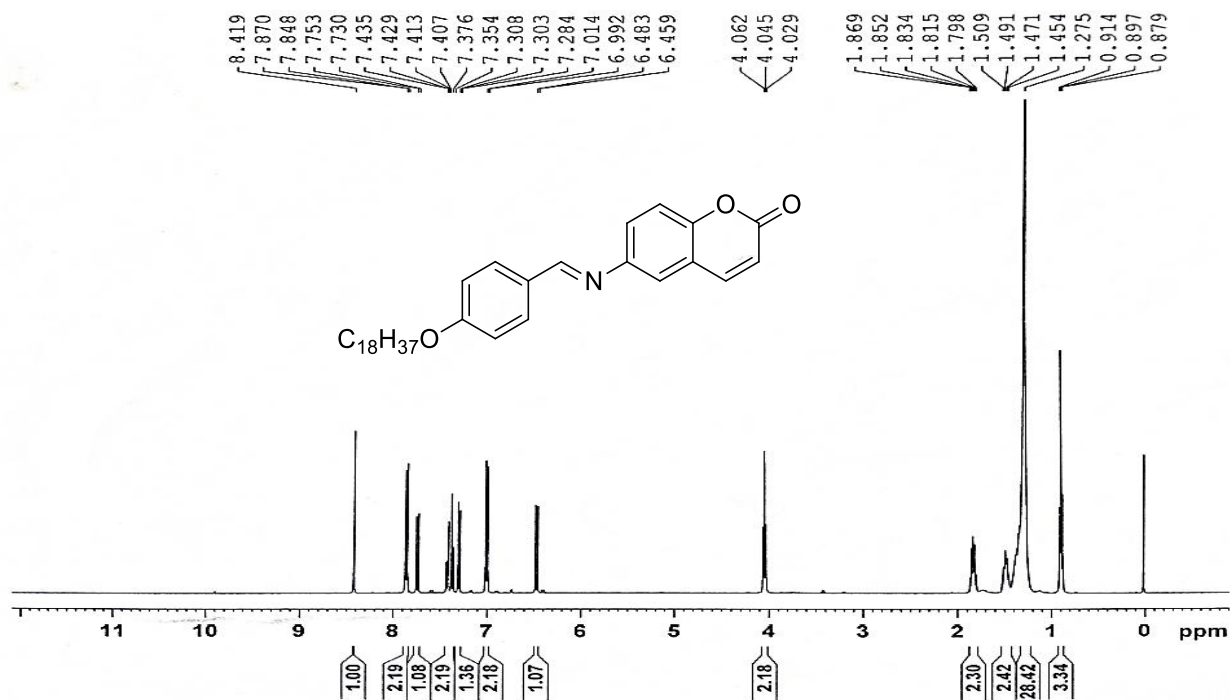
Figure- 5.8.2 ¹H-NMR of (E)-6-((4-(octadecyloxy)benzylidene)amino)-2H-chromen-2-one (10g)

Figure- 5.8.3 ^{13}C -NMR of (E)-6-((4-(octadecyloxy)benzylidene)amino)-2H-chromen-2-one (10g)

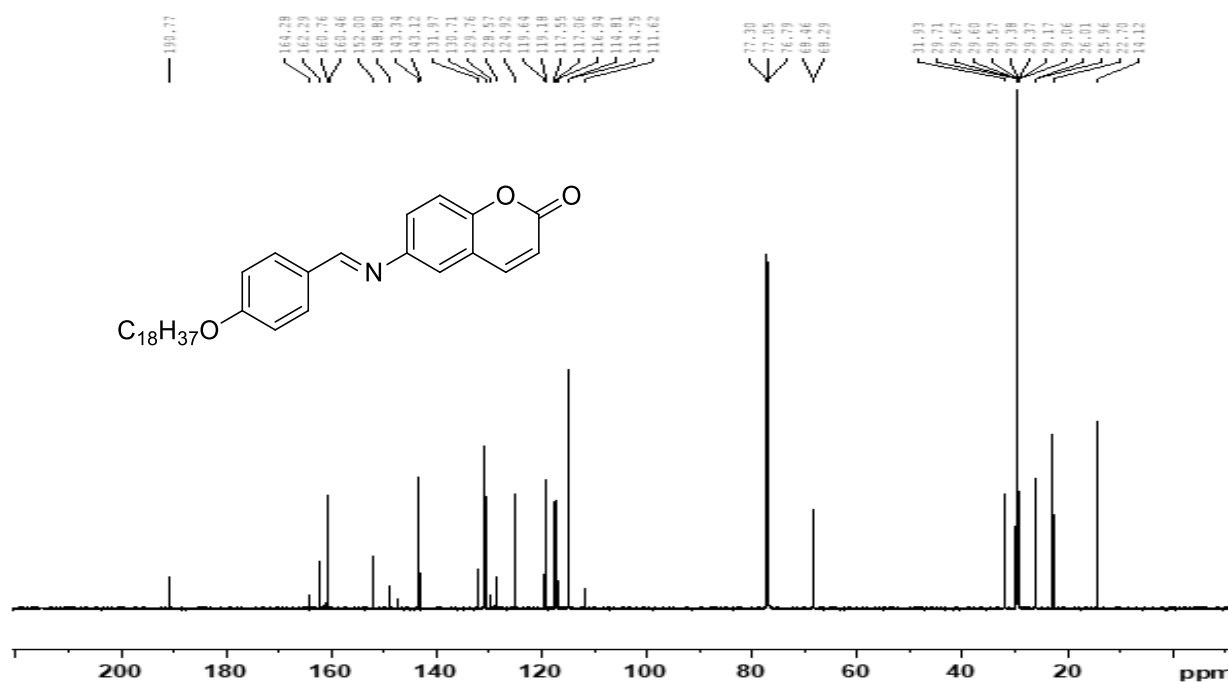


Figure- 5.8.4. Mass of (E)-6-((4-(octadecyloxy)benzylidene)amino)-2H-chromen-2-one (10g) M+H peak at 518.18

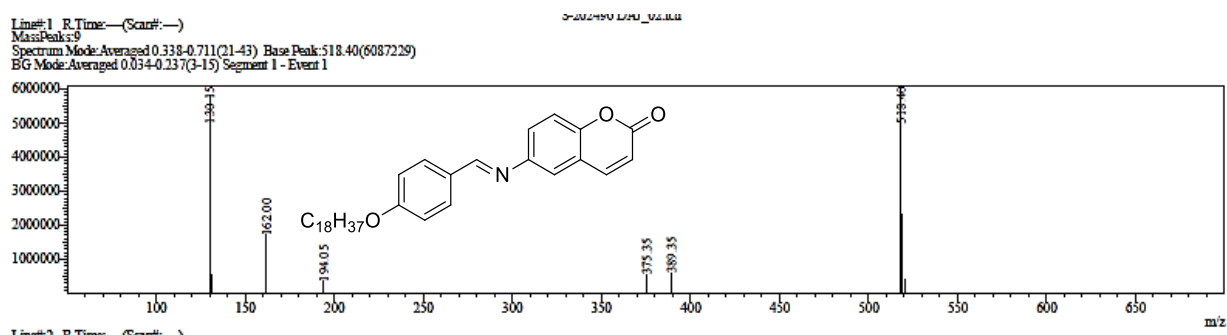


Figure- 5.9.1 IR of (E)-4-(((2-oxo-2H-chromen-6-yl)imino)methyl)phenyl 4-(butoxy)benzoate (**12a**)

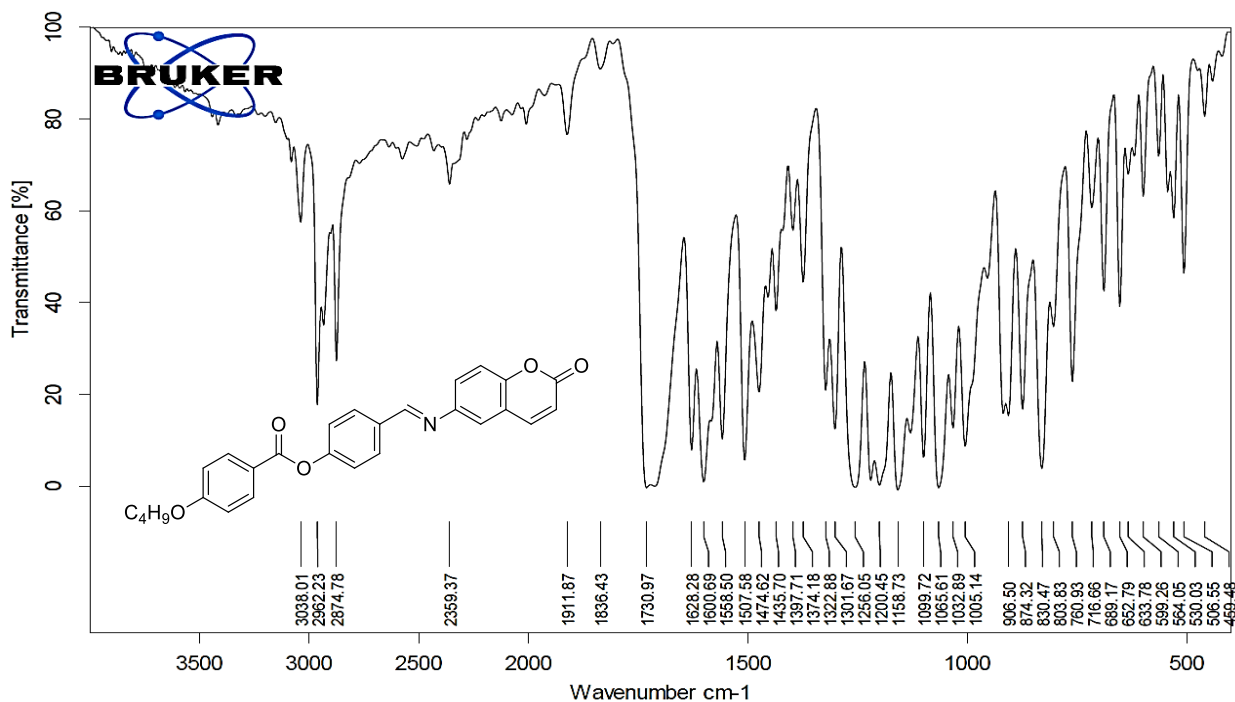


Figure- 5.9.2 $^1\text{H-NMR}$ of (E)-4-(((2-oxo-2H-chromen-6-yl)imino)methyl)phenyl 4-(butoxy)benzoate (**12a**)

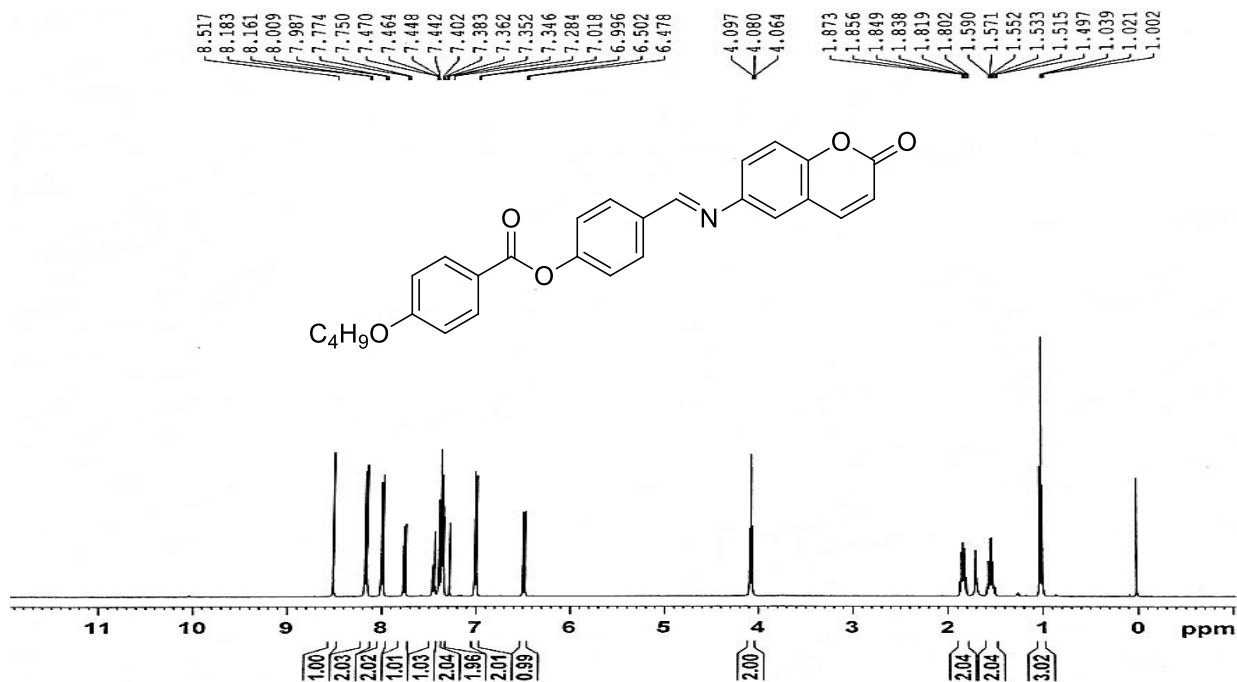


Figure- 5.10.1 IR of (E)-4-(((2-oxo-2H-chromen-6-yl)imino)methyl)phenyl 4-(hexyloxy) benzoate (**12b**)

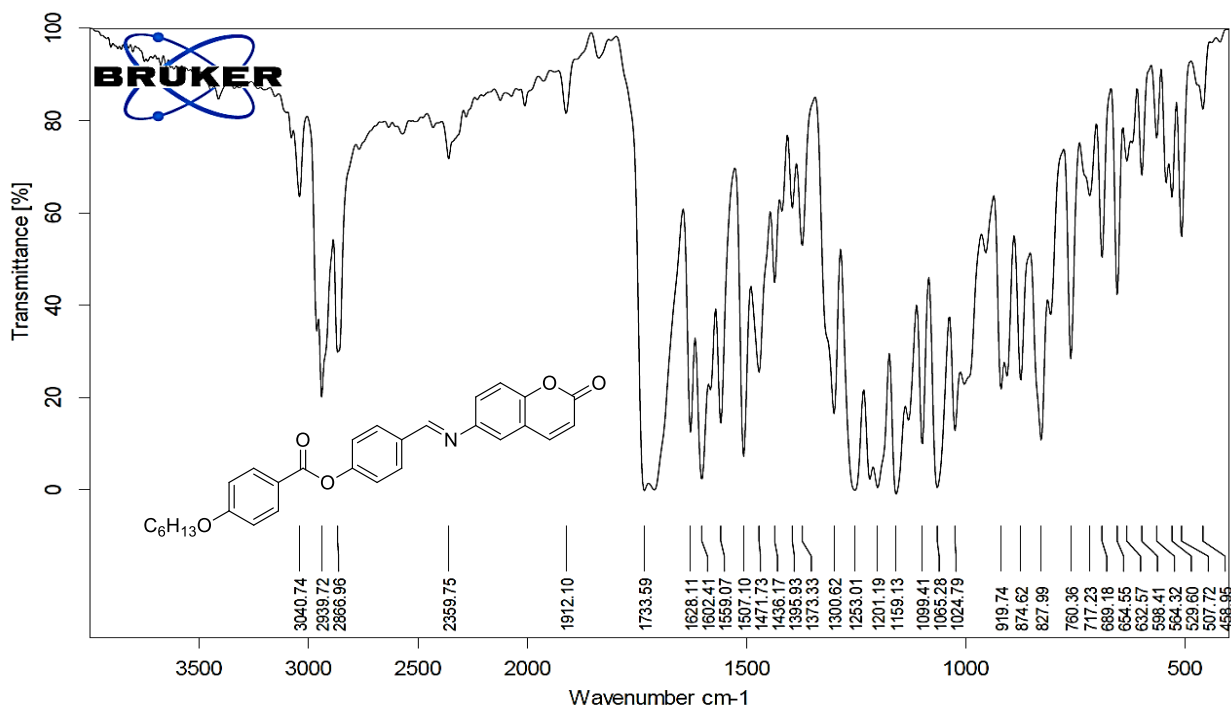


Figure- 5.10.2 $^1\text{H-NMR}$ of (E)-4-(((2-oxo-2H-chromen-6-yl)imino)methyl)phenyl 4-(hexyloxy) benzoate (**12b**)

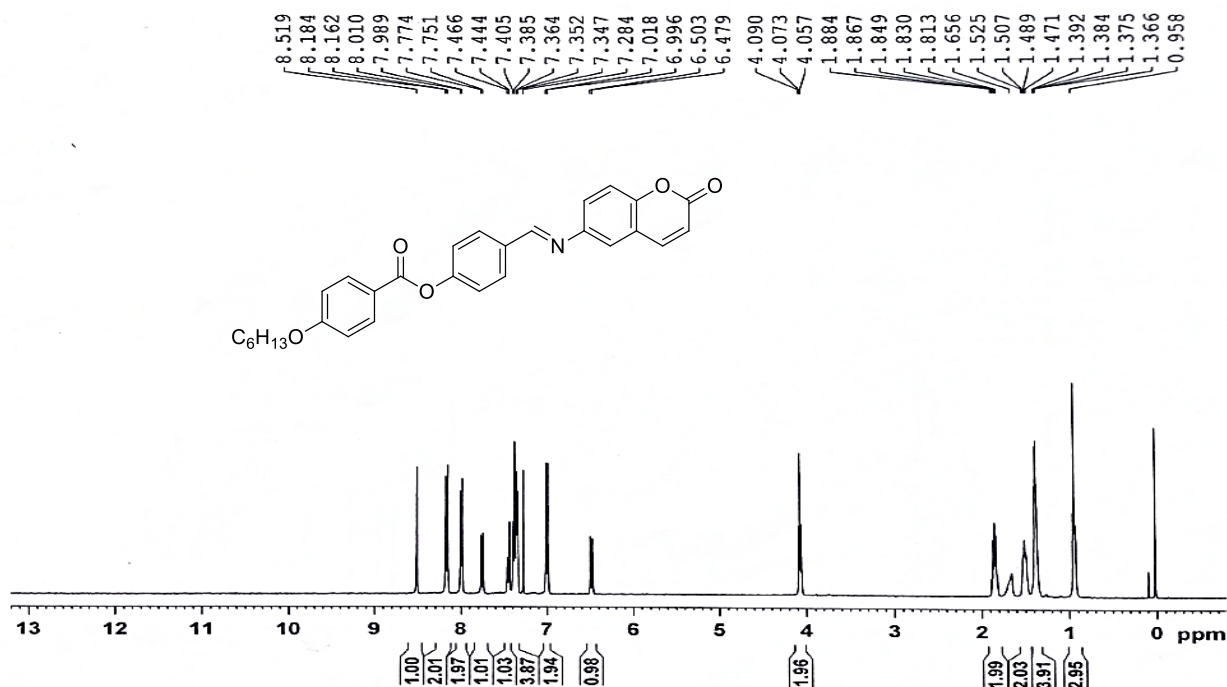


Figure- 5.10.3 ^{13}C -NMR of (E)-4-(((2-oxo-2H-chromen-6-yl)imino)methyl)phenyl 4-(hexyloxy) benzoate (**12b**)

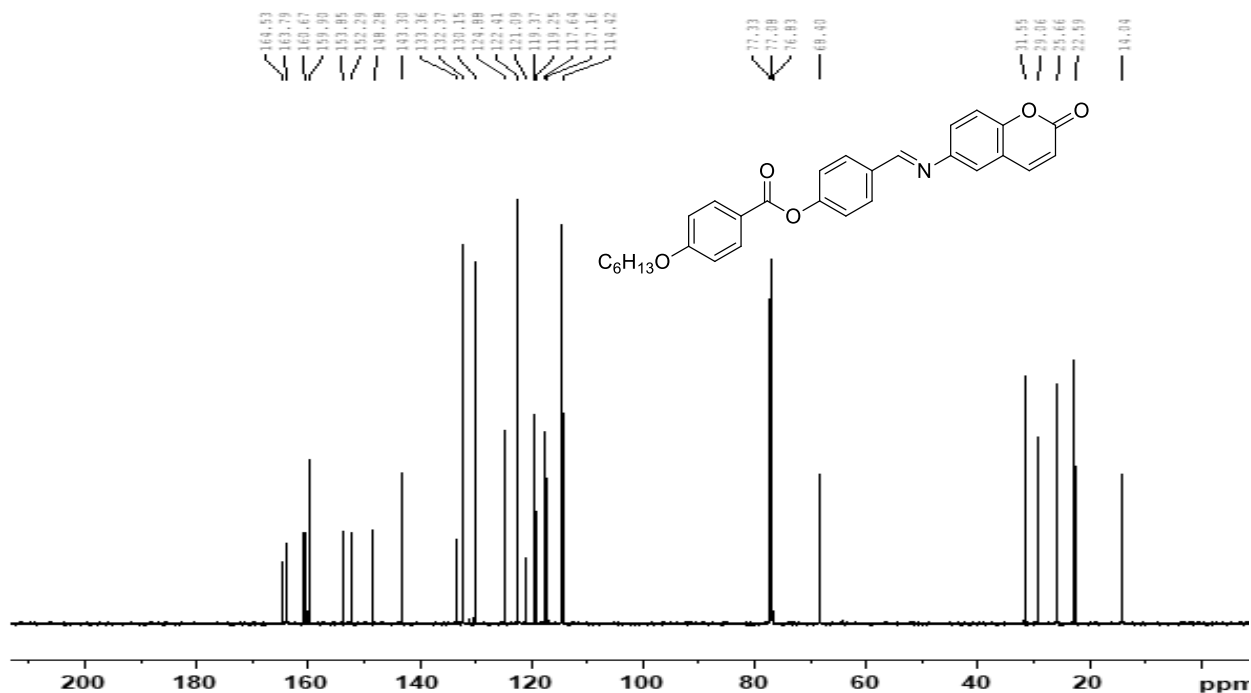


Figure- 5.11.1 IR of (E)-4-(((2-oxo-2H-chromen-6-yl)imino)methyl)phenyl 4-(octyloxy)benzoate (**12c**)

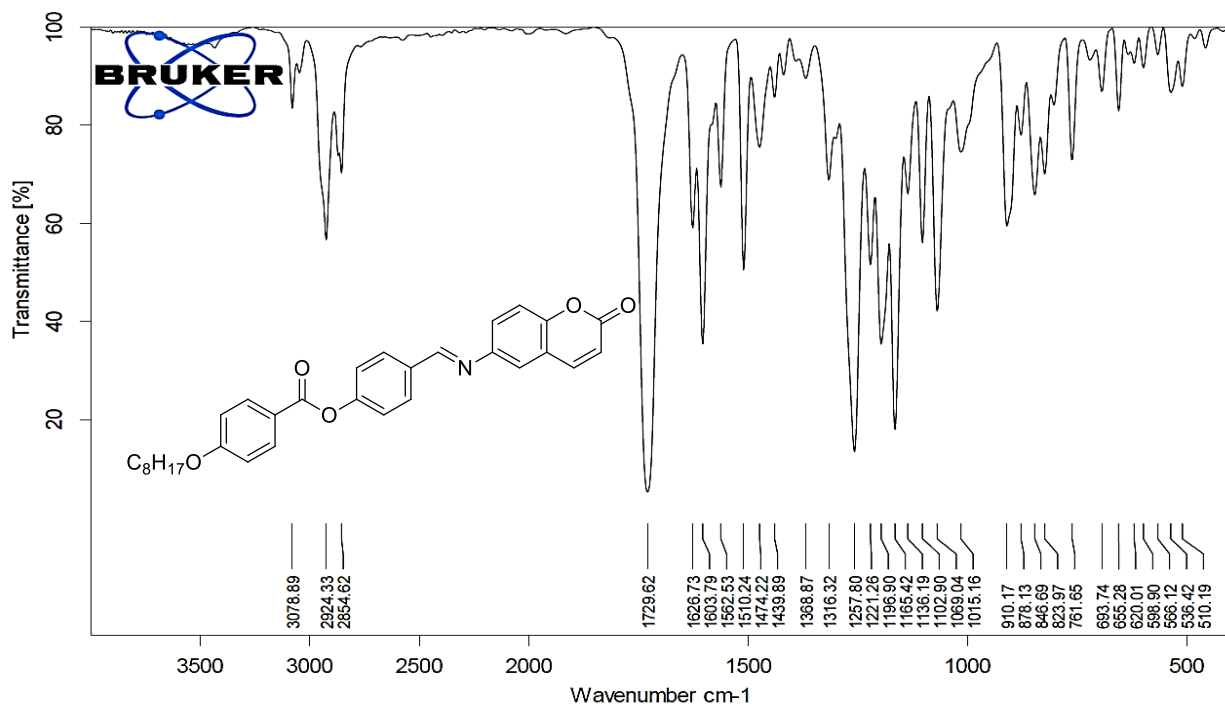


Figure- 5.12.2 $^1\text{H-NMR}$ of (E)-4-(((2-oxo-2H-chromen-6-yl)imino)methyl)phenyl 4-(octyloxy) benzoate (**12c**)

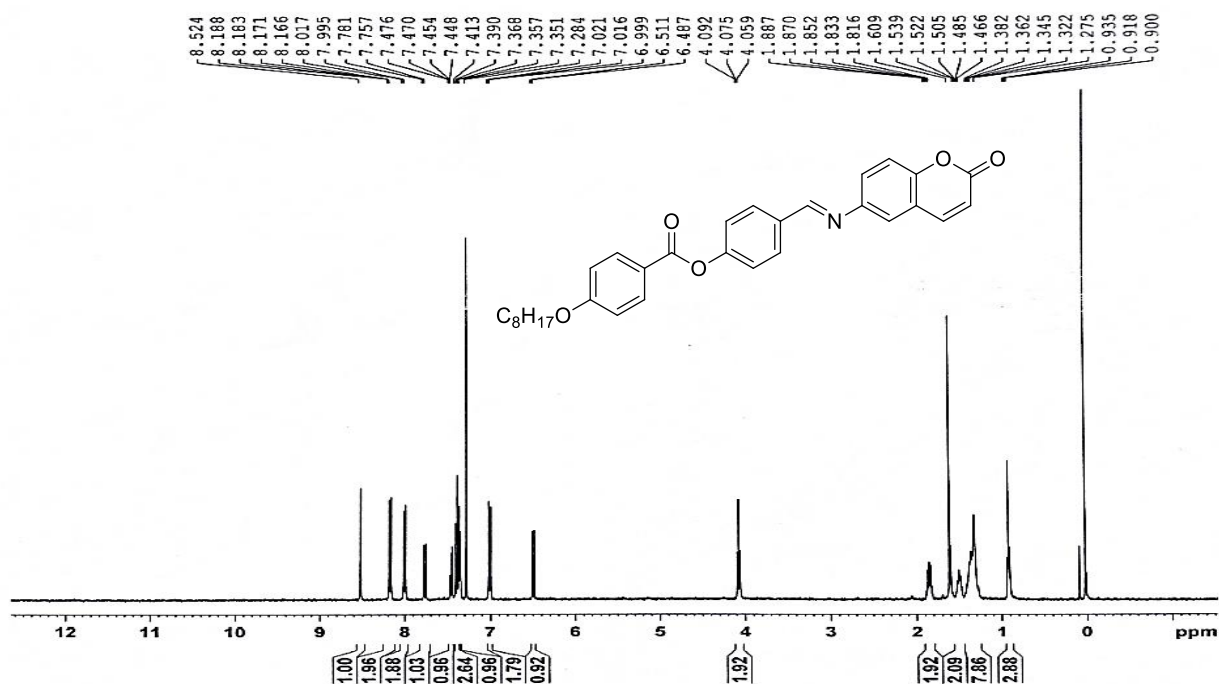


Figure- 5.11.3 $^{13}\text{C-NMR}$ of (E)-4-(((2-oxo-2H-chromen-6-yl)imino)methyl)phenyl 4-(octyloxy) benzoate (**12c**)

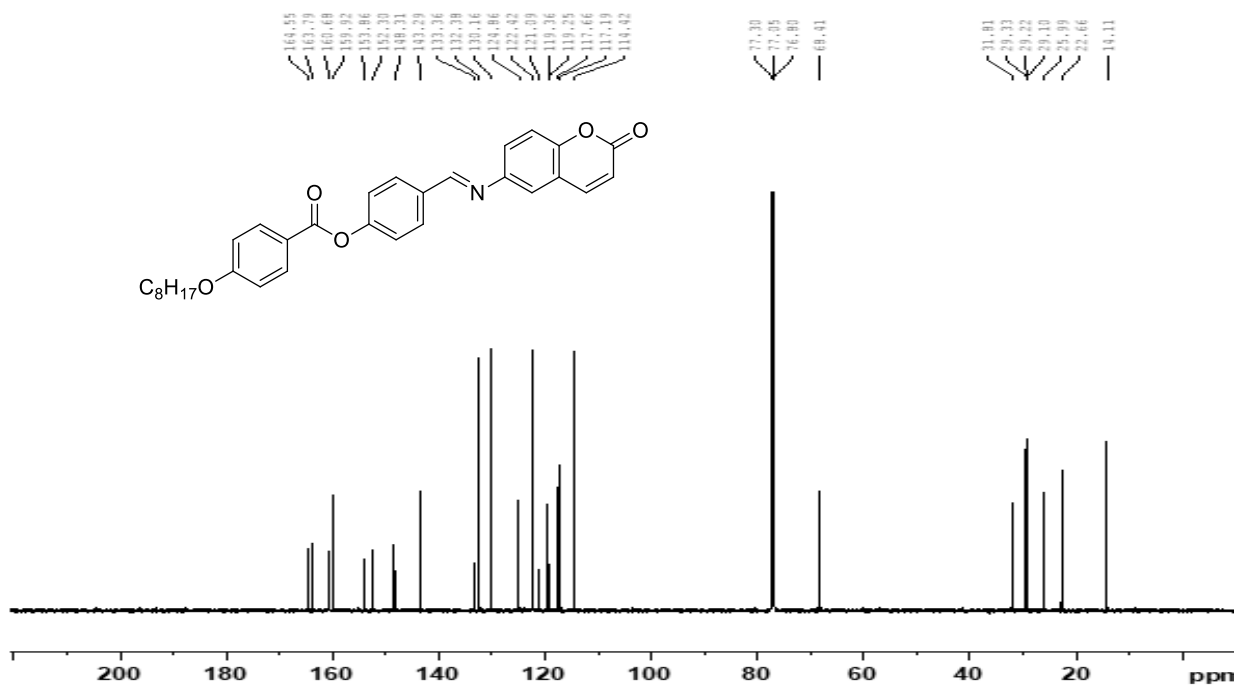


Figure- 5.11.4 Mass of (E)-4-(((2-oxo-2H-chromen-6-yl)imino)methyl)phenyl 4-(octyloxy) benzoate (**12c**) M⁺ peak at 497.63

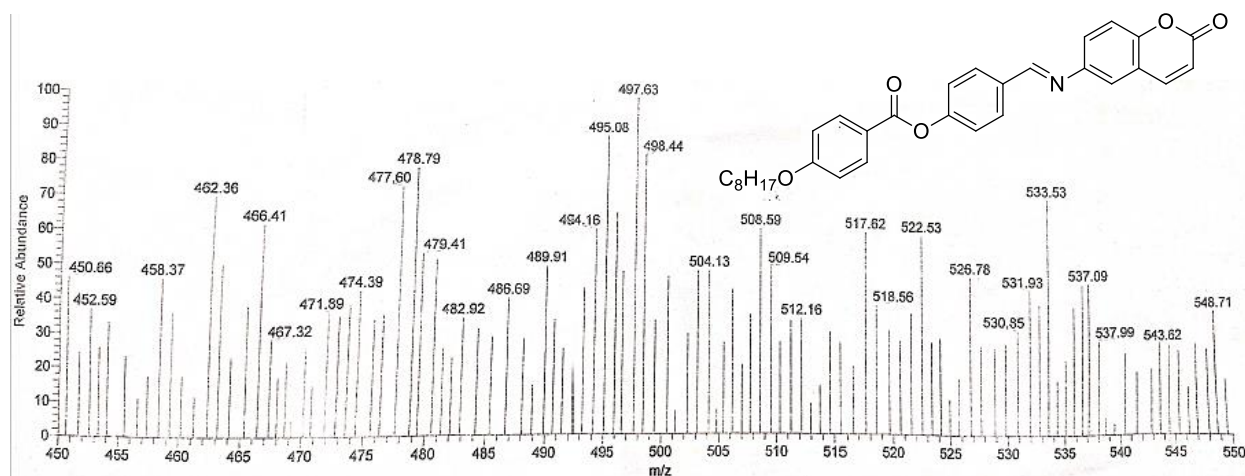


Figure- 5.12.1 IR of (E)-4-(((2-oxo-2H-chromen-6-yl)imino)methyl)phenyl 4-(decyloxy) benzoate (**12d**)

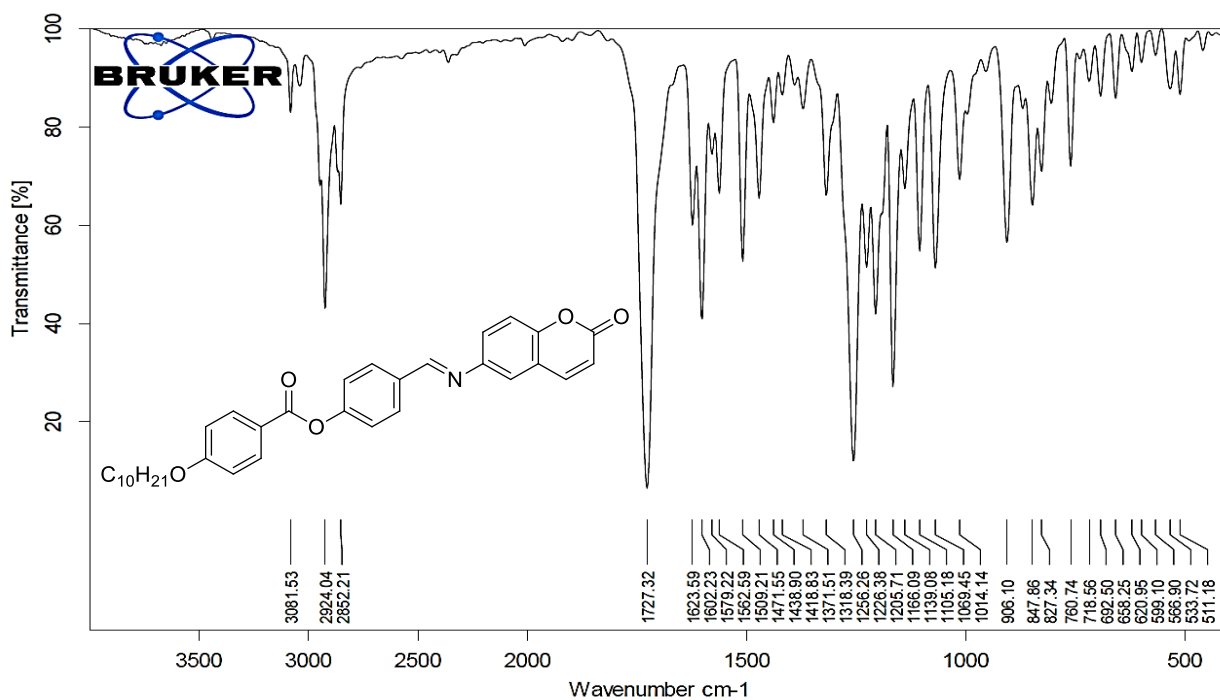


Figure- 5.12.2 $^1\text{H-NMR}$ of (E)-4-(((2-oxo-2H-chromen-6-yl)imino)methyl)phenyl 4-(decyloxy) benzoate (**12d**)

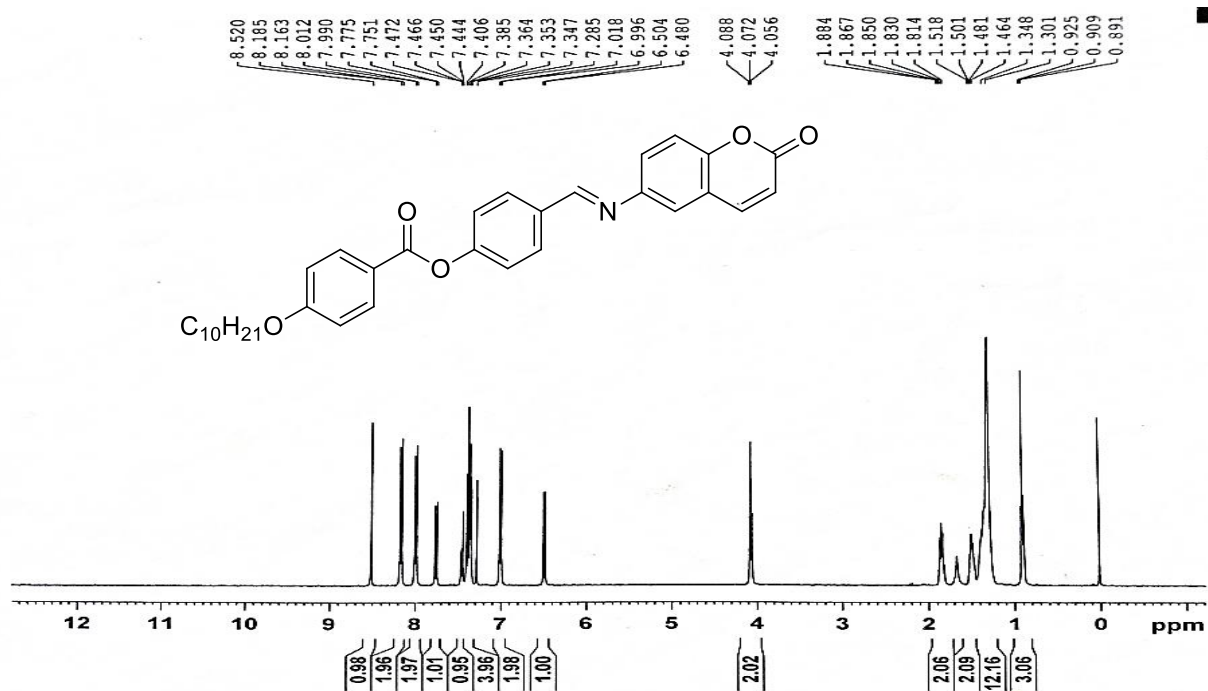


Figure- 5.12.3 $^{13}\text{C-NMR}$ of (E)-4-(((2-oxo-2H-chromen-6-yl)imino)methyl)phenyl 4-(decyloxy) benzoate (**12d**)

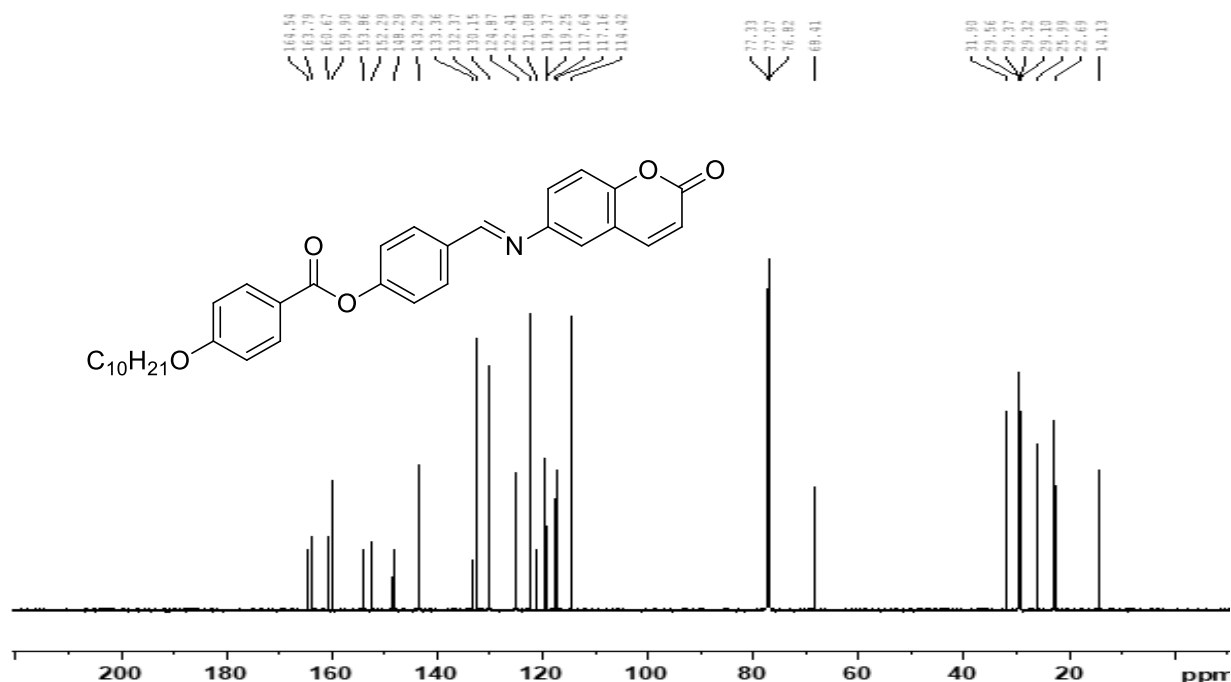


Figure- 5.13.1 IR of (E)-4-(((2-oxo-2H-chromen-6-yl)imino)methyl)phenyl 4-(dodecyloxy)benzoate (**12e**)

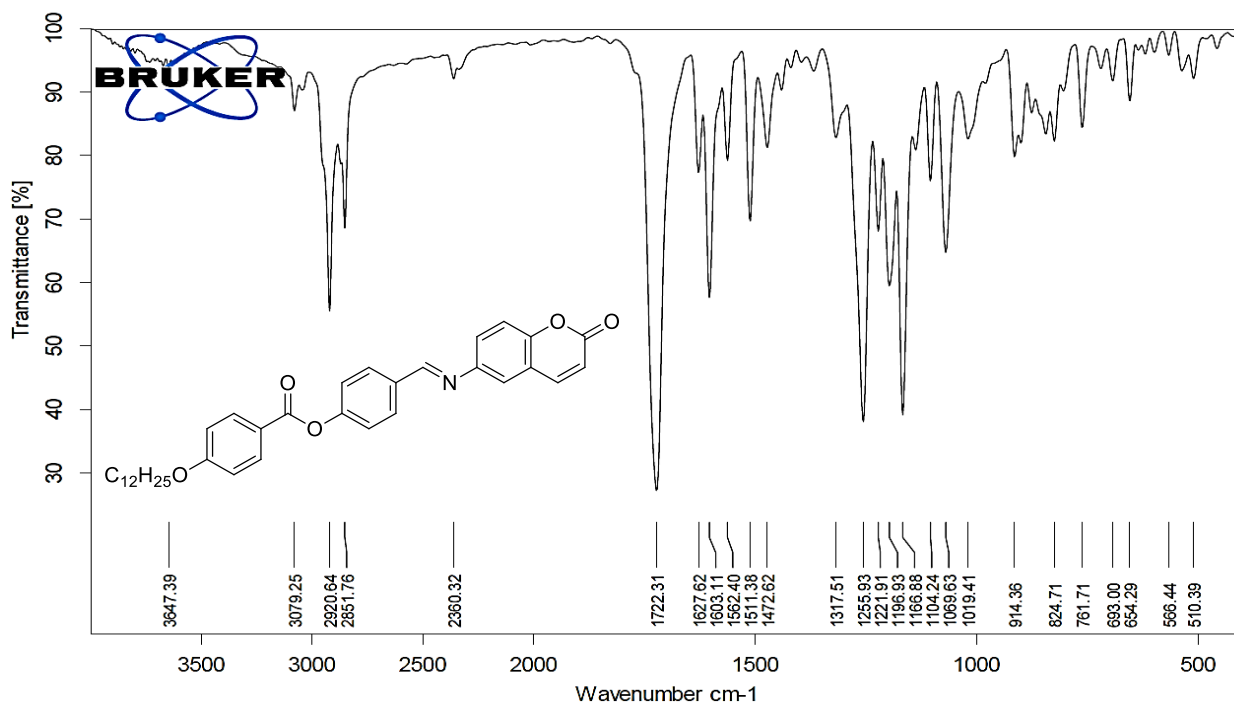


Figure- 5.13.2 ¹H-NMR of (E)-4-(((2-oxo-2H-chromen-6-yl)imino)methyl) phenyl 4-(dodecyloxy)benzoate (**12e**)

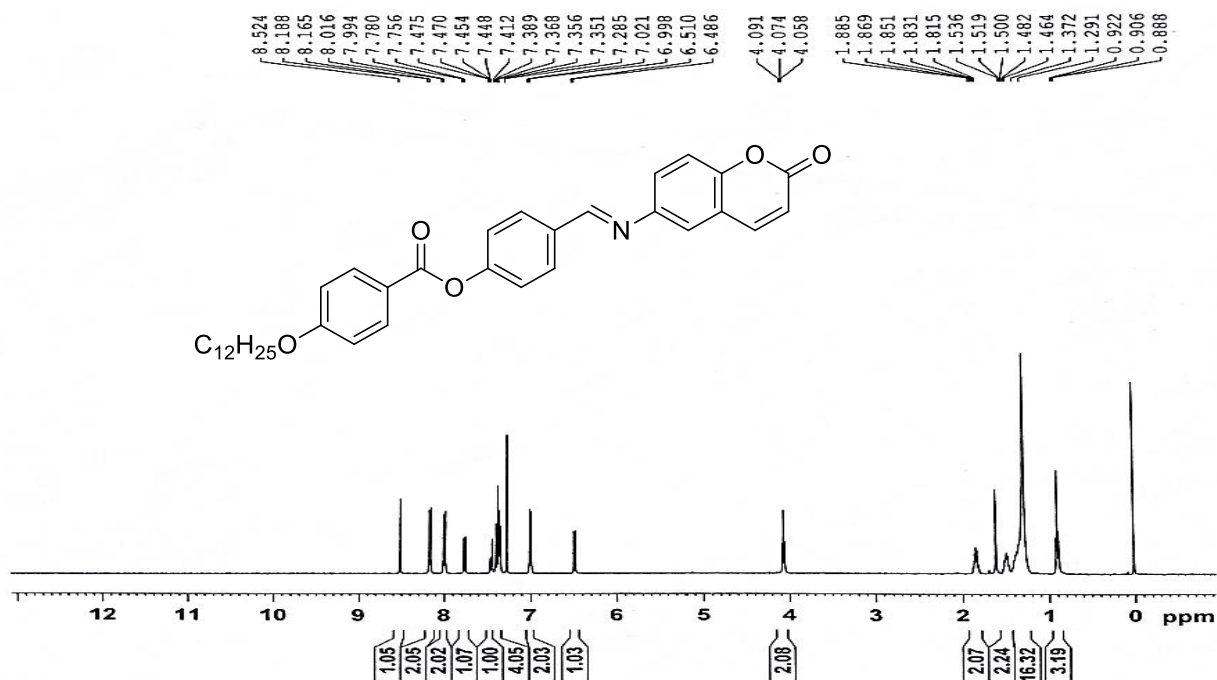


Figure- 5.13.3 ^{13}C -NMR of (E)-4-(((2-oxo-2H-chromen-6-yl)imino)methyl)phenyl 4-(dodecyloxy) benzoate (**12e**)

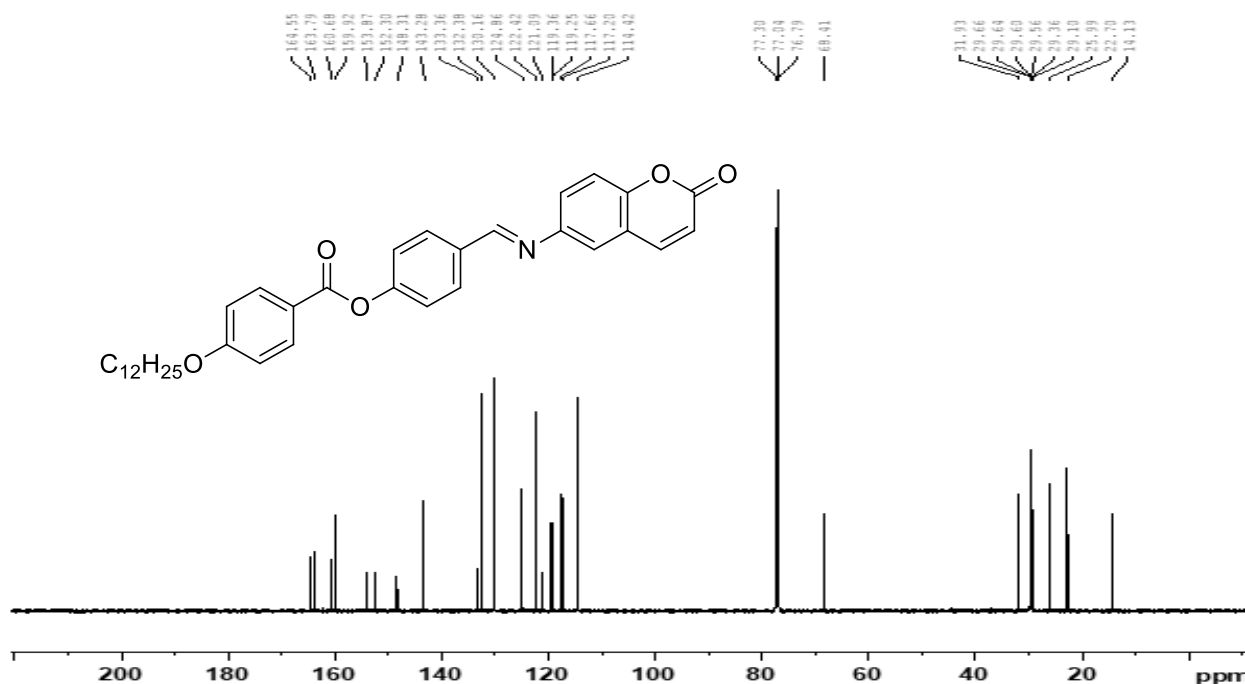


Figure- 5.14.1 IR of (E)-4-(((2-oxo-2H-chromen-6-yl)imino)methyl)phenyl 4-(tetradecyloxy) benzoate (**12f**)

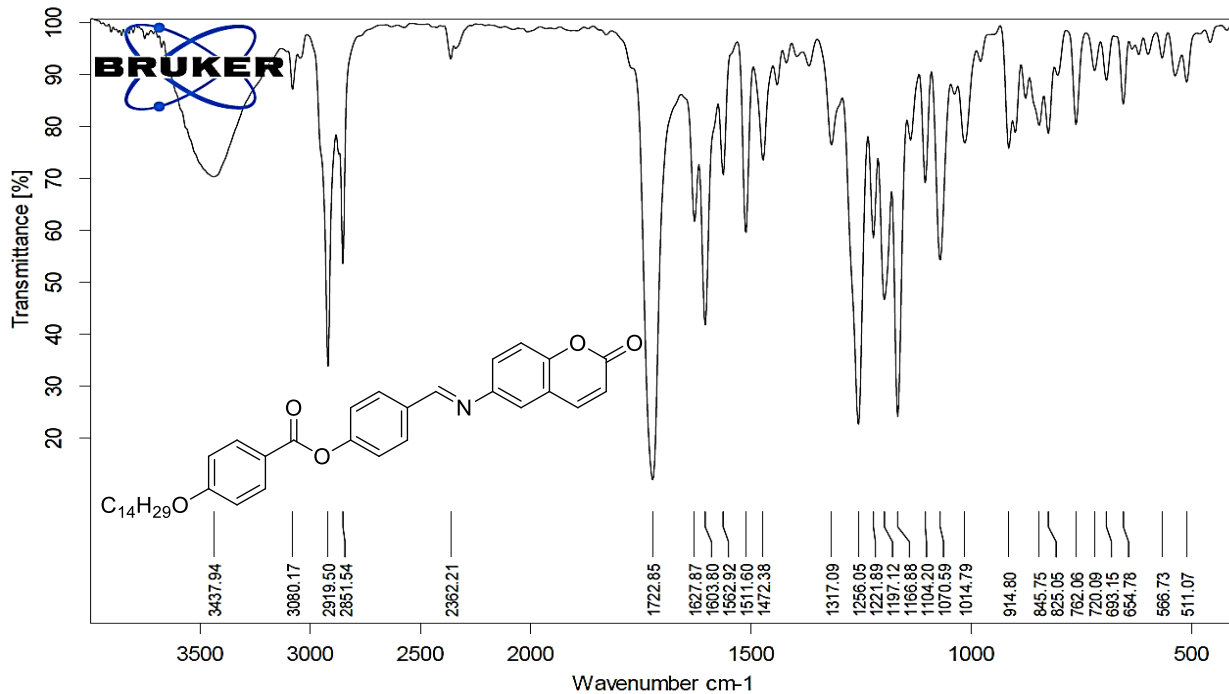


Figure- 5.14.2 $^1\text{H-NMR}$ of (E)-4-(((2-oxo-2H-chromen-6-yl)imino)methyl)phenyl 4-(tetradecyloxy)benzoate (**12f**)



Figure- 5.14.3 $^{13}\text{C-NMR}$ of (E)-4-(((2-oxo-2H-chromen-6-yl)imino)methyl)phenyl 4-(tetradecyloxy)benzoate (**12f**)

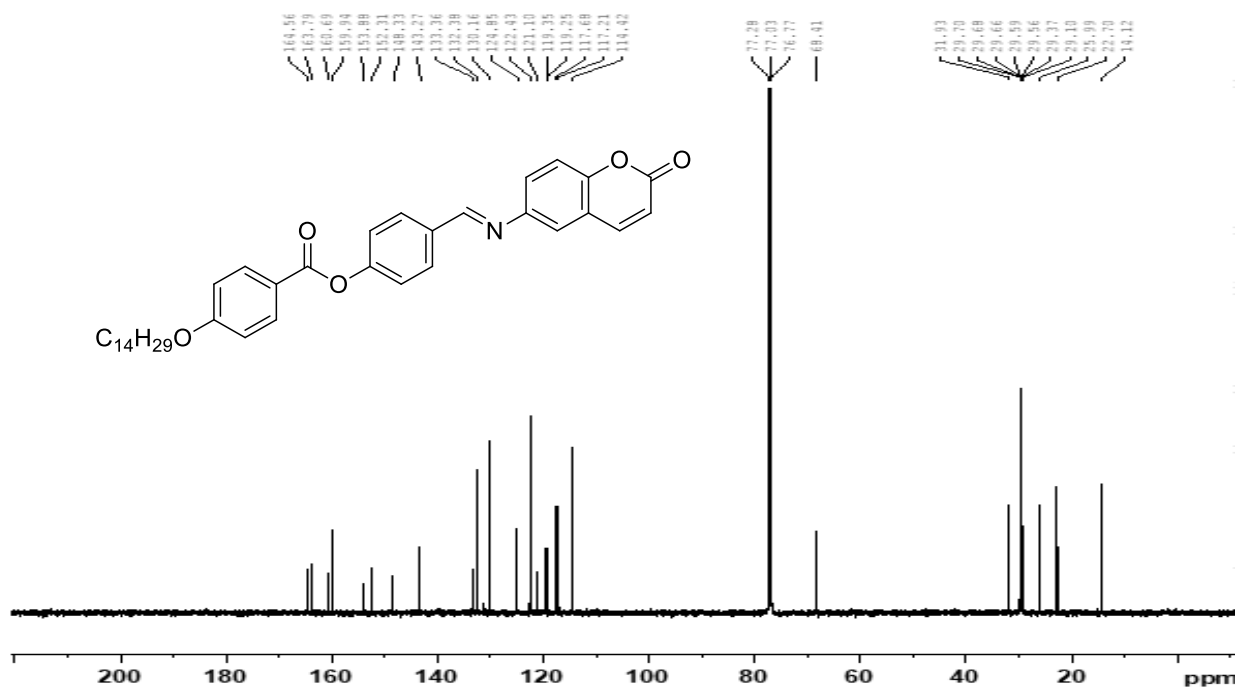


Figure- 5.15.1 IR of (E)-4-(((2-oxo-2H-chromen-6-yl)imino)methyl)phenyl 4-(hexadecyloxy) benzoate (**12g**)

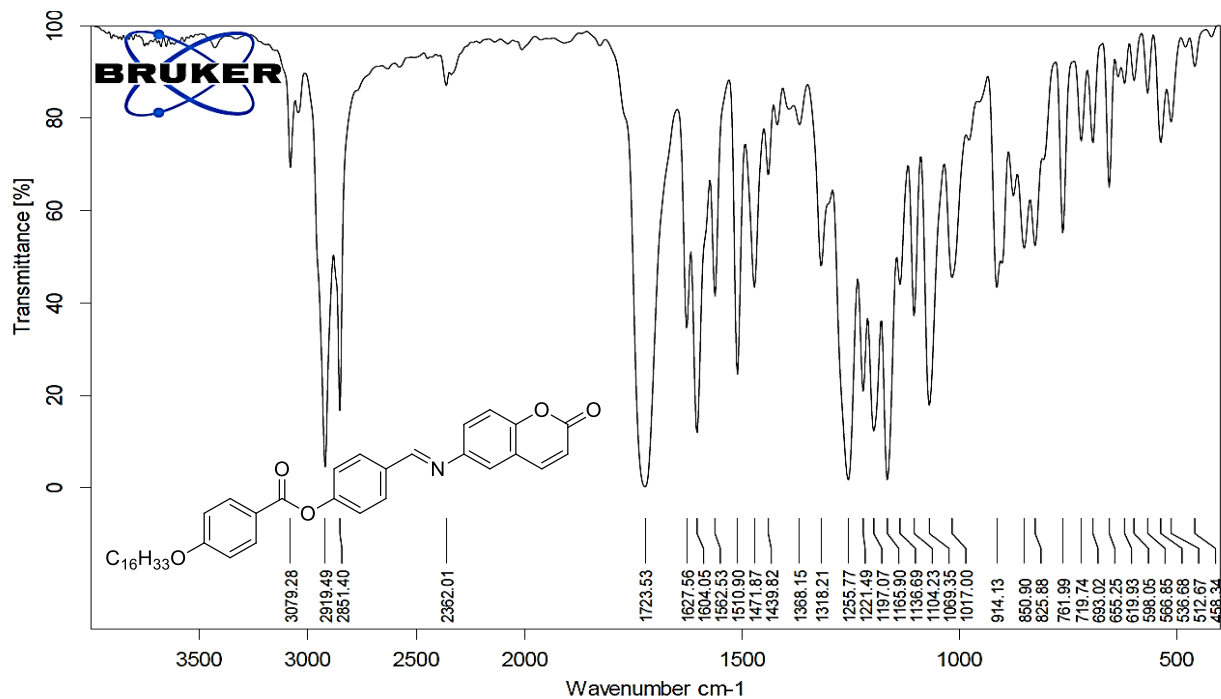


Figure- 5.15.2 $^1\text{H-NMR}$ of (E)-4-(((2-oxo-2H-chromen-6-yl)imino)methyl)phenyl 4-(hexadecyloxy) benzoate (**12g**)

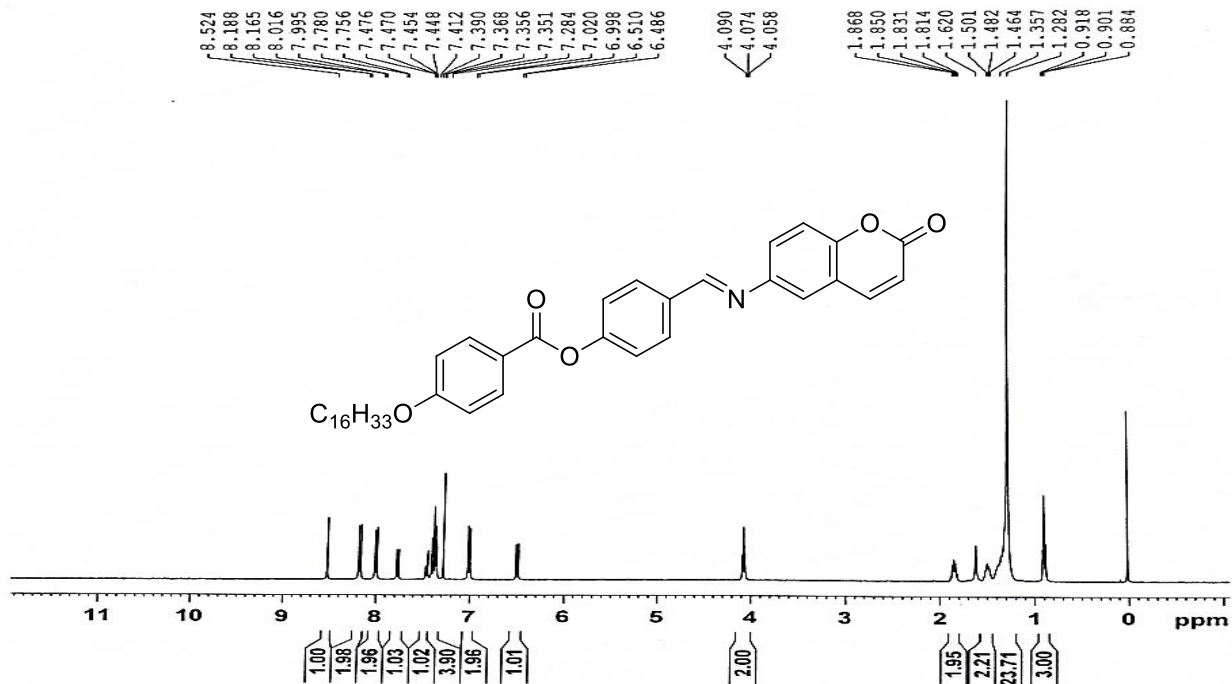


Figure- 5.15.3 ^{13}C -NMR of (E)-4-(((2-oxo-2H-chromen-6-yl)imino)methyl)phenyl 4-(hexadecyloxy) benzoate (**12g**)

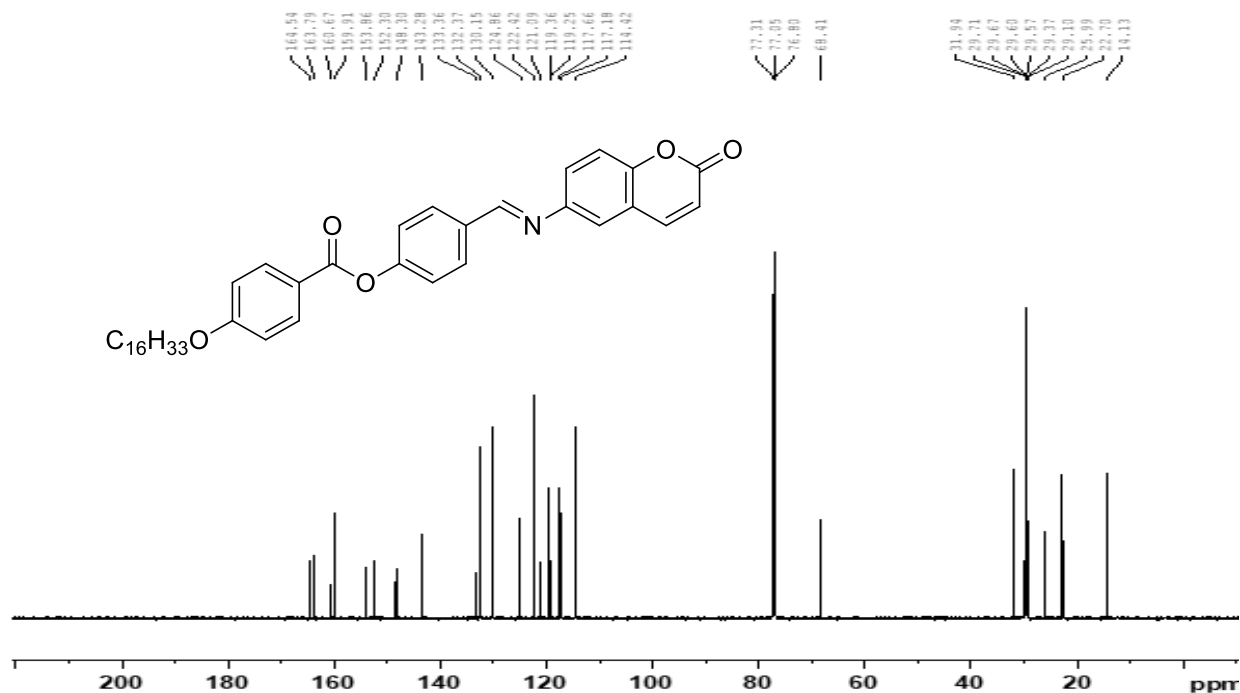


Figure- 5.16.1 IR of (E)-4-(((2-oxo-2H-chromen-6-yl)imino)methyl)phenyl 4-(octadecyloxy) benzoate (**12h**)

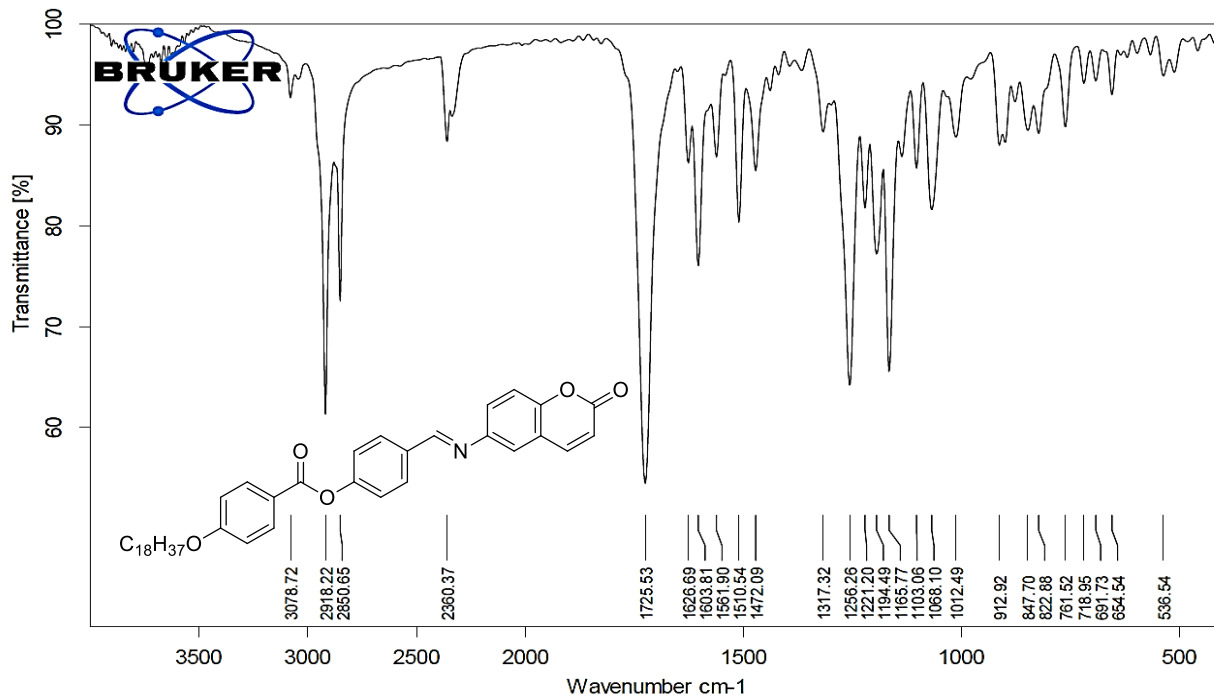
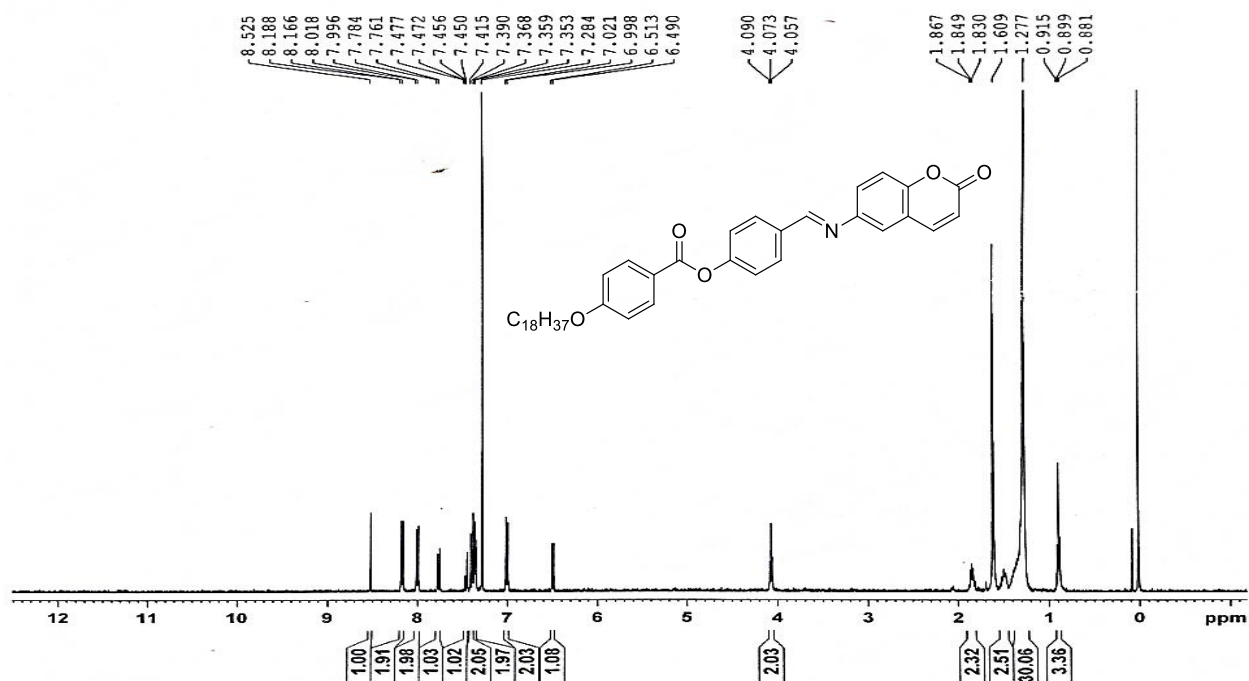


Figure- 5.16.2 $^1\text{H-NMR}$ of (E)-4-(((2-oxo-2H-chromen-6-yl)imino)methyl)phenyl 4-(octadecyloxy) benzoate (**12h**)



5.2.2 Study of mesomorphic properties:

The newly synthesized imine derivatives **10a-h** and **12a-g** were examined using a polarizing optical microscope. In order to identify mesophase texture, POM analysis of compound was performed as thin film sandwich between glass slide and cover at a rate of 10°C/min during the first cooling cycle and the second heating cycle. Additionally, all the compounds were analyzed using differential scanning calorimetry (DSC) during heating and cooling scans at a rate of 10°C/min. The thermograms generated were used to measure temperatures associated with phase transition and change in enthalpy ($\Delta H \text{ KJmol}^{-1}$). While POM analysis produced good mesophase textures and transition temperature along with enthalpy changes were calculated using DSC thermograms for all the examined substances after numerous heating and cooling cycles, are summarized in (Table-5.1).

5.2.2.1 Polarizing optical microscopy (POM) study:

Schiff base derivatives **10a-g** in which imine derivative with lower alkyloxy chain length did not showed any mesogenic behavior during heating and cooling cycle The compound **10b** with octyloxy chain length showed monotropic mesophase of nematic type (Fig-5.17) with the characteristic Schlieren texture and changed to crystalline solid on further cooling. When octyloxy chain was replaced by decyloxy chain compound **10c** exhibited enantiotropic mesophase, on heating compound **10c** crystalline solid changes to smectic A mesophase further on heating it converts to isotropic liquid while on cooling cycle isotropic liquid transformed to smectic A mesophase and again further cooling transform to crystalline solid. Compounds **10d-g** with higher alkyloxy chain length (n= 12-18) exhibited enantiotropic stable smectic A focal conic mesophase during the both heating and cooling cycle.

Schiff bases with n alkoxy ester compounds **12a-h** have been analyzed for their mesomorphic properties. When lower alkyloxy chain changed to higher chain length compound **12d** with decyloxy chain length on heating cycle exhibited smectic A mesophase (Fig-5.17) further on heating smectic A changed to nematic droplet texture which converted to isotropic liquid on further heating, while it exhibited nematic first and then smectic A mesophase on cooling. By varied higher alkyloxy chain length n=12 to 18 in compounds **12e-h** exhibited enantiotropic smectic A mesophase with very good thermal stability as well as broad temperature range.

Table 5.1: Phase assignments, transition temperature °C of compounds **10a-g** and **12a-h** as determined by POM and DSC

Compd	n	2 nd heating process ^a Temp °C (ΔH KJmol ⁻¹)	1 st cooling process ^a Temp °C (ΔH KJmol ⁻¹)
10a	6	Cr 148.0(-21.64) Iso	I 92.2(23.15) Cr
10b	8	Cr 124.0(-51.12) I	I 108.4(0.55) N 95.3 (46.25) Cr
10c	10	Cr ¹ 97.70(-8.51)Cr ² 113.1(-20.63) SmA 122.78(-1.19) I	I 116.08(1.72) SmA 94.1(21.35) Cr
10d	12	Cr 117.8(-17.90) SmA 132.2(-2.63) I	I 129.6(1.53) SmA 109 (18.01) Cr
10e	14	Cr 113.3(-15.34) SmA 137.8(-3.45) I	I 132.8(3.17)SmA 101.7(24.06)Cr
10f	16	Cr 108.0(-44.98.01) SmA 134.2(-3.31)I	I 127.0(3.11) SmA 94.8(24.47) Cr
10g	18	Cr 114.7(-39.27) SmA 139.9(-1.3) I	I 116.1(1.8) SmA 93.21(19.16) Cr
12a	4	Cr 179.1(-31.69) N 315.0(-0.42) I	I 289.4(0.57) N 115.0(9.5) Cr
12b	6	Cr 156.8(-33.01)N 292.2(-0.65) I	I 279.8(0.60)N 127.7(20.18) Cr
12c	8	Cr 155.9(-24.05)N 274.0(-0.30) I	I 262.1(0.51)N 125.0(20.01) Cr
12d	10	Cr 133.7(-44.10) SmA 248.0N* 256.1(-4.42) I	I 253.0N* 239.9(4.44) SmA 92.1 (31.00) Cr
12e	12	Cr 135.2(-33.19)SmA 255.7(-3.55) I	I 243.5(3.05)SmA 104.4(14.56)Cr
12f	14	Cr 131.7(-34.72)SmA 253.8(-4.31) I	I 243.4(1.72)SmA 109.8(22.17) Cr
12g	16	Cr 137.4(-28.65)SmA 253.6(-3.73) I	I 246.3(2.64) SmA 122.9(23.58) Cr
12h	18	Cr 113.1(-35.24) SmA 249.3(-2.05) I	I 232.7(2.68) SmA 105.3(26.19) Cr

^aCr = Crystal, Iso = isotropic liquid state, N = nematic phase, SmA= smectic A phase, I = isotropic state, *The phase transitions of the compounds were studied under POM only. The enthalpy values are enclosed in brackets

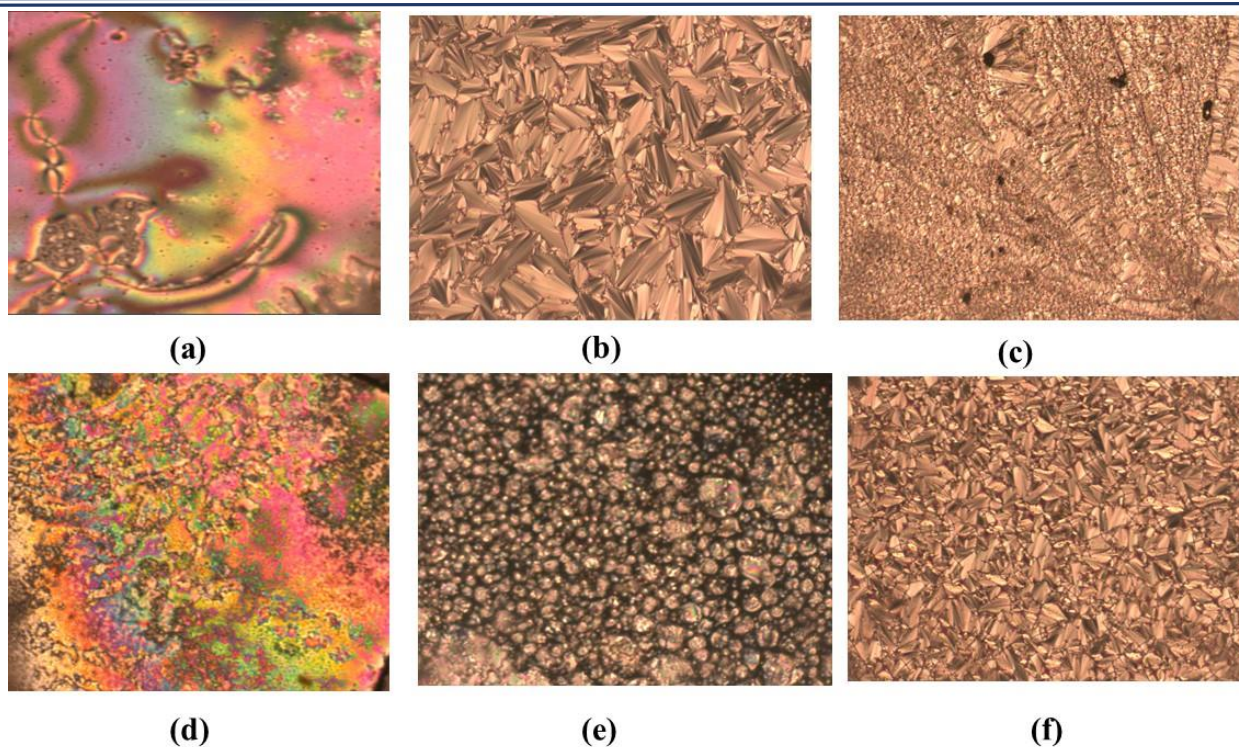


Figure- 5.17 POM textures of coumarin Schiff base mesogens (a) Nematic schlieren texture of **10b** upon cooling at 108.41°C; (b) SmA focal conic fan texture of **10d** upon heating at 132°C; (c) SmA transition of **10e** on cooling 132.8 (d) Nematic marble texture of **12d** on heating at 256.1°C; (e) Nematic droplet texture of **12d** on cooling at 175.4 °C; (f) SmA transition of **10e** on further cooling at 243.5°C

5.2.2.2 Differential scanning calorimetry study (DSC):

In order to measure exact transition temperature and associated energy, differential scanning calorimetry analysis is very important. All the compounds **10a-g** and **12a-h** were studied for DSC thermograms at a rate of 10°C min⁻¹ for both heating-cooling cycle from ambient temperature to isotropic temperature and back. In DSC studies, all the compounds exhibited clear-cut transition temperatures as well as associated enthalpy values in the DSC thermograms, which were further compiled and showed in **Table 5.1**.

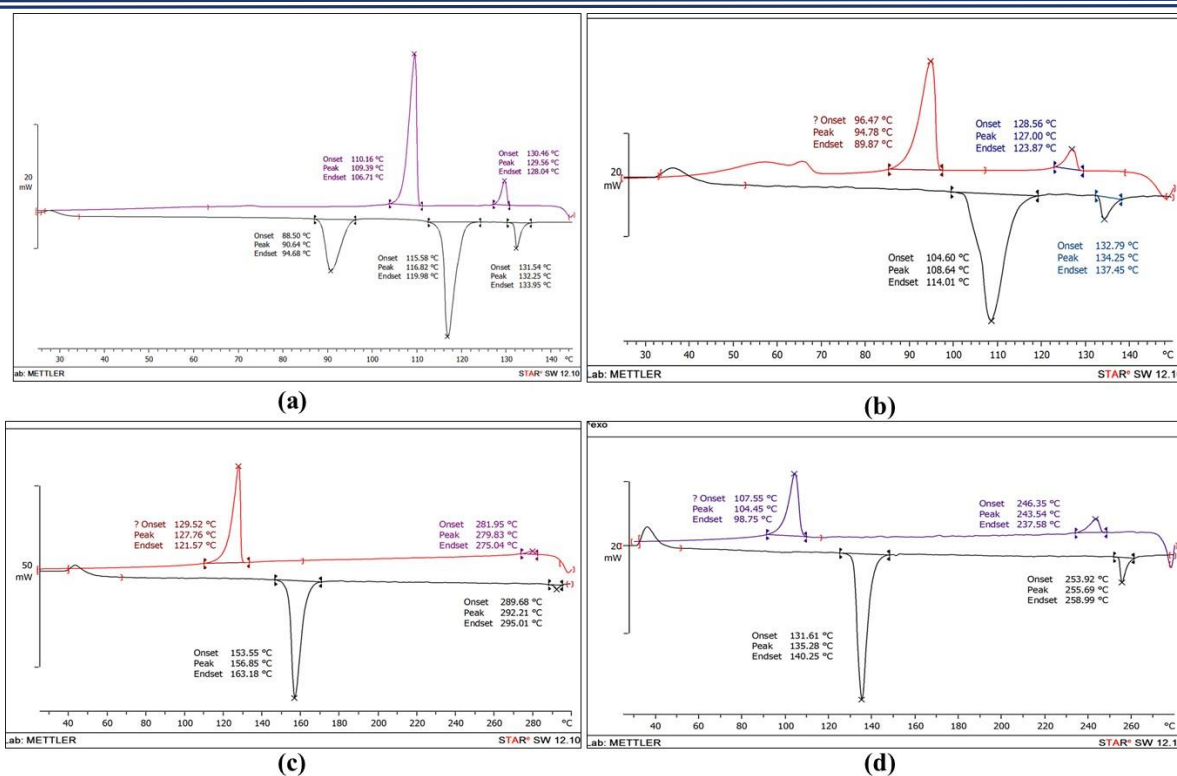


Figure-5.18 DSC thermograms of compounds (a)10d, (b)10f, (c)12b and (d) 12e

In DSC analysis, compound **10b** showed monotropic phase transition with two exothermic transition corresponding to I-N and N-Cr at 108.4°C and 95.3°C respectively, while only one endotherm for I-Cr transition at 124 °C. Compound **10c** and **10d** showed three endotherms for Cr1-Cr transition, Cr-SmA and SmA-Iso during the heating scan, while on cooling two exotherms for I-SmA and SmA-Cr(**Figure-5.18a**). From **10e-10g** all the compounds showed two endotherms for Cr-SmA and SmA-I and two exotherms from I-SmA and SmA-Cr during heating and cooling cycle respectively.

In second series, compound in which lower alkoxy ester attached Schiff base **12a** exhibited two endothermic curves for Cr-N and N-Iso at temperature 179.1 °C and 315.0 °C and two exotherms for Iso-N and N-Cr at temperature 289.4°C and 115.0°C respectively during cooling cycle. Similar set of transition peaks were observed for compound **12b** (**Figure-5.18c**) and **12c** with two endothermic curves for Cr-N and N-Iso and two exothermic curves for Iso-N and N-Cr. Replacement of octyloxy group by decyloxy group, compound **12d** showed two endotherms for Cr-SmA and SmA-I at temperature 133.7°C and 256.1°C on heating scan and two exotherms from I-SmA and SmA –Cr at temperature 239.9 °C and 92.1 °C during cooling cycle, due to very low energy nematic transition was not observed in DSC thermograms, however it is well observed and captured from POM analysis hence temperature observed in

POM analysis were reported in table. On increasing chain length to dodecyloxy in compound **12e**, resulted in enantiotropic smectic mesophase and showed two endotherm corresponds to Cr-SmA at temperature 135.2 °C and SmA to I at temperature 255.7 °C whereas two exotherms on cooling corresponds to I-SmA at temperature 243.5 °C and SmA to Cr at temperature 104.4 °C shown in (**Figure-5.18d**). Higher analogues of this series compounds **12e-h** (with n=12-18) showed two endotherm corresponds to Cr-SmA and SmA-I at and two exotherms on cooling corresponds to I-SmA and SmA-Cr.

5.2.2.3 X-ray diffraction studies:

Compounds of both the homologous series **10a-g** and **12a-h** were studied for their mesomorphic properties using POM and DSC analysis and showed very good mesophase textures and transition temperatures. Based on this, compounds **10d** and **12d** were selected and analysed for powder X-ray diffraction analysis (**Fig-5.19**) and interlayer spacing for peaks observed were calculated using Bragg's diffraction equation from the 2θ values. In powder XRD analysis of compound **10d** at 125 °C, two peaks were appeared one sharp peak with layer spacing 40.2 Å in the small angle regime while second peak as broad hump with layer spacing 4.8 Å (**Fig-5.19-a**). The sharp peak at small angle regime has confirmed the correct identification of mesophase which is smectic A. Similarly, compound **12d** showed first sharp peak in small angle regime ($d= 40.2 \text{ \AA}$) and second broad hump in wide angle regime ($d= 4.8 \text{ \AA}$) (**Fig- 5.19-b**) in powder XRD analysis at 240 °C. The same compound when analysed at 252 °C, the intensity of first sharp peak was decreased as compared to that appeared earlier for smectic A mesophase at lower temperature 240°C, which further confirms nematic mesophase in compounds **12d**. However, the diffused broad halo around 4.8 Å has remained unaffected as corresponding to liquid like nature of alkoxy terminal. The orthogonal smectic A mesophase was further confirmed by tilt angle, which was found to be near to zero.

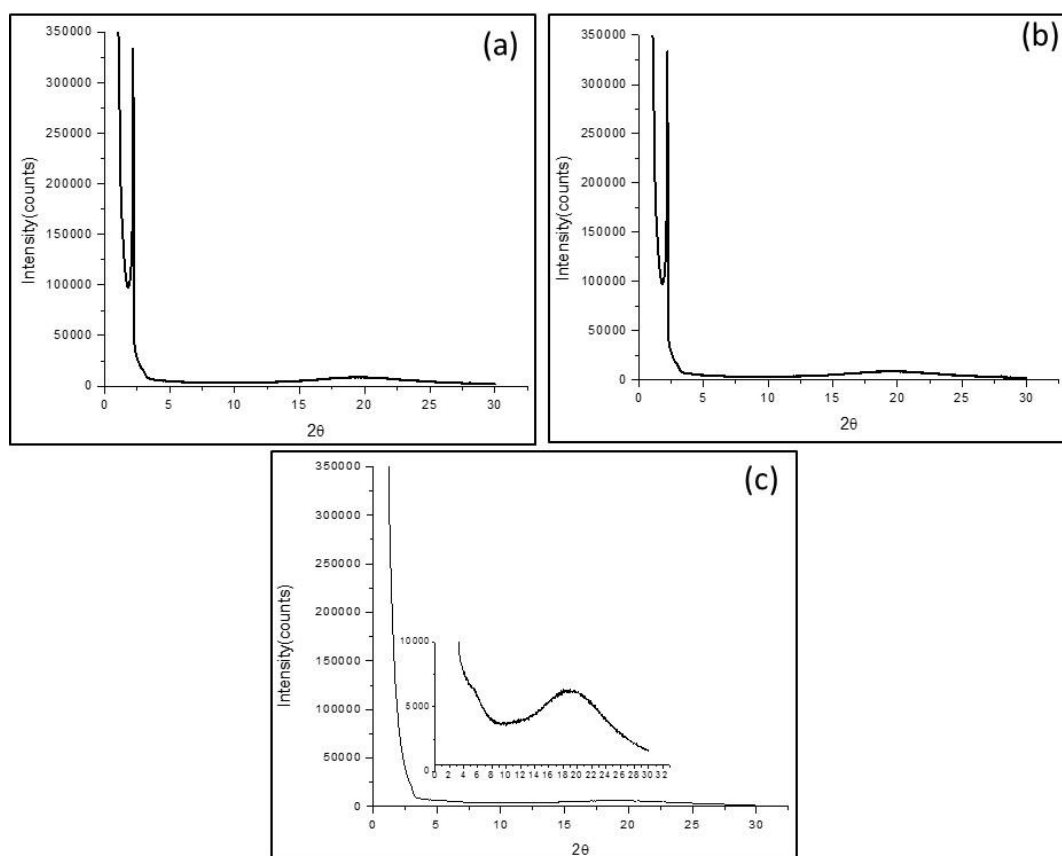


Figure- 5.19 Powder X-ray diffraction analysis graph as the scattering intensity (in counts) vs the scattering angle, 2θ (a) compound **10d** at 125 °C (b) compound **12d** at 240 °C (c) compound **12d** at 252 °C

5.3 DFT Calculations:

5.3.1 The geometrical structures:

Gaussian 9 was utilized for performing theoretical DFT calculations employing both DFT and B₃LYP-6-311G basis set. The optimized geometries of all structures were confirmed as stable, as no imaginary frequencies were observed [37]. A comparative analysis was conducted between the synthesized compound and a previously reported compound **4** which contain-OH group. The molecular structures of all these compounds are depicted in (Fig-5.20) All the optimized structures displayed excellent stability, and the frequencies of all compounds were determined using the same basis set for computing various parameters (Fig-5.20). Using the same method, basis set, and optimized molecular structures, calculations of frequency were conducted which were further used for computing different thermodynamic parameters.

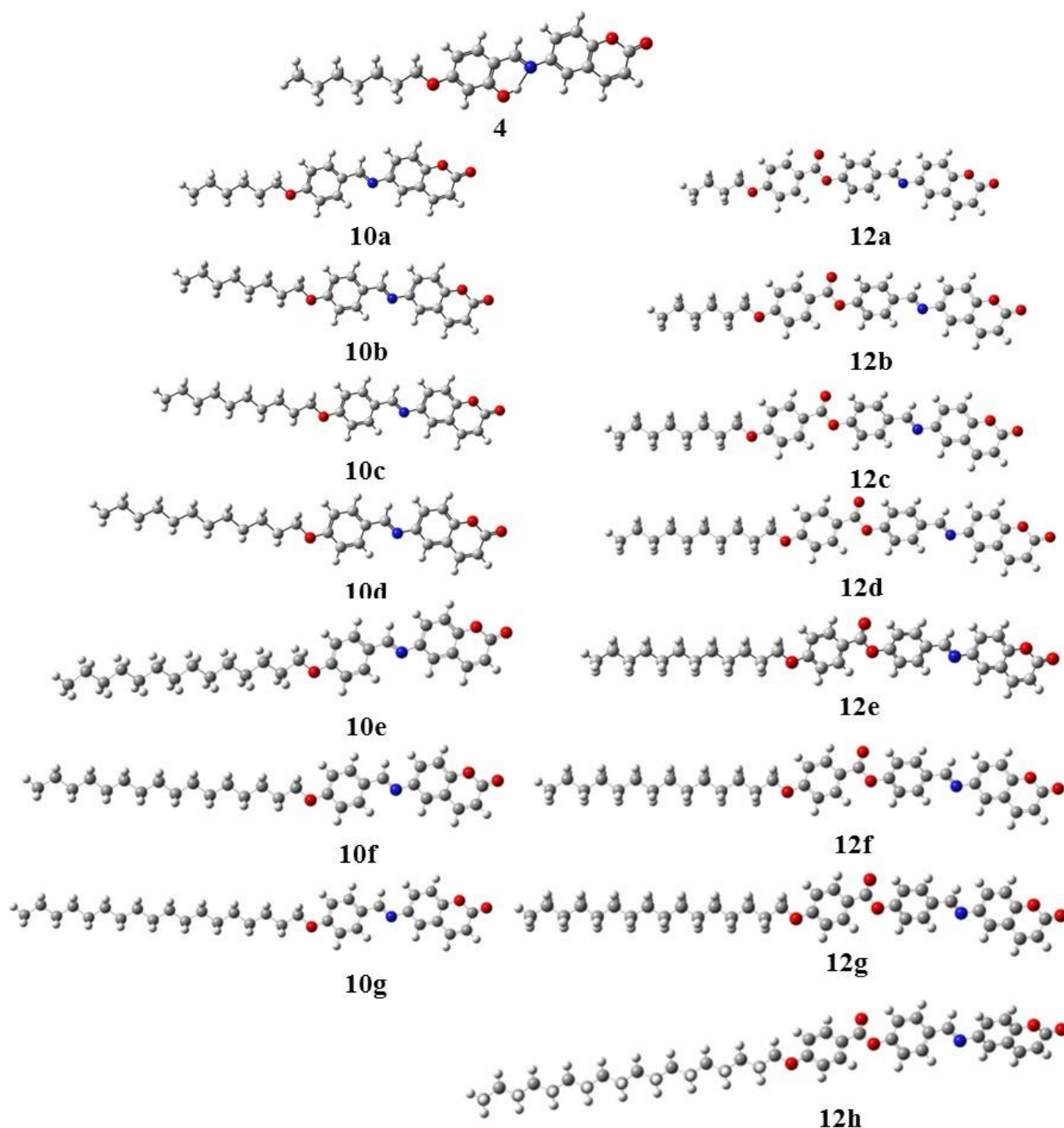


Figure- 5.20 The estimated molecular geometry of the compounds **4**, **10a-g** and **12a-h**

5.3.2 Frontier Molecular orbitals (FMO's) and Molecular Electrostatic Potential (MEP):

The highest occupied molecular orbital (HOMO) and Lowest unoccupied molecular orbital play distinct roles in the molecule, HOMO represents the highest energy level occupied by electrons functioning as electron donor. Conversely, the LUMO, characterized as orbital with lowest energy that can accept electrons and act as electron acceptor [38]. As a combined also called Frontier Molecular orbitals (FMO's) provides a reasonable qualitative prediction of both

excitation properties and electron transport capability. Additionally, these quantum chemical parameters can be used to determine the reactivity of the molecules. HOMO and LUMO images with energy gap of all the optimized structures are shown in (Table-5.2) and (Fig-5.21).

Table 5.2: Frontier molecular orbitals energies (eV), chemical hardness η (eV), and global softness (S) and other various parameters of the investigated compounds **10a-g** and **12a-h**

Compd	LUMO	HOMO	ΔE	X	η	S	ω	A=- E _{LUMO}	I=- E _{HOMO}
10a	-1.81690	-5.67058	3.85368	3.7416	1.92684	0.2595	3.63707	1.81690	5.67058
10b	-1.81582	-5.66922	3.85339	3.7416	1.92656	0.2595	3.63489	1.81582	5.66922
10c	-1.81554	-5.66840	3.85286	3.7416	1.92656	0.2595	3.63435	1.81554	5.66840
10d	-1.81418	-5.66731	3.85422	3.7416	1.92711	0.2595	3.62836	1.81418	5.66731
10e	-1.81527	-5.66786	3.85259	3.7416	1.92629	0.2595	3.63380	1.81527	5.66786
10f	-1.81527	-5.66786	3.85259	3.7416	1.92629	0.2595	3.63380	1.81527	5.66786
10g	-1.81472	-5.66759	3.85285	3.7416	1.92656	0.2595	3.63272	1.81472	5.66759
12a	-1.83514	-5.89970	4.06456	3.8667	2.03242	0.2460	3.67979	1.83514	5.89970
12b	-1.83296	-5.89806	4.06511	3.8667	2.03269	0.2460	3.67571	1.83296	5.89806
12c	-1.83241	-5.89752	4.06511	3.8640	2.03269	0.2460	3.67463	1.83241	5.89752
12d	-1.83214	-5.89752	4.06511	3.8640	2.03269	0.2460	3.67408	1.83214	5.89752
12e	-1.83187	-5.89725	4.06538	3.8640	2.03269	0.2460	3.67354	1.83187	5.89725
12f	-1.83159	-5.89725	4.06565	3.8640	2.03269	0.2460	3.67326	1.83159	5.89725
12g	-1.83159	-5.89752	4.06592	3.8640	2.03269	0.2460	3.67326	1.83159	5.89752
12h	-1.82997	-5.89562	4.06565	3.8640	2.03269	0.2460	3.67326	1.82997	5.89562

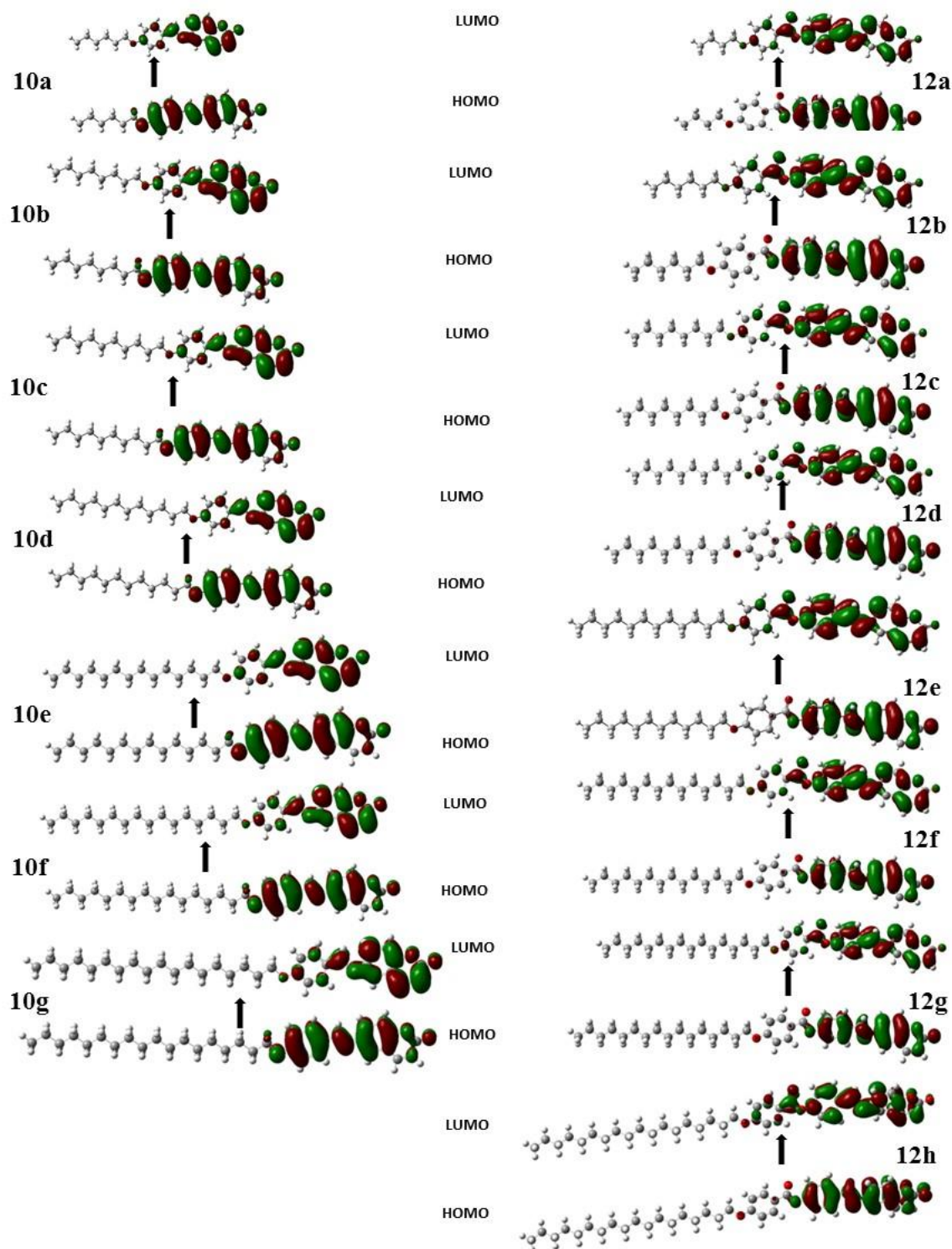


Figure- 5.21 Frontier Molecular Orbitals (FMO) HOMO-LUMO of compounds **10a-g** and **12a-h**

The HOMO and LUMO, their energies and energy gap of some representative compounds **10b** and Schiff base derivative with ester linkage **12c** were compared with the reported compound **4**, it is observed that HOMO is mainly appeared on coumarin and attached aromatic ring in compounds **4** and **10b**. While LUMO is mainly found on coumarin ring however in compound **10b** distribution of LUMO is on coumarin ring as well as aromatic ring partially (**Fig-5.23**). In Schiff base derivative **12c** with ester linkages, HOMO is located on coumarin and imine part, however LUMO is located on coumarin, imine aromatic ring as well as on ester linkage. Various parameters such as chemical hardness(η) and global softness (S) can be calculated from these HOMO and LUMO energies [39]. These parameters provide information of charge transfer resistance and photoelectric behavior of the compounds whose results are shown in (**Table-5.2**). These parameters serve as determinants for assessing the suitability of employing LCs in specific applications. For all the studied compounds, the energy values of the HOMO and LUMO were calculated and used for calculating other parameters such as the global softness and chemical hardness. An observation can be made that the energy gap between **4** and **10b** these FMOs not much affected by the additionally –OH group on compound **4** (**Table-5.3**), while in **12c** with ester linkage effect on energy gap, its ΔE value is greater than the Schiff base derivatives **4** and **10b**, therefore, does not exert an influence on the global softness and so that on chemical hardness as well.

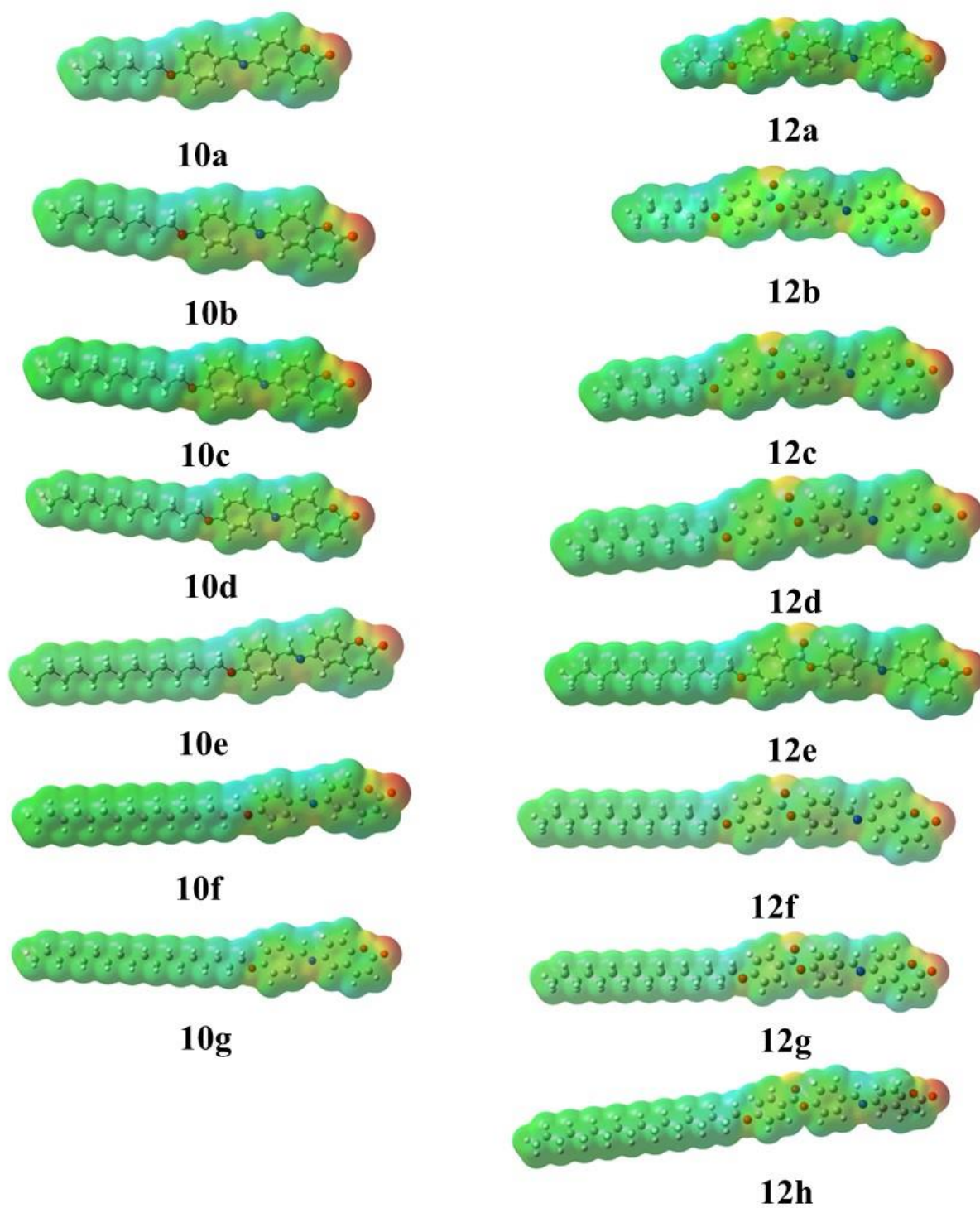


Figure- 5.22 Molecular Electrostatic Potential (MEP) of compounds **10a-g** and **12a-h**

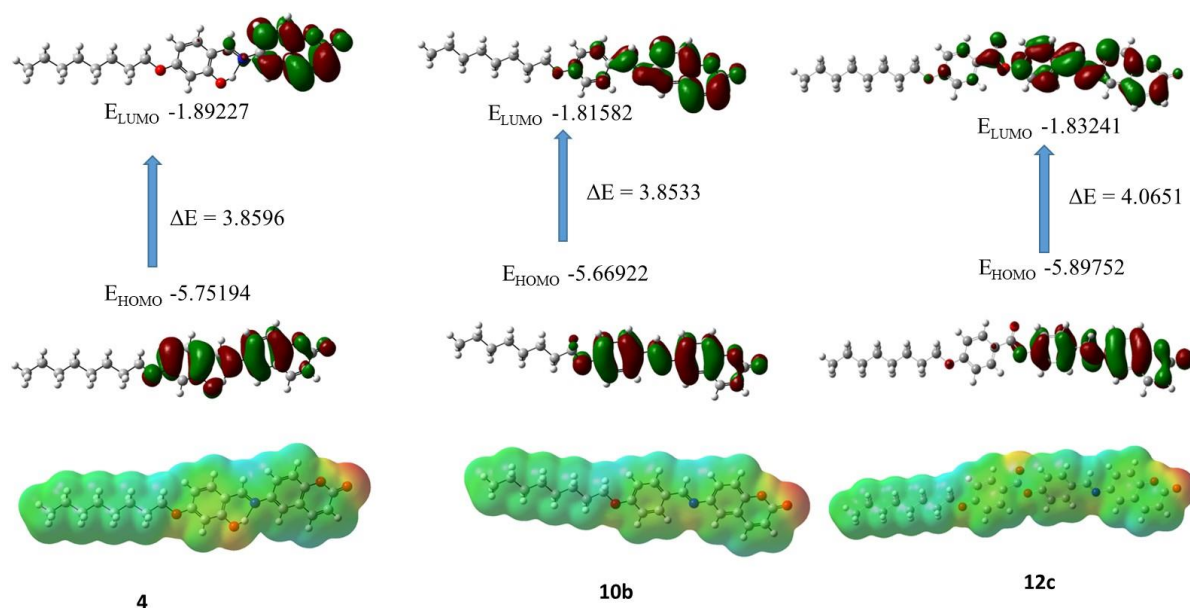


Figure- 5.23 Frontier Molecular orbitals (FMOs) and Molecular electrostatic potentials (MEP) for the prepared compounds **4**, **10b** and **12c**

Table 5.3: Frontier molecular orbitals energies (eV), chemical hardness η (eV), and global softness S of the investigated compounds **4**, **10b** and **12c**

Compd	LUMO (eV)	HOMO (eV)	ΔE (eV)	χ	n	s	ω
4	-1.89227	-5.75194	3.85967	-3.8221	1.9298	0.2590	3.78496
10b	-1.81582	-5.66922	3.85339	-3.7416	1.92656	0.2595	3.63489
12c	-1.83241	-5.89752	4.06511	-3.8640	2.03269	0.2460	3.67463

5.3.3 Polarizability, Aspect Ratio and Dipole moment:

The impact of polarizability is influenced by various factors, including the size of studied compounds, the type of mesogenic core as well as on the polarity of terminal moiety. Polarizability refers to the sensitivity of a molecular system's electron cloud to the presence of a charge [40]. Consequently, larger molecules exhibit higher polarizability compared to smaller ones. Moreover, the mesophase stability of the liquid crystalline compounds can be affected by change in polarizability of the mesogenic core compounds [28]. As a result, our theoretical methodology encompasses the computation of polarizability for the compounds under investigation, with the numerical outcomes presented in (Table 5.4). Upon comparing the calculated values for **10a-g** and **12a-h** it is evident that greater terminal alkoxy chain lengths

lead to heightened polarizability for the entire compound. It also observed that Schiff base derivatives with ester linkages **12a-h** variant displays greater polarizability than **10a-g**. Additionally, the compound **12a-h** exhibits a broader nematic and smectic mesophase range as compared to the compounds **10a-g**. Conversely, the absence of a mesophase in the **10a** compound could be attributed to its low polarizability value, leading to reduced end-to-end interactions and subsequently lowering molecular packing density.

Table 5.4: Mesomorphic parameters for heating cycle ($^{\circ}\text{C}$), polarizability (Bohr^3), dipole moment (Debye), the estimated dimensions (\AA), and the aspect ratio of the studied compounds. **10a-g** and **12a-h**

Comp	n	ΔT_{Cr}	ΔT_{SmA}	ΔT_{N}	Dipole Moment	Polarizability	Dimensions (\AA)		Aspect Ratio L/D
							Length (L)	Width (D)	
10a	6	-	-	-	7.769	307.16	22.31	5.50	4.05
10b	8	12.7		12.7	7.818	330.70	24.88	5.50	4.53
10c	10	22.0	22.0		7.844	353.93	26.66	5.49	4.86
10d	12	20.6	20.0		7.858	376.99	30.00	5.48	5.47
10e	14	31.1	31.1		7.872	399.97	32.56	5.48	5.94
10f	16	32.2	32.2		7.879	422.88	35.13	5.48	6.41
10g	18	23.7	23.7		7.882	445.73	37.69	5.47	6.88
12a	4	174.4		174.4	9.609	374.11	26.07	5.41	4.82
12b	6	152.1		152.1	9.716	398.06	28.64	5.60	5.12
12c	8	137.1		137.1	9.767	421.489	31.20	5.68	5.49
12d	10	160.9	146.9	14.0	9.796	444.67	33.77	5.73	5.89
12e	12	139.3	139.3		9.810	467.66	36.33	5.76	6.31
12f	14	133.6	133.6		9.819	490.580	38.899	5.77	6.74
12g	16	123.4	123.4		9.826	513.463	41.464	5.77	7.18
12h	18	127.4	127.4		9.768	536.478	44.017	5.47	8.04

The term aspect ratio pertains to the proportion between the length and width of an elongated molecule. This concept holds particular significance in the study of liquid crystals, especially those with rod like structures [41]. The aspect ratio serves as a vital structural characteristic that can elucidate the behavior of liquid crystals and impact their various mesophases. By determining the ratio of molecular length to width, the aspect ratio offers insight into the collision diameter of these molecules. Consequently, this ratio can influence both lateral and terminal interactions between molecules, a correlation that varies based on these values [29, 42].

Molecules characterized by higher aspect ratios, indicative of elongation and anisotropy, tend to exhibit a greater tendency for organizing into ordered mesophases, particularly within the smectic and nematic phases. L/D values effectively encapsulate the length-to-diameter ratio of the molecules and their respective aspect ratios, indicating their shape and propensity for certain liquid crystal phases [31,43]. These values describe the dimensions of the molecules and their aspect ratios, which are crucial for determining the types of liquid crystal phases that can form. These findings have been compiled in a tabulated form shown in (Table-5.4), in which the Schiff base derivatives **10a-g**, it was noted that there is an overall increase in the range of mesophase as the aspect ratio increases. For instance, compound **10b**, featuring an octyloxy chain length, a nematic mesophase range was evident due to its lower aspect ratio compared to **10c-g**. However, the prevalence of nematic stability diminishes with longer terminal alkoxy groups, with predominance shifting toward shorter chain lengths due to increasing terminal intermolecular interactions. For compounds **10c-g** it is observed that stability range of smectic mesophase was increased with the increment of aspect ratio.

In another series involving homologous Schiff bases **12a-h** with ester linkages, different trend emerged. For compounds **12a-d**, with $n = 4$ to 10, there was a decrease in the range of nematic mesophase up to $n = 8$ as the aspect ratio increases. Conversely, compound **12d** exhibited a notably limited nematic mesomorphic range compared to **12a-c** with further increase in aspect ratio. Subsequent compounds **12e-h** ($n = 10$ up to 18) experienced an increment of the smectic A mesophase range. Evidently, increase in the aspect ratios correlate with increased intermolecular interaction. These interactions as area expands, alongside give rise in the degree of π - π interaction. Consequently, greater molecular packing density enhances the appearance of the more ordered smectic mesophase in higher analogues prevailing over nematic mesophase [29,36,44].

Out of all the electronic parameters, dipole moment is one of them which affects the mesomorphic stability of thermotropic liquid crystalline compounds [45]. Dipole moment value is low for compound **10a** has resulted in absence of any mesophase, while on increasing chain length has increased the dipole moment as a result of that weak intermolecular interactions leading to nematic mesophase in compound **10b** (Table-5.4). Further, on increasing chain length from $n=10$ to 18, the relatively increase in dipole moment value allowed side-side interactions which overall resulted in the orthogonal smectic A mesophase. When ester linkage is introduced in between terminal alkoxy group in compounds **12a-h** dipole moment values were relatively high as compared to that of compounds **10a-g** and hence showed

very good total mesophase range stability. In this particular series with ester linkage, compounds **12a-c** with lower dipole moment resulted in terminal interaction to produce stable nematic mesophase. As terminal alkoxy chain length increased in compounds **12d-h** resulted in rise of dipole moment as well as parallel interaction to give rise stable smectic A mesophase (Fig-5.24).

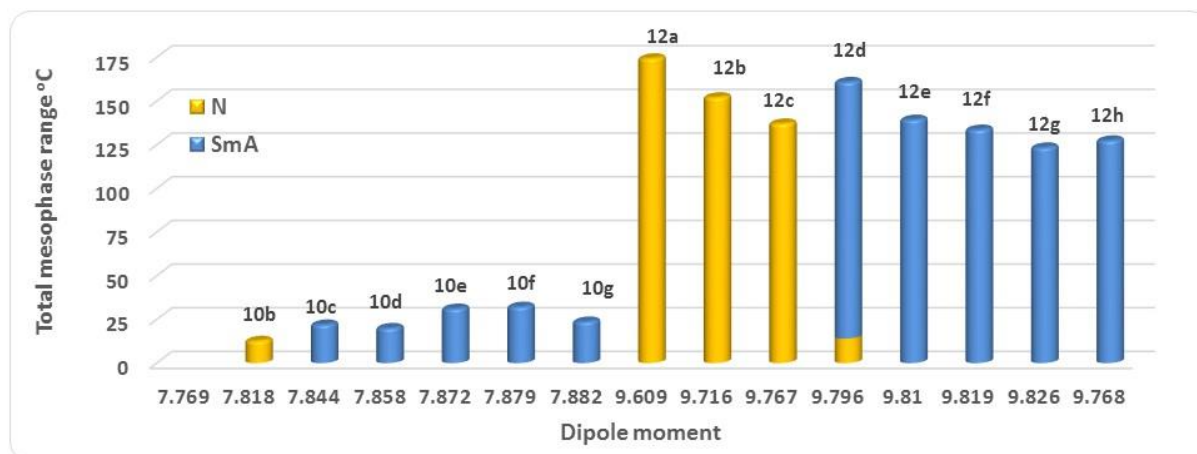


Figure- 5.24 Graph of the dipole moment versus the total mesophase range of compounds **10a-g** and **12a-h**

Electronic parameters such as polarizability and dipole moment of compounds **10b** and **12c** were compared with reference compound **4** (Table-5.5). Compound **4** with intramolecular hydrogen bonding, has shown very good polarizability leading to stable smectic A mesophase. However, removal of hydroxyl group in compound **10b**, resulted in drop in polarizability and overall formation of comparatively less stable nematic mesophase (Figure-5.25). On introduction of ester linkage in compound **12c** lead to increase in total polarizability to easily form terminal aggregation and resulted in stable nematic mesophase formation.

Table 5.5: Mesomorphic data for heating cycle (°C), polarizability (Bohr³), and dipole moment (Debye) of the studied compounds. **4**, **10b** and **12c**

Comp	ΔT_{Cr}	ΔT_{SmA}	ΔT_N	Dipole Moment	Polarizability	Aspect Ratio L/D
4	43.4	43.4		6.674	335.42	4.79
10b	12.74	-	12.74	7.818	330.70	4.53
12c	137.1	-	137.1	9.767	421.489	5.49

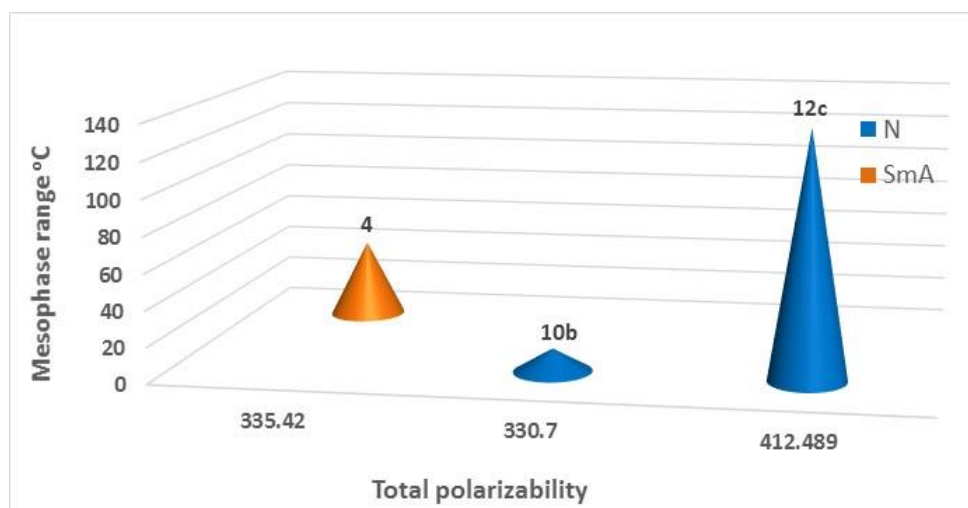


Figure- 5.25 Graphical relation between the polarizability and the thermal stability of nematic smectic A mesophase for compounds **4**, **10b** and **12c**.

5.4 Conclusion

In the first series of Schiff base derivatives of 6-aminocoumarin, compounds **10a-g** were designed with void of hydroxyl group. All the compounds were synthesized, characterized and their mesomorphic properties were studied using POM and DSC analysis. Removal of hydroxyl group on aldehyde part in compounds **10a-h** has resulted in decrease in parallel interaction in lower analogue **10b** with $n=8$ leading to show monotropic nematic mesophase. Higher analogues of this series, compounds **10c-h** ($n=10-18$) have showed enantiotropic Smectic A mesophase, however their stability were lower as compared to that reported for compounds with ortho hydroxyl group on aldehyde part. In second series, ester linkage has been introduced along with Schiff base in compounds **12a-h**. In which, compounds **12a-c** ($n=4-8$) have shown very stable enantiotropic nematic mesophase, while higher analogues **12d-h** ($n=10-18$) have shown enantiotropic smectic A mesophase. Transition of nematic to smectic A mesophase has been observed in compound **12d** ($n=10$), however stability of nematic mesophase was very low energy and could not detected in DSC thermograms. Hence, compounds **10d** from first series and **12d** from second series were studied for powder XRD analysis to identify the type of mesophase, which further confirmed orthogonal smectic A mesophase for compound **10d** at 125°C and **12d** at 240°C . Further compound **12d** showed nematic behavior at 252°C in powder XRD analysis. Compounds of both the series as well as reference compound **4** were optimized using DFT calculations. Based on optimized geometries, various structural and electronic parameters were calculated and compared. Overall dipole moments values for compounds **12a-h** with ester linkage were found to be higher as compared to that of compounds **10a-g** leading to more intermolecular interactions as well as higher mesophase stability. At the same time removal of hydroxyl group from reference compound **4** in compound **10b**, has resulted in decrease in polarizability and hence lower intermolecular interaction with less stable nematic mesophase. However, introduction of ester linkage in compound **12c** has enhanced the polarizability which has affected the parallel interactions within the molecules and lead to formation of highly stable smectic A mesophase.

5.5 Experimental

After being purified, all of the chemicals and solvents were bought from commercial suppliers. Silica gel F254 plates (Merck & Co., Kenilworth, NJ, USA) were utilized for the thin-layer chromatography analysis. The purification process uses column chromatography and Avra's silica gel (60-120 mesh). All reactions took place in a typical atmosphere. Melting points (M.P.) were uncorrected measurements taken in open capillary tubes. By using KBr pellet IR spectra were captured using a Bruker spectrometer. On an Advance Bruker Neo 400 spectrometer (400 MHz), $^1\text{H-NMR}$ and $^{13}\text{C-NMR}$ spectral data were collected with CDCl_3 or $\text{DMSO-}d_6$ as the solvent and J values in Hz. Utilizing a Polarizing Optical Microscope (POM) LEICA DM 2500P (Wien, Austria) coupled with a CAMERA-LEICA-DFC 295, liquid crystalline properties were investigated. With the sample in a thin film sandwiched between a glass slide and cover, polarized light with a crossed polarizer at an angle of 45 degrees and 10x magnification were used to observe the textures of the compounds. By employing the DSC-822 from Mettler Toledo (Greifensee, Switzerland), which has STARe software, during both heating and cooling cycles at a rate of 10.0 °C/min, differential scanning calorimetry (DSC) analysis was performed. 6-aminocoumarin, 4-alkoxy benzaldehyde, 4-alkoxy benzoic acid, and Schiff base derivatives was synthesized according to literature methods [29, 30, 34,35].

Synthesis of 6-nitrocoumarin (7)

To a cold solution of coumarin (10.0 g, 68.5 mmol) in concentrated H_2SO_4 (50 mL), was added 20 ml of mixed acid (HNO_3 : H_2SO_4 = 1:3, v/v). The resulting mixture was stirred at 0 °C for 15 mins and then at room temperature for 2 hours. The reaction mixture was poured into ice-cold water to give white solid. The solid was filtered washed with cold water and recrystallized using acetic acid.

Synthesis of 6-amino coumarin (8)

To a suspension of 6-Nitrocoumarin (10.0 g, 52.38 mmol) and Fe powder (20 g) in water (170 mL) was added ammonium chloride (3.25 g, 60.75 mmol) in several portions over a period of 10 mins. The resulting mixture was heated at 80°C for 6 hours. The completion of reaction was checked by TLC. After completion of reaction, the reaction mixture was filtered and brown solid was dissolved in ethyl acetate. The organic layer was filtered to remove insoluble solid and filtrate was concentrated on a rotavapor to give compound as silky golden crystals (m. p. 158°C)

4-Alkyloxy benzaldehyde (9)

To a solution of 4-hydroxy benzaldehyde (1.0 eq) in DMF (20 mL) was added anhydrous K_2CO_3 (2.5 eq) and stirred at room temperature for 10-15 min. To this mixture, alkyl bromide (1.0 mmol) was added and resulting solution was stirred at room temperature for 16-18 hours. The completion of reaction was checked by TLC. After completion of reaction, the reaction mixture was poured into ice-cold water. The crude compounds were obtained were directly used for next step. Yield: 70-85%.

Synthesis of 4-(n-alkyloxy) benzoic acid

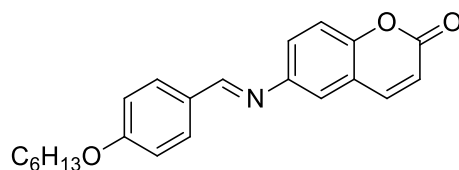
To a solution of 4-hydroxy benzoic acid (3.5g, 0.03 mmol, 1 eq) in methanol (25ml) was added potassium hydroxide followed by N-alkyl bromide (1.2 eq) and refluxed for 7-8 hours. Afterward, potassium hydroxide (20% solution, 5 ml) was added and again refluxed for additional two hours. In order to precipitate 4-(n-alkyloxy) benzoic acid, the reaction mixture was poured into ice-cold water and acidified with dil.HCl. The solid separated out was filtered, dried, and recrystallized from ethanol.

Synthesis of ester (n-alkyl benzoic acid) (11)

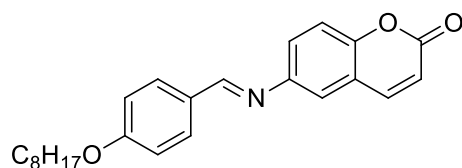
EDC (1.5 eq) and HOBt (1.0 eq.) were added to a solution of 4-(n-alkyloxy) benzoic acid (0.5 g, 1.0 eq) in DCM (25 ml) (2.5 eq.) followed by TEA (2.5 eq) and cooled to 0-5°C. To this, 4-hydroxy benzaldehyde (0.20 g, 1.0 eq.) was added and stirred at 0-5°C for additional 30 minutes and subsequently at room temperature for 20 hours. After the reaction was completed on TLC, the mixture was diluted with water (30 mL) and extracted with DCM (3 x 20 mL). The organic layer was separated, washed with water (20 mL), brine solution (20 mL), dried over anhydrous Na_2SO_4 , filtered, and concentrated on a rotavapor. The residue was scratched in methanol, filtered and dried to give compound **11** as white solid.

General procedure for Schiff Base (10a-g) and (12a-h):

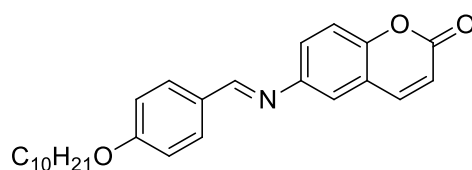
To a suspension of 6-amino-chromen-2-one (1.0 eq) and 4-alkoxy benzaldehyde/4-formylphenyl 4-(n-alkyloxy) benzoate (1.0 eq) in ethanol (10 mL) was added 3-4 drops of acetic acid and then refluxed for 18–20 hours. During the heating, the solid separated out. The mixture was cooled, filtered and washed with cold ethanol to give desired compound. All were recrystallized from ethanol.

(E)-6-((4-(hexyloxy)benzylidene)amino)-2H-chromen-2-one (10a)

Yield: 87%; Melting Point :146-148°C; IR (KBr) : 3429, 3086, 2935, 2868, 1725, 1625, 1605, 1564, 1511, 1483, 1421, 1392, 1308, 1252, 1189, 1170, 1138, 1105, 1024, 970, 908, 835, 808, 773, 710, 639, 601 cm^{-1} ; $^1\text{H-NMR}$ (400 MHz CDCl_3) : δ ppm 0.94 (t, $J = 6.8\text{Hz}$, 3H), 1.35-1.39 (m, 4H), 1.48-1.51 (m 2H), 1.74-1.87 (m, 2H), 4.04 (t, $J = 6.8\text{Hz}$, 2H), 6.47 (d, $J = 9.6\text{Hz}$, 1H), 7.00 (d, $J = 8.8\text{Hz}$, 2H), 7.30 (d, $J = 2.0\text{Hz}$, 1H), 7.36 (d, $J = 8.8\text{Hz}$, 1H), 7.42 (dd, $J = 2.4\text{Hz}$, and 8.8Hz , 1H), 7.74 (d, $J = 9.6\text{Hz}$, 1H), 7.85 (d, $J = 8.8\text{Hz}$, 2H), 8.42 (s, 1H); $^{13}\text{C-NMR}$ (100 MHz CDCl_3) : 14.03, 22.59, 25.68, 29.13, 31.56, 68.28, 114.81, 117.04, 117.54, 119.18, 119.20, 124.93, 128.60, 130.68, 143.36, 148.83, 151.98, 160.47, 160.77, 162.26 δ ppm; ESI-MS: 350.17 $[\text{M}+\text{H}]^+$; Anal. Calc. for $\text{C}_{22}\text{H}_{23}\text{NO}_3$; C, 75.62; H, 6.63; N, 4.01 found: C, 75.64; H, 6.60; N, 4.03%.

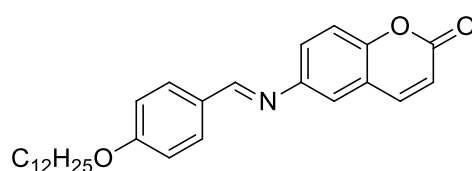
(E)-6-((4-(octyloxy)benzylidene)amino)-2H-chromen-2-one (10b)

Yield: 88%; Melting Point :122-124°C; IR (KBr) : 3044, 2924, 2852, 1731, 1624, 1606, 1564, 1511, 1482, 1467, 1436, 1422, 1389, 1370, 1308, 1255, 1187, 1168, 1136, 1103, 1020, 908, 832, 757, 713, 638 cm^{-1} ; $^1\text{H-NMR}$ (400 MHz CDCl_3) : δ ppm 0.91 (t, $J = 6.4\text{Hz}$, 3H), 1.31-1.50 (m, 10H), 1.79-1.86 (m, 2H), 4.04 (t, $J = 6.4\text{Hz}$, 2H), 6.45 (d, $J = 9.2\text{Hz}$, 1H), 7.01 (d, $J = 8.8\text{Hz}$, 2H), 7.29 (d, $J = 2.4\text{Hz}$, 1H), 7.34 (d, $J = 8.8\text{Hz}$, 1H), 7.42 (dd, $J = 2.4\text{Hz}$, 8.8Hz , 1H), 7.73 (d, $J = 9.6\text{Hz}$, 1H), 7.84 (d, $J = 8.4\text{Hz}$, 2H), 8.41 (s, 1H); $^{13}\text{C-NMR}$ (100 MHz CDCl_3) : δ ppm 14.11, 22.65, 26.01, 29.16, 29.22, 29.34, 31.81, 68.44, 114.81, 117.03, 117.53, 119.18, 119.20, 124.94, 128.60, 130.68, 143.36, 148.83, 151.97, 160.46, 160.76, 162.26; ESI-MS: 378.10 $[\text{M}+\text{H}]^+$; Anal. Calc. for $\text{C}_{24}\text{H}_{27}\text{NO}_3$; C, 76.36; H, 7.21; N, 3.71 found: C, 76.34; H, 7.23; N, 3.72%

(E)-6-((4-(decyloxy)benzylidene)amino)-2H-chromen-2-one (10c)

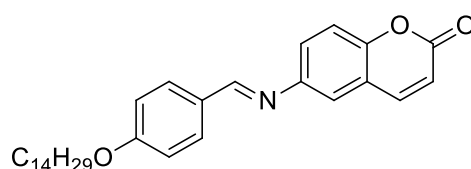
Yield: 86%; Melting Point :122-124°C; IR (KBr) : 3035, 2925, 2858, 1719, 1627, 1599, 1561, 1510, 1474, 1436, 1390, 1301, 1254, 1168, 1132, 1103, 1018, 985, 955, 908, 831, 718, 628, 600 cm^{-1} ; $^1\text{H-NMR}$ (400 MHz CDCl_3) : δ ppm 0.90 (t, $J = 6.4\text{Hz}$, 3H), 1.26-1.37 (m, 12H), 1.47-1.51 (m, 2H), 1.80-1.85 (m, 2H), 4.04 (t, $J = 6.4\text{Hz}$, 2H), 6.47 (d, $J = 9.6\text{Hz}$, 1H), 7.00 (d, $J = 8.4\text{Hz}$, 2H), 7.30 (d, $J = 2.4\text{Hz}$, 1H), 7.36 (d, $J = 8.8\text{Hz}$, 1H), 7.43, (dd, $J = 8.8\text{Hz}$, 2.4Hz, 1H), 7.74 (d, $J = 9.6\text{Hz}$, 1H), 7.85 (d, $J = 8.8\text{Hz}$, 2H), 8.42 (s, 1H); $^{13}\text{C-NMR}$ (100 MHz CDCl_3) : δ ppm 14.12, 22.68, 26.01, 29.17, 29.32, 29.32, 29.38, 29.56, 29.57, 31.90, 68.28, 114.81, 117.04, 117.54, 119.18, 119.20, 124.93, 128.59, 130.68, 143.35, 148.83, 151.98, 160.47, 160.77, 162.26 ESI-MS: 405.52 $[\text{M}^+]$; Anal. Calc. for $\text{C}_{26}\text{H}_{31}\text{NO}_3$; C, 77.01; H, 7.71; N, 3.45 found: C, 77.04; H, 7.73, N, 3.47%

(E)-6-((4-(dodecyloxy)benzylidene)amino)-2H-chromen-2-one (10d)



Yield: 85%; Melting Point :132-134°C; IR (KBr) : 3033, 2923, 1718, 1627, 1599, 1560, 1511, 1474, 1435, 1374, 1302, 1255, 1221, 1170, 1129, 1100, 1024, 1000, 954, 914, 877, 830, 755, 719, 627, 600 cm^{-1} ; $^1\text{H-NMR}$ (400 MHz CDCl_3) : δ ppm 0.90 (t, $J = 6.4\text{Hz}$, 3H), 1.28-1.37 (m, 16H), 1.45-1.51 (m, 2H), 1.80-1.85 (m, 2H), 4.04 (t, $J = 6.4\text{Hz}$, 2H), 6.47 (d, $J = 9.6\text{Hz}$, 1H), 7.00 (d, $J = 8.8\text{Hz}$, 2H), 7.30 (d, $J = 2.4\text{Hz}$, 1H), 7.36 (d, $J = 8.8\text{Hz}$, 1H), 7.43 (dd, $J = 2.4\text{Hz}$, 8.4Hz, 1H), 7.74 (d, $J = 9.6\text{Hz}$, 1H), 7.85 (d, $J = 8.4\text{Hz}$, 2H), 8.42 (s, 1H); $^{13}\text{C-NMR}$ (100 MHz CDCl_3) : δ ppm 14.13, 22.69, 26.01, 29.06, 29.17, 29.35, 29.38, 29.55, 29.57, 29.66, 31.92, 68.28, 114.81, 117.04, 117.53, 119.17, 119.20, 124.93, 128.60, 130.68, 143.35, 148.83, 151.98, 160.45, 160.76, 162.26; ESI-MS: 434.26 $[\text{M}+\text{H}]^+$; Anal. Calc. for $\text{C}_{28}\text{H}_{35}\text{NO}_3$; C, 77.56; H, 8.14; N, 3.23 found: C, 77.52; H, 8.11; N, 3.21%

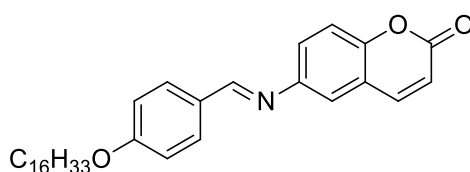
(E)-6-((4-(tetradecyloxy)benzylidene)amino)-2H-chromen-2-one (10e)



Yield: 84%; Melting Point :138-140°C; IR (KBr) : 3032, 2920, 2852, 2362, 1711, 1624, 1600, 1560, 1510, 1471, 1305, 1253, 1222, 1163, 1136, 1105, 1014, 915, 834, 721, 628 cm^{-1} ; $^1\text{H-NMR}$ (400 MHz CDCl_3) : δ ppm 0.90 (t, $J = 6.8\text{Hz}$, 3H), 1.28 (broad s, 20H), 1.37-1.51 (m,

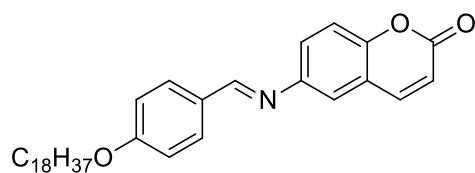
2H), 1.64-1.66 (m, 2H), 1.80-1.85 (m, 2H), 4.04 (t, $J = 6.8\text{Hz}$, 2H), 6.48 (d, $J = 9.6\text{Hz}$, 1H), 7.00 (d, $J = 8.8\text{Hz}$, 2H), 7.30 (d, $J = 2.4\text{Hz}$, 1H), 7.37 (d, $J = 8.8\text{Hz}$, 1H), 7.43 (dd, $J = 2.4\text{Hz}$, 8.8Hz, 1H), 7.74 (d, $J = 9.6\text{Hz}$, 1H), 7.86 (d, $J = 8.8\text{Hz}$, 2H), 8.42 (s, 1H); ^{13}C -NMR (100 MHz CDCl_3) : δ ppm 14.13, 22.70, 26.01, 29.17, 29.37, 29.38, 29.57, 29.60, 29.66, 29.68, 29.70, 31.93, 68.28, 114.81, 117.04, 117.54, 119.18, 119.20, 124.93, 128.60, 130.68, 143.35, 148.83, 151.99, 160.46, 160.76, 162.26; ESI-MS: 462.60 $[\text{M}+\text{H}]^+$; Anal. Calc. for $\text{C}_{30}\text{H}_{39}\text{NO}_3$; C, 78.05; H, 8.52; N, 3.03 found: C, 78.09; H, 8.51; N, 3.06%

(E)-6-((4-(hexadecyloxy)benzylidene)amino)-2H-chromen-2-one (10f)



Yield: 88%; Melting Point :134-136°C; IR (KBr) : 3031, 2920, 2851, 1712, 1626, 1599, 1560, 1511, 1470, 1438, 1375, 1304, 1253, 1221, 1188, 1164, 1134, 1104, 1018, 918, 880, 834, 772, 722, 627, 600 cm^{-1} ; ^1H -NMR (400 MHz CDCl_3) : δ ppm 0.90 (t, $J = 6.4\text{Hz}$, 3H), 1.28 (broad s, 24H), 1.33-1.1.51 (m, 2H), 1.81-1.85 (m, 2H), 4.04 (t, $J = 6.4\text{Hz}$, 2H), 6.46 (d, $J = 9.6\text{Hz}$, 1H), 7.00 (d, $J = 8.8\text{Hz}$, 2H), 7.30 (d, $J = 2.0\text{Hz}$, 1H), 7.35 (d, $J = 8.4\text{Hz}$, 1H), 7.42 (dd, $J = 2.4\text{Hz}$, 8.8Hz, 1H), 7.73 (d, $J = 9.6\text{Hz}$, 1H), 7.85 (d, $J = 8.8\text{Hz}$, 2H), 8.42 (s, 1H) ^{13}C -NMR (100 MHz CDCl_3) : δ ppm 14.12, 22.70, 25.97, 26.01, 29.06, 29.17, 29.37, 29.38, 29.55, 29.57, 29.60, 29.66, 29.70, 31.93, 68.45, 114.81, 117.05, 117.55, 119.18, 119.20, 124.93, 128.59, 130.69, 143.35, 148.82, 151.99, 160.46, 160.76, 162.27 ESI-MS: 489.13 $[\text{M}+\text{H}]^+$; Anal. Calc. for $\text{C}_{32}\text{H}_{43}\text{NO}_3$; C, 78.49; H, 8.85; N, 2.86 found: C, 77.47; H, 8.83; N, 2.84%

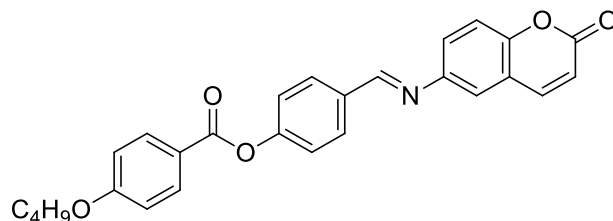
(E)-6-((4-(octadecyloxy)benzylidene)amino)-2H-chromen-2-one (10g)



Yield: 86%; Melting Point :136-138°C; IR (KBr) : 3031, 2920, 2851, 2859, 1712, 1626, 1599, 1560, 1511, 1468, 1438, 1375, 1305, 1254, 1221, 1188, 1165, 1135, 1105, 1016, 919, 834, 773, 722, 627, 600 cm^{-1} ; ^1H -NMR (400 MHz CDCl_3) : δ ppm 0.90 (t, $J = 6.8\text{Hz}$, 3H), 1.28 (broad s, 28H), 1.45-1.51 (m, 2H), 1.80-1.87 (m, 2H), 4.05 (t, $J = 6.8\text{Hz}$, 2H), 6.47 (d, $J = 9.6\text{Hz}$, 1H), 7.00 (d, $J = 8.8\text{Hz}$, 2H), 7.30 (d, $J = 2.0\text{Hz}$, 1H), 7.36 (d, $J = 8.8\text{Hz}$, 1H), 7.42 (dd, $J = 2.4\text{Hz}$, 8.8Hz, 1H), 7.74 (d, $J = 9.2\text{Hz}$, 1H), 7.85 (d, $J = 8.8\text{Hz}$, 2H), 8.42 (s, 1H) ^{13}C -NMR (100 MHz CDCl_3) : δ ppm 14.12, 22.70, 25.96, 26.01, 29.06, 29.17, 29.37, 29.38, 29.57, 29.60,

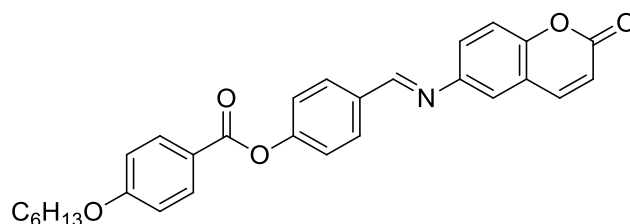
29.67, 29.71, 31.93, 68.46, 114.81, 117.06, 117.55, 119.18, 119.64, 124.92, 128.57, 130.71, 143.34, 148.80, 152.00, 160.46, 160.76, 162.29 ESI-MS: 518.18 $[M+H]^+$; Anal. Calc. for $C_{34}H_{47}NO_3$; C, 78.87; H, 9.15; N, 2.71 found: C, 77.85; H, 9.14; N, 2.72%

(E)-4-(((2-oxo-2H-chromen-6-yl)imino)methyl)phenyl 4-(butoxy)benzoate (12a)

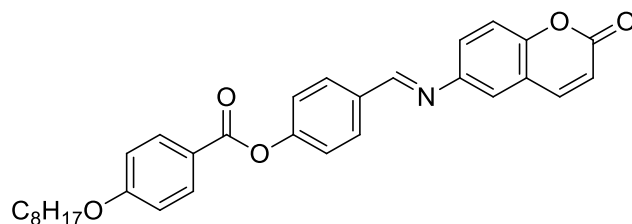


White solid; Yield: 84%; M.P: 312-314°C; IR (KBr): 3038, 2962, 2875, 1731, 1628, 1601, 1559, 1508, 1475, 1398, 1374, 1323, 1302, 1256, 1200, 1159, 1100, 1033, 907, 830, 761, 653 cm^{-1} ; 1H -NMR (400 MHz, $CDCl_3$): δ ppm 1.02 (t, $J = 7.4Hz$, 3H), 1.49-1.59 (m, 2H), 1.80-1.87 (m, 2H), 4.07 (t, $J = 6.6Hz$, 2H), 6.48 (d, $J = 9.6Hz$, 1H), 7.0 (d, $J = 9.2Hz$, 2H), 7.34-7.39 (m, 4H), 7.45 (dd, $J = 8.8, 2.4Hz$, 1H), 7.75 (d, $J = 9.6Hz$, 1H), 7.99 (d, $J = 8.4Hz$, 2H), 8.16 (d, $J = 8.8Hz$, 2H), 8.51 (s, 1H); ESI-MS: 442.16 $[M+H]^+$; Anal. Calc. for $C_{27}H_{23}NO_5$; C, 73.46; H, 5.25; N, 3.17 found: C, 73.44; H, 5.23, N, 3.20%

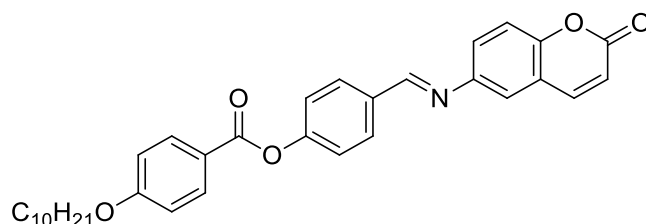
(E)-4-(((2-oxo-2H-chromen-6-yl)imino)methyl)phenyl 4-(hexyloxy)benzoate (12b)



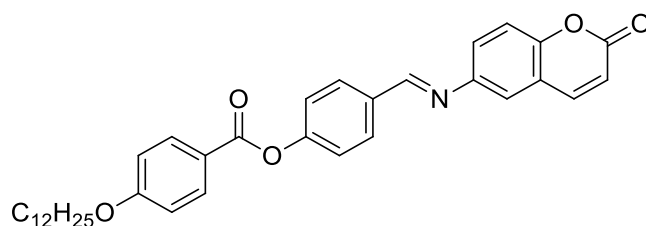
White solid; Yield: 84 %; M.P: 292-294 °C ; IR (KBr): 3041, 2940, 2867, 2360, 1734, 1628, 1602, 1559, 1507, 1472, 1436, 1373, 1301, 1253, 1201, 1159, 1099, 1065, 920, 875, 828, 760, 655 cm^{-1} ; 1H -NMR (400 MHz, $CDCl_3$): δ ppm 0.94 (t, $J = 6.8Hz$, 3H), 1.37-1.39 (m, 4H), 1.47-1.53 (m, 2H), 1.81-1.88 (m, 2H), 4.07 (t, $J = 6.8Hz$, 2H), 6.49 (d, $J = 9.6Hz$, 1H), 7.01 (d, $J = 8.8Hz$, 2H), 7.35-7.41 (m, 4H), 7.46 (d, $J = 8.8Hz$, 1H), 7.76 (d, $J = 9.2Hz$, 1H), 8.0 (d, $J = 8.4Hz$, 2H), 8.17 (d, $J = 8.8Hz$, 2H), 8.52 (s, 1H); ^{13}C -NMR (125 MHz, $CDCl_3$): δ ppm 14.04, 22.59, 25.66, 29.06, 31.55, 68.40, 114.42, 117.16, 117.64, 119.25, 119.37, 121.09, 122.41, 124.88, 130.15, 132.37, 133.36, 143.30, 148.28, 152.29, 153.85, 159.90, 160.67, 163.79, 164.53. ESI-MS: 470.15 $[M+H]^+$; Anal. Calc. for $C_{29}H_{27}NO_5$; C, 74.18; H, 5.80; N, 2.98 found: C, 74.16; H, 5.48; N, 2.96%

(E)-4-(((2-oxo-2H-chromen-6-yl)imino)methyl)phenyl 4-(octyloxy)benzoate (12c)

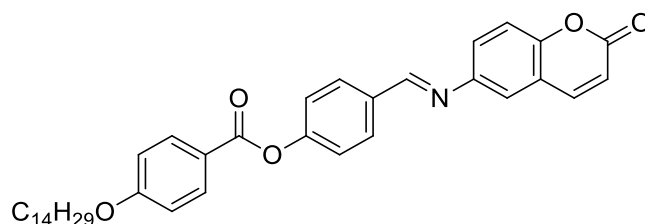
White solid; Yield:86%; M.P:274-276°C; IR (KBr): 3079, 2924, 2855, 1730, 1627, 1604, 1563, 1510, 1474, 1316, 1258, 1221, 1197, 1165, 1103, 1069, 910, 847, 762, 655, 536 cm^{-1} ; $^1\text{H-NMR}$ (400 MHz, CDCl_3): δ ppm 0.92 (t, $J = 7.0\text{Hz}$, 3H), 1.32-1.38 (m, 8H), 1.47-1.52 (m, 2H), 1.82-1.89 (m, 2H), 4.08 (t, $J = 6.4\text{Hz}$, 2H), 6.50 (d, $J = 9.6\text{Hz}$, 1H), 7.01 (d, $J = 8.8\text{Hz}$, 2H), 7.35-7.41 (m, 4H), 7.46 (dd, $J = 8.8, 2.4\text{Hz}$, 1H), 7.77 (d, $J = 9.6\text{Hz}$, 1H), 8.01 (d, $J = 8.8\text{Hz}$, 2H), 8.18 (d, $J = 8.8\text{Hz}$, 2H), 8.52 (s, 1H); $^{13}\text{C-NMR}$ (125 MHz, CDCl_3): δ ppm 14.11, 22.66, 25.99, 29.10, 29.22, 29.33, 31.81, 68.41, 114.42, 117.19, 117.66, 119.25, 119.36, 121.09, 122.42, 124.86, 130.16, 132.38, 133.36, 143.29, 148.31, 152.30, 153.86, 159.92, 160.68, 163.79, 164.55; ESI-MS: 497.22 $[\text{M}^+]$; Anal. Calc. for $\text{C}_{31}\text{H}_{31}\text{NO}_5$; C, 74.83; H, 6.28; N, 2.81 found: C, 77.85; H, 6.25; N, 2.84%

(E)-4-(((2-oxo-2H-chromen-6-yl)imino)methyl)phenyl 4-(decyloxy)benzoate (12d)

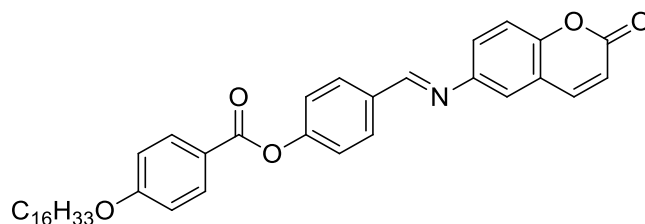
White solid; Yield: 85%; M.P: 254-256°C; IR (KBr): 3082, 2924, 2852, 1727, 1624, 1602, 1563, 1509, 1472, 1439, 1372, 1318, 1256, 1206, 1166, 1105, 1069, 1014, 906, 848, 761, 658 cm^{-1} ; $^1\text{H-NMR}$ (400 MHz, CDCl_3): δ ppm 0.91 (t, $J = 6.4\text{Hz}$, 3H), 1.30-1.35 (br s, 12H), 1.46-1.52 (m, 2H), 1.81-1.88 (m, 2H), 4.07 (t, $J = 6.4\text{Hz}$, 2H), 6.49 (d, $J = 9.6\text{Hz}$, 1H), 7.01 (d, $J = 8.8\text{Hz}$, 2H), 7.35-7.39 (m, 4H), 7.46 (dd, $J = 8.8, 2.4\text{Hz}$, 1H), 7.76 (d, $J = 9.6\text{Hz}$, 1H), 8.0 (d, $J = 8.8\text{Hz}$, 2H), 8.17 (d, $J = 8.8\text{Hz}$, 2H), 8.52 (s, 1H); $^{13}\text{C-NMR}$ (125 MHz, CDCl_3): δ ppm 14.13, 22.69, 25.99, 29.10, 29.32, 29.37, 29.56, 31.90, 68.41, 114.42, 117.16, 117.64, 119.25, 119.37, 121.08, 122.41, 124.87, 130.15, 132.37, 133.36, 143.29, 148.29, 152.29, 153.86, 159.90, 160.67, 163.79, 164.54; ESI-MS: 526.25 $[\text{M}+\text{H}]^+$; Anal. Calc. for $\text{C}_{33}\text{H}_{35}\text{NO}_5$; C, 75.40; H, 6.71; N, 2.66; found: C, 77.43; H, 6.74; N, 2.69%

(E)-4-(((2-oxo-2H-chromen-6-yl)imino)methyl)phenyl 4-(dodecyloxy)benzoate (12e)

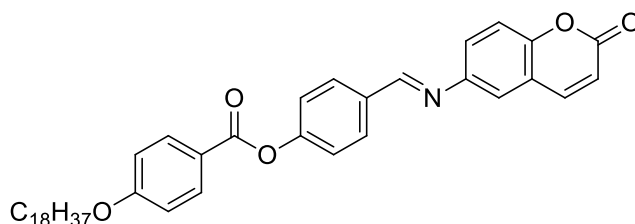
White solid; Yield:84%; M.P: 256-258°C; IR (KBr): 3079, 2921, 2852, 1722, 1628, 1603, 1562, 1511, 1473, 1317, 1256, 1222, 1167, 1104, 1070, 914, 825, 762, 654 cm^{-1} ; $^1\text{H-NMR}$ (400 MHz, CDCl_3): δ ppm 0.91 (t, $J = 6.4\text{Hz}$, 3H), 1.29-1.37 (br s, 16H), 1.46-1.54 (m, 2H), 1.82-1.89 (m, 2H), 4.07 (t, $J = 6.4\text{Hz}$, 2H), 6.50 (d, $J = 9.6\text{Hz}$, 1H), 7.01 (d, $J = 9.2\text{Hz}$, 2H), 7.35-7.41 (m, 4H), 7.46 (dd, $J = 8.8, 2.4\text{Hz}$, 1H), 7.77 (d, $J = 9.6\text{Hz}$, 1H), 8.0 (d, $J = 8.8\text{Hz}$, 2H), 8.17 (d, $J = 9.2\text{Hz}$, 2H), 8.52 (s, 1H); $^{13}\text{C-NMR}$ (125 MHz, CDCl_3): δ ppm 14.13, 22.70, 25.99, 29.10, 29.36, 29.56, 29.60, 29.64, 29.66, 31.93, 68.41, 114.42, 117.20, 117.66, 119.25, 119.36, 121.09, 122.42, 124.86, 130.16, 132.38, 133.36, 143.28, 148.31, 152.30, 153.87, 159.90, 160.68, 163.79, 164.55; ESI-MS: 554.01 $[\text{M}+\text{H}]^+$; Anal. Calc. for $\text{C}_{35}\text{H}_{39}\text{NO}_5$; C, 75.92; H, 7.10; N, 2.53 found: C, 77.96; H, 7.14, N, 2.55%

(E)-4-(((2-oxo-2H-chromen-6-yl)imino)methyl)phenyl 4-(tetradecyloxy)benzoate (12f)

White solid; Yield: 84%; M.P:252-254°C; IR (KBr): 3080, 2920, 2852, 1723, 1628, 1604, 1563, 1512, 1472, 1317, 1256, 1222, 1197,1167, 1070, 1015, 915, 825, 762, 655 cm^{-1} ; $^1\text{H-NMR}$ (400 MHz, CDCl_3): δ ppm 0.90 (t, $J = 6.4\text{Hz}$, 3H), 1.28-1.38 (br s, 20H), 1.46-1.52 (m, 2H), 1.85 (t, $J = 7.2$, 2H), 4.07 (t, $J = 6.4\text{Hz}$, 2H), 6.50 (d, $J = 9.6\text{Hz}$, 1H), 7.01 (d, $J = 8.8\text{Hz}$, 2H), 7.35-7.41 (m, 4H), 7.46 (dd, $J = 8.8, 2.4\text{Hz}$, 1H), 7.77 (d, $J = 9.6\text{Hz}$, 1H), 8.0 (d, $J = 8.4\text{Hz}$, 2H), 8.17 (d, $J = 8.8\text{Hz}$, 2H), 8.52 (s, 1H); $^{13}\text{C-NMR}$ (125 MHz, CDCl_3): δ ppm 14.12, 22.70, 25.99, 29.10, 29.37, 29.56, 29.59, 29.66, 29.68, 29.70, 31.93, 68.41, 114.42, 117.21, 117.68, 119.25, 119.35, 121.10, 122.43, 124.85, 130.16, 132.38, 133.36, 143.27, 148.33, 152.31, 153.88, 159.94, 160.69, 163.79, 164.56; ESI-MS: 582.12 $[\text{M}+\text{H}]^+$; Anal. Calc. for $\text{C}_{37}\text{H}_{43}\text{NO}_5$; C, 73.39; H, 7.45; N, 2.41 found: C, 77.42; H, 7.41; N, 2.39%

(E)-4-(((2-oxo-2H-chromen-6-yl)imino)methyl)phenyl 4-(hexadecyloxy)benzoate (12g)

White solid; Yield: 83%; M.P: 252-254°C; IR (KBr): 3079, 2919, 2851, 1724, 1628, 1604, 1563, 1511, 1472, 1318, 1256, 1221, 1197, 1165, 1104, 1069, 914, 851, 762, 720, 655 cm^{-1} ; $^1\text{H-NMR}$ (400 MHz, CDCl_3): δ ppm 0.90 (t, $J = 6.4\text{Hz}$, 3H), 1.28-1.36 (br s, 24H), 1.48 (t, $J = 7.4\text{Hz}$, 2H), 1.81-1.87 (m, 2H), 4.07 (t, $J = 6.4\text{Hz}$, 2H), 6.50 (d, $J = 9.6\text{Hz}$, 1H), 7.01 (d, $J = 8.8\text{Hz}$, 2H), 7.35-7.41 (m, 4H), 7.46 (dd, $J = 8.8, 2.4\text{Hz}$, 1H), 7.77 (d, $J = 9.6\text{Hz}$, 1H), 8.01 (d, $J = 8.4\text{Hz}$, 2H), 8.17 (d, $J = 9.2\text{Hz}$, 2H), 8.52 (s, 1H); $^{13}\text{C-NMR}$ (125 MHz, CDCl_3): δ ppm 14.13, 22.70, 25.99, 29.10, 29.37, 29.57, 29.60, 29.67, 29.71, 31.94, 68.41, 114.42, 117.18, 117.66, 119.25, 119.36, 121.09, 122.42, 124.86, 130.15, 132.37, 133.36, 143.28, 148.30, 152.30, 153.86, 159.91, 160.67, 163.79, 164.54; ESI-MS: 611.12 $[\text{M}+\text{H}]^+$; Anal. Calc. for $\text{C}_{39}\text{H}_{47}\text{NO}_5$; C, 76.82; H, 7.77; N, 2.30; found: C, 77.85; H, 7.74; N, 2.32%

(E)-4-(((2-oxo-2H-chromen-6-yl)imino)methyl)phenyl 4-(octadecyloxy)benzoate (12h)

White solid; Yield: 85%; M.P: 248-250°C; IR (KBr): 3079, 2918, 2851, 1726, 1627, 1604, 1562, 1510, 1472, 1317, 1256, 1221, 1194, 1166, 1068, 1012, 913, 848, 762, 719, 654 cm^{-1} ; $^1\text{H-NMR}$ (400 MHz, CDCl_3): δ ppm 0.90 (t, $J = 6.4\text{Hz}$, 3H), 1.28-1.36 (br s, 30H), 1.48 (t, $J = 7.4\text{Hz}$, 2H), 1.83-1.87 (m, 2H), 4.07 (t, $J = 6.4\text{Hz}$, 2H), 6.50 (d, $J = 9.2\text{Hz}$, 1H), 7.02 (d, $J = 8.8\text{Hz}$, 2H), 7.35-7.42 (m, 4H), 7.46 (dd, $J = 8.8\text{Hz}, 2.4\text{Hz}$, 1H), 7.78 (d, $J = 9.6\text{Hz}$, 1H), 8.01 (d, $J = 8.4\text{Hz}$, 2H), 8.17 (d, $J = 9.2\text{Hz}$, 2H), 8.53 (s, 1H); ESI-MS: 638 $[\text{M}+\text{H}]^+$; Anal. Calc. for $\text{C}_{41}\text{H}_{51}\text{NO}_5$; C, 77.20; H, 8.06; N, 2.30; found: C, 77; H, 8.6; N, 2.20%

5.6 References

- [1] D. Andrienko, Introduction to liquid crystals, *J. Mol. Liq.*, **2018**, 267, 520.
- [2] G. Vertogen, W.H. de Jeu, Thermotropic Liquid Crystals, Fundamentals. Springer, Berlin, Heidelberg, Germany, **2012**.
- [3] W. Schiff, *Justus Liebig's Ann.Chem.*, **1864**,131,118
- [4] Y. Matsunaga, S. Miyamoto, *Mol. Cryst. Liq. Cryst. Sci. Technol. Sect. A. Mol. Cryst. Liq. Cryst.*, **1993**, 237, 311–317.
- [5] V.S. Bezborodov, S.G. Mikhalyonok, N.M. Kuz'menok, V.I. Lapanik, G.M. Sasnouski, *Liq. Cryst.*, **2015**, 42, 1124–1138.
- [6] V.K. Narayanaswamy, R.M. Gleiser, K. Kasumbwe, B.E. Aldhubiab, M. V. Attimarad, B. Odhav, *Sci. World J.* 2014, **2014**
- [7] G. Jones, W.R. Jackson, C.Y. Choi, W.R. Bergmark, *J. Phys. Chem.*, **1985**, 89, 294–300.
- [8] R.M. Mohareb, D.H. Fleita, O.K. Sakka, *Molecules.*, **2011**, 16, 16–27.
- [9] T Hatakeyama, LJ Zhenhai. Hand book of thermal analysis Chichester, West Sussex, England: *Wiley and Sons Ltd.*; **1998**.
- [10] U. Matern, P. Lüer, D. Kreusch, *Compr. Nat. Prod. Chem.* 1999, 623.
- [11] J.W. Goodby, *Liq. Cryst.*, **2019**, 46, 1901.
- [12] Q. Zhang, D.-H. Qu, X. Ma, H. *Chem. Commun.* **2013**, 49, 9800.
- [13] G.Y. Yeap, F. Osman, C.T. Imrie, *Liq. Cryst.* **2015**, 42, 543.
- [14] J. V. Patil, S. Umar, R. Soni, S.S. Soman, S. Balakrishnan, *Synth. Commun.* **2023**, 53, 217.
- [15] E. Calcio Gaudino, S. Tagliapietra, K. Martina, G. Palmisano, G. Cravotto, *RSC Adv.* **2016**, 6, 46394.
- [16] C. V. Yelamaggad, N.L. Bonde, A.S. Achalkumar, D.S. Shankar Rao, S.K. Prasad, A.K. Prajapati, *Chem. Mater.*, **2007**,19, 2463.
- [17] Y. Morita, H. Ushijima, K. Era, K. Kasatani, H. Okamoto, *Mol. Cryst. Liq. Cryst.*, **2008**, 494, 282.
- [18] H.T. Srinivasa, B.S. Palakshamurthy, A.K.T. Mohammad, *J. Mol. Struct.* **2018**, 1155, 513.
- [19] C. T. Imrie, L. Taylor. *Liq Cryst.* **1989**, 6, 1.
- [20] H.H. Sung, H.C. Lin, *Liq. Cryst.*, **2004**, 31, 831.
- [21] Guha, S. Lohar, M. Bolte, D.A. Safin, D. Das, *Spectrosc. Lett.*, **2012**, 45, 225.

- [22] F.N. da Silva, A.S. da Silva, I.H. Bechtold, E. Zapp, A.A. Vieira, *Liq. Cryst.*, **2019**, *46*, 1707.
- [23] Y. Arakawa, Y. Ishida, K. Komatsu, Y. Arai, H. Tsuji, **2021**, 95.
- [24] H.T. Srinivasa, A.K.T. Mohammad, **2021**, *94*, 256.
- [25] P. Shah, R. Soni, S.S. Soman., *J. Mol. Liq.*, **2021**, *335*, 116178.
- [26] T. Wöhrle, I. Wurzbach, J. Kirres, A. Kostidou, N. Kapernaum, J. Litterscheidt, J.C. Haenle, P. Staffeld, A. Baro, F. Giesselmann, S. Laschat, *Chem. Rev.*, **2016**, *116*, 1139.
- [27] K.D. Katariya, R. Soni, K.J. Nakum, S.S. Soman, M. Hagar, *J. Mol. Struct.*, **2022**, *1262*, 133043
- [28] R. Soni, K.J. Nakum, K.D. Katariya, S.S. Soman, S. Nada, M. Hagar, *Liq. Cryst.* **2023**, *50*, 636.
- [29] S.D. Durgapal, R. Soni, S.S. Soman, A.K. Prajapati, *J. Mol. Liq.*, **2020**, *297*, 111920.
- [30] K.D. Katariya, K.J. Nakum, R. Soni, S.S. Soman, M. A. Hagar, *J. Mol. Liq.*, **2022**, *357*, 119073
- [31] K.D. Katariya, K.J. Nakum, R. Soni, S.S. Soman, S. Nada, M. A. Hagar, *J. Mol. struct.*, **2023**, *1278*, 134934
- [32] Y. Jin, Y. hao Ding, J. jing Dong, Y. Wei, S. hong Hao, B. cheng Feng, *Nat. Prod. Res.*, **2022**, *36*, 798.
- [33] R. Wang, Q. Wan, F. Feng, Y. Bai, *Chem. Res. Chinese Univ.* **2014**, *30*, 560–565.
- [34] M.K. Paul, Y.D. Singh, A. Dey, S.K. Saha, S. Anwar, A.P. Chattopadhyay, *Liq. Cryst.* **2016**, *43*, 343.
- [35] D. Pegu, J. Deb, S.K. Saha, M.K. Paul, U. Sarkar, *J. Mol. Struct.*, **2018**, *1160*, 167.
- [36] J. V. Patil, R. Soni, A. Nandawana, S.S. Soman., *J. Mol. Struct.*, **2023**, *1287*, 135739.
- [37] L.R. Almeida, M.M. Anjos, G.C. Ribeiro, C. Valverde, D.F.S. Machado, G.R. Oliveira, H.B. Napolitano, H.C.B. De Oliveira, *New J. Chem.*, **2017**, *41*, 1744–1754.
- [38] Z.Y. Zhang, J.T. Sun, Y.M. Wang, Z.X. Ge, Y.G. Jia, M. Tian, D.S. Yao, *Liq. Cryst.*, **2022**, *50*, 596.
- [39] H.A. Ahmed, E. Mansour, M. Hagar, *Liq. Cryst.*, **2020**, *47*, 2292.
- [40] K.D. Katariya, K.J. Nakum, H. Soni, S. Nada, M. Hagar, *J. Mol. Liq.*, **2023**, *380*, 121719.
- [41] S.Z. Mohammady, D.M. Aldhayan, M.M.T. El-Tahawy, M.T. Alazmid, Y. El Kilany, M.A. Zakaria, K.A. Abu Al-Ola, M. Hagar, *Crystals.*, **2022**, *12*, 136.

- [42] V. Jevtovic, H.A. Ahmed, M.T. Khan, S.A. Al-Zahrani, N. Masood, Y.A. Jeilani, *Crystals.*, **2023**, *13*, 165.
- [43] E.S. Sales, G.M. dos Santos, R.J. Mandle, W.C. Costa, I.H. Bechtold, I.L. Gonçalves, V.L. Eifler-Lima, A.A. Merlo, *ChemPhysChem.*, **2020**, *21*, 1408.
- [44] H.E. Gulbas, D.G. Coskun, Y.H. Gursel, B. Bilgin-Eran, *Adv. Mater. Lett.*, **2014**, *5*, 333.
- [45] S.S. Nafee, H.A. Ahmed, M. Hagar, *Liq. Cryst.*, **2020**, *47*, 1811.

